Q-SWITCHED AND MODE-LOCKED MID-IR FIBER LASERS

by

Gongwen Zhu

A Dissertation Submitted to the Faculty of the

COLLEGE OF OPTICAL SCIENCES

In Partial Fulfillment of the Requirements

For the Degree of

DOCTOR OF PHILOSOPHY

In the Graduate College

THE UNIVERSITY OF ARIZONA

2015

THE UNIVERSITY OF ARIZONA
GRADUATE COLLEGE

As members of the Dissertation Committee, we certify that we have read the dissertation prepared by Gongwen Zhu, titled Q-switched and Mode-locked Mid-IR Fiber Lasers and recommend that it be accepted as fulfilling the dissertation requirement for the Degree of Doctor of Philosophy.

_____ Date: 08/03/2015
Nasser Peyghambarian

_____ Date: 08/03/2015
Xiushan Zhu

_____ Date: 08/03/2015
Robert A. Norwood

Final approval and acceptance of this dissertation is contingent upon the candidate's submission of the final copies of the dissertation to the Graduate College.

I hereby certify that I have read this dissertation prepared under my direction and recommend that it be accepted as fulfilling the dissertation requirement.

_____ Date: 08/03/2015
Dissertation Director: Nasser Peyghambarian

STATEMENT BY AUTHOR

This dissertation has been submitted in partial fulfillment of the requirements for an advanced degree at the University of Arizona and is deposited in the University Library to be made available to borrowers under rules of the Library.

Brief quotations from this dissertation are allowable without special permission, provided that an accurate acknowledgement of the source is made. Requests for permission for extended quotation from or reproduction of this manuscript in whole or in part may be granted by the head of the major department or the Dean of the Graduate College when in his or her judgment the proposed use of the material is in the interests of scholarship. In all other instances, however, permission must be obtained from the author.

SIGNED: Gongwen Zhu

ACKNOWLEDEMENT

Firstly, I would like to take this opportunity to express my sincere gratitude to my academic advisor Dr. Nasser Peyghambarian who financially supported my research in the past four years. Without his help I cannot conduct my research in College of Optical Sciences.

I would also like to thank my research advisor Dr. Xiushan Zhu who has been directly supervising my research and gives me tremendous help in the past four years. Without his guidance and persistent support this dissertation would not have been accomplished.

My deep gratitude also goes to Dr. Robert A. Norwood who serves as my dissertation committee member and provides me very valuable suggestions.

Thanks also goes to Jie Zong, Qiang Fang, Yevgeniv Merzlyak, Dmitriy Churin, Chen Wei, Kaushik Balakrishnan, Roland Himmelhuber, Lixiang Geng, Jingwei Wu, Minghong Tong, Shujing Liu, Jian Yuan, Bin Li, Yitian Ding, Daniel Sickinger, Tianquan Su, Yi Qin, Weibo Cheng for their help and useful discussions.

I would also like to express my deepest gratitude to my parents for their love, support, encouragement and sacrifice, and to my sisters who are helping me all the time.

Finally I would like to thank my wife Xin Zi who are always standing by me and makes my life happier and more meaningful.

DEDICATION

To my parents and my wife

TABLE OF CONTENTS

TABLE OF CONTENTS-Continued

TABLE OF CONTENTS-Continued

LIST OF FIGURES

LIST OF FIGURES-Continued

LIST OF FIGURES-Continued

LIST OF FIGURES-Continued

LIST OF FIGURES-Continued

LIST OF FIGURES-Continued

LIST OF FIGURES-Continued

LIST OF FIGURES-Continued

LIST OF FIGURES-Continued

LIST OF TABLES

ABSTRACT

Mid-infrared (IR) lasers (2-12 μm) have found tremendous applications in medical surgeries, spectroscopy, remote sensing, etc. Nowadays, mid-IR emissions are usually generated from semiconductor lasers, gas lasers, and solid-state lasers based on nonlinear wavelength conversion. However, they usually have disadvantages including poor beam quality, low efficiency, and complicated configurations. Mid-IR fiber lasers have the advantages of excellent beam quality, high efficiency, inherent simplicity, compactness, and outstanding heat-dissipating capability, and have attracted significant interest in recent years. In this dissertation, I have studied and investigated Q-switched and mode-locked fiber lasers in the mid-IR wavelength region.

My dissertation includes six chapters: In Chapter 1, I review the background of mid-IR lasers and address my motivation on the research of mid-IR fiber lasers; In Chapter 2, I present the experimental results of microsecond and nanosecond Er^{3+}-doped and Ho^{3+}-doped fiber lasers in the 3 μm wavelength region Q-switched by Fe^{2+}:ZnSe and graphene saturable absorbers. In Chapter 3, Q-switched 3 μm laser fiber amplifiers are investigated experimentally and theoretically and their power scaling are discussed. In Chapter 4, a graphene mode-locked Er^{3+}-doped fiber lasers at 2.8 μm with a pulse width < 50 ps is presented. In Chapter 5, extending the spectral range of mid-IR fiber lasers by use of nonlinear wavelength conversion is addressed and discussed. I have proposed 10-watt-level 3-5 μm Raman lasers using tellurite fibers as the nonlinear gain medium and pumped by our Er^{3+}-doped fiber lasers at 2.8 μm. In the last chapter, the prospect of mid-IR fiber laser is addressed and further research work is discussed.

CHAPTER 1

Introduction

1.1 Brief introduction to lasers, optical fibers and fiber lasers

The term “laser” originated as an acronym for “light amplification by stimulated emission of radiation”. Since the invention of the first functioning lasers in 1960 by Theodore H. Maiman [1], lasers are playing a more and more important role in a large number of fields such as scientific research (Raman spectroscopy, laser cooling, nuclear fusion, etc), medical application (cosmetic surgery, laser scalpel, laser therapy, etc), industrial and commercial application (laser cutting, laser welding, laser printers, etc), defense technology (defensive countermeasures, laser weapons, laser guidance, etc). The first working laser is a solid state ruby laser with chromium ions doped in the ruby crystal. Since then many types of lasers have been invented and vastly developed such as the gas lasers, semiconductor laser, photonic crystal lasers, fiber lasers, dye lasers, free-electron lasers, etc. Among them, fiber lasers have attracted great attentions due to their great advantages such as the inherent simplicity, high efficiency, high output power, flexibility, maintenance-free, low cost, outstanding heat-dissipating capability, and excellent beam quality, etc.

The first optical fiber laser was constructed in 1961 by Elias Snitzer and his colleagues shortly after the invention of laser [2]. Unlike other types of lasers, the laser cavity is usually formed by fusion splicing fiber Bragg gratings (FBGs) with the gain fibers to form a laser cavity. The gain fiber is usually doped with rare earth (RE) ions such as erbium (Er^{3+}), ytterbium (Yb^{3+}), thulium (Tm^{3+}), holmium (Ho^{3+}), neodymium

(Nd^{3+}), and praseodymium (Pr^{3+}), etc. As a large number of energy levels exist in the RE ions, it provides tremendous flexibility in operating wavelength ranges. In the next few decades, fiber lasers have been greatly developed in different aspects, such as different operating wavelengths, multi-wavelength, high power, high energy, short pulse width, narrow linewidth, etc. Various kinds of optical fibers have also been developed to reach low attenuation, low cost, high power, new operation wavelength, high dopant concentration, etc.

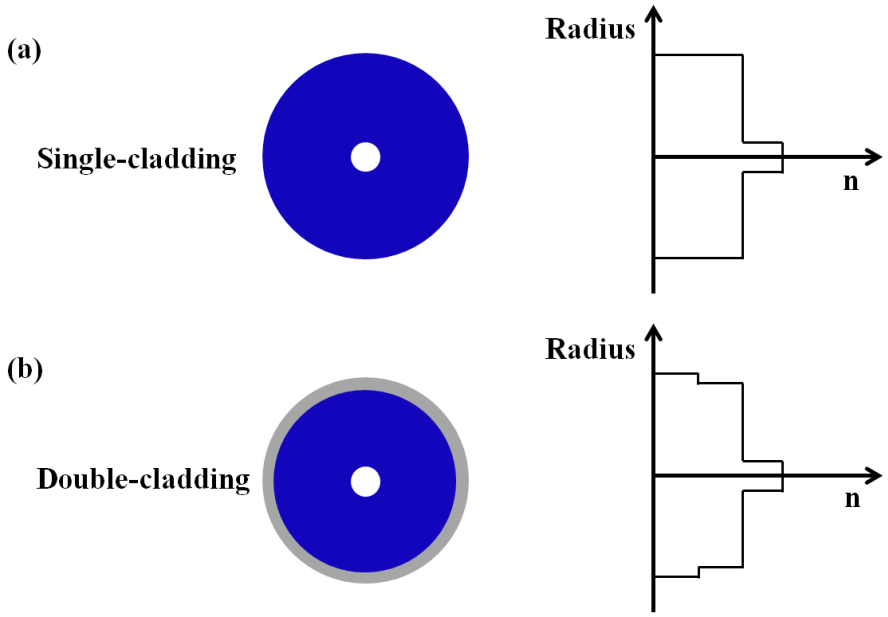

Fig. 1.1 Schematic of (a) the single-cladding and (b) the double-cladding optical fibers (left) and the corresponding refractive indexes (right).

The typical structure of the single-cladding and double cladding optical fibers are shown in Fig. 1.1. The single-cladding fiber usually consists a core and a cladding whose refractive index is lower than that of the core so that the light can be guided in the core by total internal reflection (TIR). While the double-cladding fiber consists of a core, an inner

cladding and an outer cladding. Double-cladding fibers are usually used in the cladding pump scheme where the pump laser is restricted to the inner cladding by an outer cladding with lower refractive index. The pump laser also partly propagates in the single-mode core, where it can be absorbed by the laser-active ions. On the outside of the cladding, buffer coatings are usually used to protect the cladding and core from moisture and physical damages (not shown in the figure).

Optical fibers have a very wide operation wavelength bandwidth ranging from ultraviolet (UV) to mid-infrared (mid-IR) depending on the host materials. Among them, the most commonly used ones are fused silica fibers which can operate in the 0.3 μm - 2 μm wavelength range. Silica fibers are chemically very stable, have high mechanical strength, high damage threshold, very low loss especially at the optical fiber communication wavelength around 1.55 μm (less than 0.2 dB/km) [3]. However, the maximum phonon energy is high ($\approx 1100\ cm^{-1}$) which limits the emission wavelength. Another commonly used type of fibers are phosphate fibers with the primary advantage of their high solubility for RE ions. High concentrations of laser-active RE ions can be doped in the phosphate glasses fibers without detrimental effects such as clustering, which is essential for single frequency operation [4]. In the mid-IR region, ZBLAN glass, which consists of a mixture of ZrF_4-BaF_2-LaF_3-AlF_3-NaF with a molar composition of 53% ZrF_4, 20% BaF_2, 4% LaF_2, 3% AlF_3, and 20% NaF, considered as the most stable glass practical for optical fiber applications, was reported first by Ohsawa et al of the Furukawa Electic Co. in 1981 [5]. ZBLAN fiber has always been considered as ideal host for lasing materials at wavelengths where silica fiber lasers are absent for its extended infrared edge (> 5 μm), low maximum phonon energy (< 600 cm^{-1}), and low loss (< 0.1

dB/m) [6,7]. Due to the low phonon energy in ZBLAN glass, RE dopant ions exhibit a strongly reduced tendency for quenching processes caused by multi-phonon transitions. Therefore, the lifetimes of various metastable energy levels can be strongly increased compared with silica fibers [8]. However, compared with silica fibers, ZBLAN glass fibers have some drawbacks such as fragility and hydroscopicity. Tellurite glass has also been extensively used in nonlinear photonics devices in the mid-IR due to its good optical transparency in the wavelength range of 0.5-5 μm and high nonlinear refractive index of 5.9×10^{-19} m^2/W[9]. Compared to other mid-IR transmitting glasses such as ZBLAN and chalcogenide glasses, tellurite glass exhibits higher robustness, stronger corrosion resistance, and better thermal stability [10]. In addition, they are non-hygroscopic, which allows storage in ambient air without degradation and makes tellurite glass devices require less protection. However, the maximum phonon energy is relatively high (800 cm^{-1}) compared with other mid-IR fibers and the longest fluorescent wavelengths that could be observed in tellurite glass can hardly go beyond 3 μm so RE-doped tellurite fiber lasers are not efficient in the mid-IR region [10]. Chalcogenide glass fiber is another kind of commonly used mid-IR fibers which has high transmission in the mid-IR or even long-wave IR region [11]. Chalcogenide glass is a member of the group of non-oxide glass that contains one or more of the chalcogen elements: S, Se or Te. It is environmentally durable and has a low toxicity. It also has very high nonlinearity ($n_2=1.5\times10^{-17}$ m^2/W [12]) and would be ideal for some applications such as mid-IR nonlinear wavelength conversions (supercontinuum generation and Raman laser), etc. However, compare with other mid-IR fibers, it is less robust. Besides, the low achievable

RE doping level (~ 0.1 mol%) and low damage threshold limits the output power in chalcogenide fiber lasers.

The transmission spetra of silica, ZBLAN [13], tellurite [14], chalcogenide [15] fibers are shown in Fig. 1.2. Silica fibers, due to its excellent physical and chemical properties, dominant in the wavelength region below 2 μm. However, in some upconversion lasers, the upper-state lifetimes of rare earth ions are particularly important. In silica fibers where multi-phonon transitions are strong, the upper-state lifetimes are usually too short for the laser transitions. In ZBLAN fibers, however, the multi-phonon transitions are largely suppressed and the upper-state lifetimes of the RE-ions are greatly increased, and thulium doped blue upconversion fiber laser and erbium-doped green upconversion fiber laser have been achieved in ZBLAN glass [8,16]. In the 2 - 4 μm wavelength region, ZBLAN glass fibers become dominant for fiber lasers due to its low propagation loss and high solubility of RE-ions. Currently most RE-doped mid-IR fiber lasers are built on ZBLAN glass fiber. Tellurite and chalcogenide fibers, however, are usually used in nonlinear wavelength conversions because of their high nonlinearities[17,18]. A comparison of selected properties for tellurite, silica, fluoride and chalcogenide glasses are also shown in Table 1.1 [10].

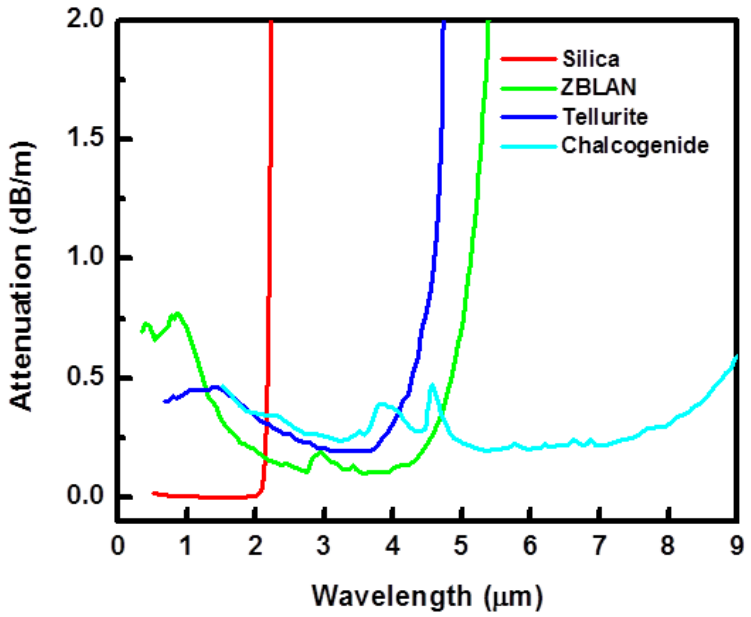

Fig. 1.2 The attenuation of silica, ZBLAN, tellurite and chalcogenide fibers as a function of wavelength.

Property	Tellurite	Silica	Fluoride	Chalcogenide
Optical properties (typical values)				
Refractive index (n)	1.8-2.3	1.46	1.5	2.83
Abbe number (v)	10-20	80	60-110	
Nonlinear refractive index (n_2, m^2/W)	2.5×10^{-19}	10^{-20}	10^{-21}	10^{-17}
Transmission range (μm)	0.4-5.0	0.2-2.5	0.2-7.0	0.8-16
Highest phonon energy (cm^{-1})	800	1000	500	300
Longest fluorescent wavelength (μm)	2.8	2.2	4.4	7.4
Bandgap (eV)	≈3	≈10		1-3
Acousto-optical figure of merit, p^2n^6 / rv^3 (10^{-18} s^3/g)	24	1-19	-	
Physical properties (typical values)				
Glass transition (T_g, ℃)	300	1000	300	300
Thermal expansion (10^{-7} ℃)	120-170	5	150	140
Density (g/cm^3)	5.5	2.2	5.0	4.51
Dielectric constant (ϵ)	13-35	4.0	-	
Fiber loss	-	0.2 dB/km (1.5 μm)	15-25 dB/km (1.5-2.75 μm)	0.4 dB/km (6.5 μm)
Bonding	covalent-ionic	Ionic-covalent	ionic	covalent
Solubility in water	$<10^{-2}$	$<10^{-3}$	soluble	$<10^{-4}$

Table 1.1 A comparison of selected properties for tellurite, silica, fluoride and chalcogenide glasses [10].

Fiber lasers are usually based on glass fibers which are doped with laser-active RE ions. The wavelength of these lasers are usually determined by the transitions between the energy levels of the RE ions. The common laser-active ions include erbium (Er^{3+}) , ytterbium(Yb^{3+}), thulium (Tm^{3+}), holmium (Ho^{3+}), neodymium (Nd^{3+}), praseodymium (Pr^{3+}), dysprosium (Dy^{3+}), etc. Table 1.2 shows the common RE ions used in fiber lasers

and their host glasses and important emission wavelength [19]. These common ions can generate laser emission spanning from visible to mid-IR region.

Ion	Host glasses	Important wavelengths
Erbium (Er^{3+})	silicate , phosphate glasses and fluoride glasses	1.55 μm, 2.8 μm
Ytterbium(Yb^{3+})	silicate glass	0.976μm, 1.0-1.1 μm
Thulium (Tm^{3+})	silicate , phosphate glasses and fluoride glasses	0.48 μm, 0.81 μm, 1.48 μm, 1.9 μm
Holmium (Ho^{3+})	silicate and fluoride glasses	1.2 μm, 2.1 μm, 2.9 μm
Neodymium (Nd^{3+})	silicate and phosphate glasses	0.90-0.94 μm, 1.06 μm, 1.32 μm
Praseodymium (Pr^{3+})	silicate and fluoride glasses	0.49 μm, 0.52 μm, 0.635 μm, 1.3 μm
Dysprosium (Dy^{3+})	silicate and fluoride glasses	1.1 μm, 1.3 μm, 2.9 μm

Table 1.2 Common RE ions, their host glasses and important emission wavelengths [19].

The partial energy level diagrams of these RE ions are shown in Fig. 1.3. The important transitions of these laser-active ions are also shown in the figure, covering a broad wavelength band ranging from visible to mid-IR.

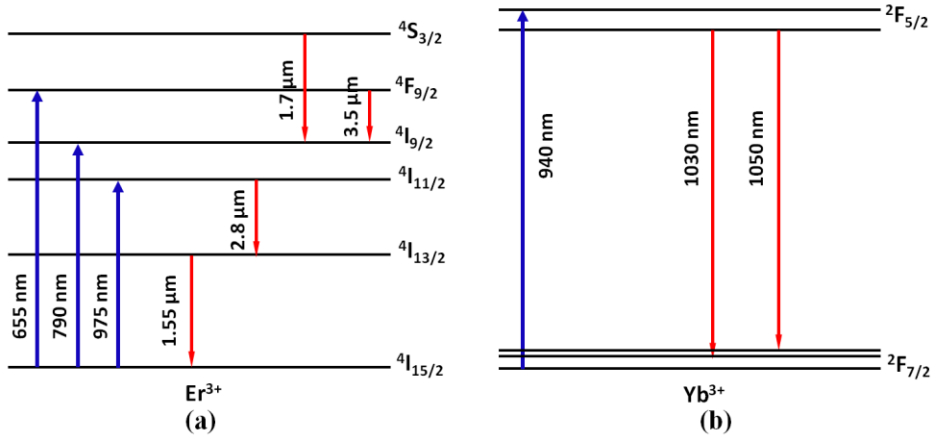

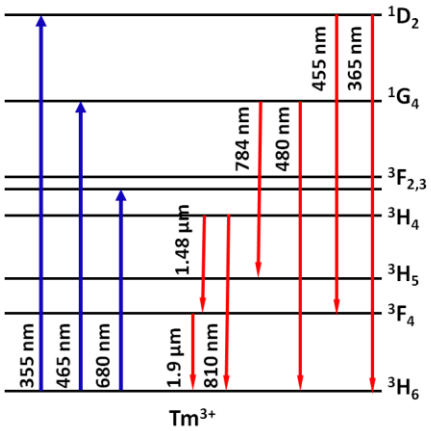
$^1D_2$
$^1G_4$
$^3F_{2,3}$
$^3H_4$
$^3H_5$
$^3F_4$
$^3H_6$
355 nm
465 nm
680 nm
1.9 µm
810 nm
1.48 µm
784 nm
480 nm
455 nm
365 nm
Tm^{3+}

(c)

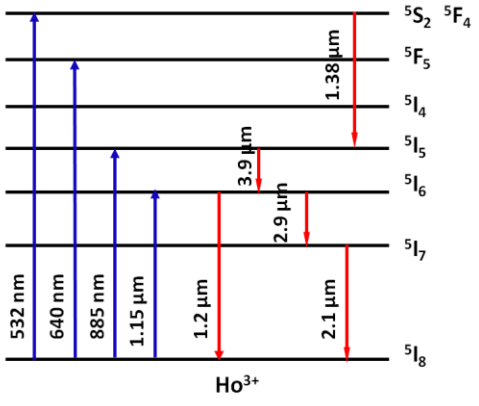
$^5S_2$ $^5F_4$
$^5F_5$
$^5I_4$
$^5I_5$
$^5I_6$
$^5I_7$
$^5I_8$
532 nm
640 nm
885 nm
1.15 µm
1.2 µm
2.1 µm
2.9 µm
3.9 µm
1.38 µm
Ho^{3+}

(d)

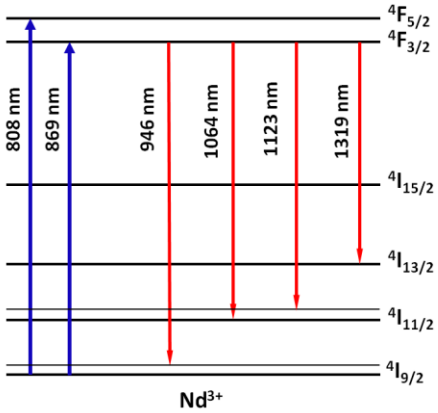
$^4F_{5/2}$
$^4F_{3/2}$
$^4I_{15/2}$
$^4I_{13/2}$
$^4I_{11/2}$
$^4I_{9/2}$
808 nm
869 nm
946 nm
1064 nm
1123 nm
1319 nm
Nd^{3+}

(e)

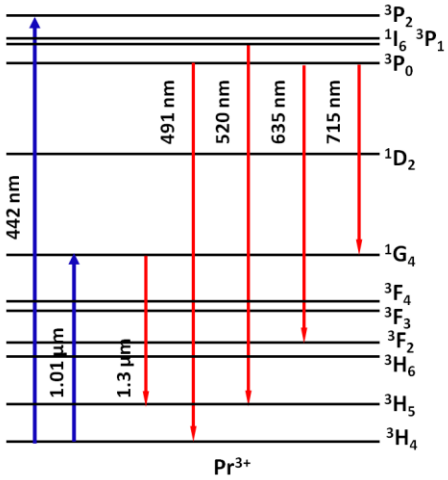
$^3P_2$
$^1I_6$ $^3P_1$
$^3P_0$
$^1D_2$
$^1G_4$
$^3F_4$
$^3F_3$
$^3F_2$
$^3H_6$
$^3H_5$
$^3H_4$
442 nm
491 nm
520 nm
635 nm
715 nm
1.01 µm
1.3 µm
Pr^{3+}

(f)

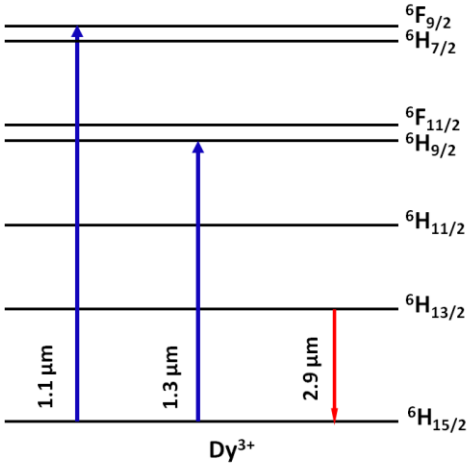
$^6F_{9/2}$
$^6H_{7/2}$
$^6F_{11/2}$
$^6H_{9/2}$
$^6H_{11/2}$
$^6H_{13/2}$
$^6H_{15/2}$
1.1 µm
1.3 µm
2.9 µm
Dy^{3+}

(g)

Fig. 1.3 The partial energy level diagrams of the common laser-active ions and their important transitions. (a) Erbium, (b) Ytterbium, (c) Thulium, (d) Holmium, (e) Neodymium, (f) Praseodymium, (g) Dysprosium.

Since the invention of fiber lasers, development of high power is always a priority. In the past few decades, the average output power of continuous-wave (CW) fiber lasers has been increasing exponentially and the maximum power reached 10 kW in 2009 [20,21]. A record high peak power of 3.8 GW directly from a fiber chirped-pulse amplification system was also reported [22]. The development of fiber lasers at new operation wavelengths have also attracted great attentions in recent decades. The highest output power from published demonstrations of infrared fiber lasers as a function of the emitted wavelength are shown in Fig. 1.4 [23]. The maximum output power from fiber lasers shows an exponential decrease as a function of emission wavelength as shown in Fig. 1.4. The primary cause of this power drop is the increase in quantum defect at longer wavelengths which creates heat that becomes a large fraction of the absorbed pump power [23]. Developing efficient longer-wavelength pump sources and using more appropriate laser transitions can effectively reduce the quantum defects and improve output performance. The development of high power fiber lasers at new operation wavelengths provides numerous opportunities in scientific research and industrial applications.

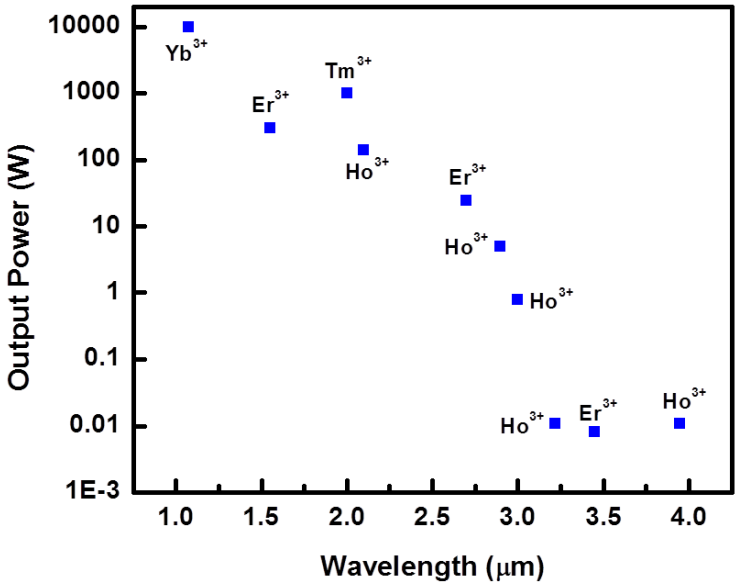

Fig. 1.4 The maximum output power from published demonstrations of infrared fiber lasers as a function of wavelength [23].

1.2 Introduction mid-IR lasers

1.2.1 Mid-IR lasers and mid-IR fiber lasers

Mid-infrared (mid-IR) lasers are generally referred to lasers with wavelength from 3 μm to 12 μm. Sometimes people may also consider mid-IR region starts at 2 μm. Mid-IR lasers have attracted great attentions in the recent decays due to its large application in spectroscopy, medical surgery, frequency metrology, missile countermeasures, remote sensing and materials processing, high-efficiency pump sources for nonlinear wavelength converters, etc [24-31]. Particularly pulsed mid-IR lasers with high peak powers have attracted great attentions in recent decades for their numerous important applications. Pulsed mid-IR lasers, especially at 3 μm, are highly demanded in laser surgeries due to

the high water absorption at this wavelength as shown in Fig. 1.5 [32]. The peak absorption coefficient near 3 μm of pure water is approximately 12,000 cm^{-1}. In tissue, which is typically 70% water, the optical penetration depth, should be approximately 1 μm, which is much less than that of lasers at other operation wavelengths (e.g. CO_2 laser with a wavelength of 10.6 μm has a penetration depth of more than 10 μm) [33]. 3 μm pulsed laser with high power and short pulses is also essential since they can significantly reduce collateral damages. Compared with normal-spiking-mode pulses (pulse duration ≈ 200 μs) which typically leave 10-50 μm of collagen damage, Q-switched pulses (pulse duration ≈ 90 ns) typically only cause 5-10 μm of damage in all tissues [33].

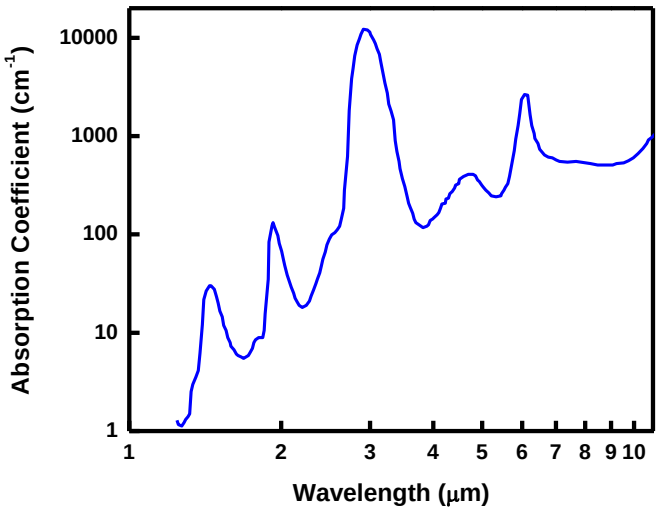

Fig. 1.5 Absorption spectrum (absorption coefficient vs. wavelength) of liquid water.

Another important application for mid-IR pulsed fiber lasers at 3 μm is serving as the pump sources for nonlinear wavelength conversion. With proper laser resonator, fiber laser sources operating at any wavelength within the 3-5 μm atmospheric transparency

window can be achieved by employing 1st-and 2nd-order Raman scattering of tellurite fibers when pumped at 2.8 μm [31]. Q-switched pump lasers also have much higher conversion efficiency and much lower threshold than corresponding cw pump lasers [31]. 3 μm pulsed fiber lasers is also very important in supercontinuum generation (SC) in the long-wavelength mid-IR region. Mid-IR SC with a long wavelength edge of 4.65 μm in a W-type tellurite fiber pumped by a mid-IR picosecond laser, and mid-IR SC with a long wavelength edge up to 12 μm in a chalcogenide photonic crystal fiber (PCF) pumped by a mid-IR femtosecond laser at 2.8 μm, were reported [14]. Pulsed mid-IR lasers also has many other important applications such as mid-IR frequency comb generation for precision spectroscopy of molecules [34], gas sensing [29], etc.

Mid-IR coherent emissions can generally be produced by electrically and optically-pumped semiconductor lasers (e.g. lead-salt, antimonide, IV-VI semiconductors, quantum cascade lasers)[35-38], optically-pumped ion-doped (Rare-earth: Er, Pr, Ho, Dy, etc. or transition-metal: Cr, Fe, etc) crystal lasers [39-41], solid-state laser-pumped optical parametric oscillators (OPOs) and difference frequency generation (DFG) sources [42-45], and optically or electrically-pumped gas (e.g. CO_2, CO, C_2H_2, HCN) lasers [46-49]. Mid-IR laser sources are firstly obtained from various types of lead salt lasers which are comprised of PbTe, PbSe, and PbS and various alloys of these compounds with the same materials above and with SnSe, SnTe, CdS and other materials [35]. However, lead salt lasers need to be operated at cryogenic temperatures (normally well below 200 K). Besides, they can only provide very low powers (typically in the order of 1 mW), and their electrical-to-optical power efficiency is very low compared with that of shorter-wavelength laser diodes. Quantum cascade lasers are a relatively recent development in

the area of semiconductor lasers which utilize intersubband transitions. The photon energy (and thus the wavelength) of transitions can be varied in a wide range by engineering the details of the semiconductor layer structure. Nevertheless, the beam quality is usually very poor and the output power is still in the mW-level [36]. Besides, Quantum cascade lasers operating in CW mode produce a large amount of heat and most of the injected electrical power is converted into heat. Given that the area of the active region is small, it will be a challenge to create high-power single-mode infrared light conveniently from these sources [23]. Solid-state lasers based on Cr^{2+}:ZnSe or Fe^{2+}:ZnSe crystals generally have better performance in terms of output power, but they usually require low temperature to achieve high efficiency and suffer from relatively poor beam quality [39-41]. OPO is an alternative route for laser radiation in the mid-IR region and recent developments show a 22 W of output power in the 3-5 μm range with a beam quality factor $M^2 \approx 1.4$ can be achieved in a $ZnGeP_2$ based OPO [42]. However, OPO sources generally have a more complex configuration requiring careful alignment and maintenance. DFG is also a wide spread method in mid-IR laser radiation, especially for the generation of fs pulse lasers in the 6 - 12 μm wavelength range [42]. But they have similar drawbacks as OPO sources. Gas lasers have also gained interest in recent years for generating coherent radiation in the mid-IR region [46-48]. However, these sources usually have very low efficiency and need numerous free-space accessories.

Compared to these laser sources, mid-IR fiber lasers, like other fiber lasers, have the advantages of high efficiency, inherent simplicity, compactness, low cost, outstanding heat-dissipating capability, and excellent beam quality, etc. Mid-IR fiber lasers generally include RE-doped (such as Er, Ho, Dy-doped, etc) fluoride, tellurite, and chalcogenide

fiber lasers[50-63], nonlinear wavelength conversion fiber lasers (supercontinuum and Raman) [17,31,64], etc.

The partial energy level diagram of Er^{3+} ions are plotted in Fig. 1.3 (a). The first Er^{3+}-doped fluorozirconate fiber laser operating near 3 μm was reported by M. C. Brierley et al by pumping a large core, low concentration ZBLANP fluoride glass fiber at 476.5 nm [50]. This unusual CW lasing of the self terminating transition was explained by ESA depleting the lower level $^4I_{13/2}$ and maintaining the population inversion ($^4I_{11/2}$ level lifetime 6.9 ms, $^4I_{13/2}$ level lifetime 9 ms). Although pumping around 980 nm directly into the upper laser level provides the highest Stokes efficiency, ESA at 980 nm from the $^4I_{11/2}$ upper laser level [65] was detrimental to lasing for low-doped, core pumped Er^{3+}-doped ZBLAN fiber lasers. Experimentally, the best pump wavelength is near 792 nm since this wavelength is at the peak of ESA from the $^4I_{13/2}$ lower laser level [66,67]. Colasing at 1.7 μm via transition $^4S_{3/2} \rightarrow {}^4I_{9/2}$ was suggested to suppress the competitive lasing on the 850 nm transition $^4S_{3/2} \rightarrow {}^4I_{13/2}$ and achieve the population inversion [68]. However, this type of cascade lasing is only efficient in low-doped, core-pumped fiber lasers and cannot be used for diode-pumped high-power fiber lasers. Over the last decade, great efforts have been made to escalate the power of CW RE-doped mid-IR fiber lasers. By now, energy transfer process between Er^{3+} ions and codoped Pr^{3+} ions and energy transfer upconversion process between Er^{3+} and Er^{3+} ions have been proven to be the most efficient way to depopulate the lower laser level $^4I_{13/2}$ and solve the population bottleneck. With recent commercially available high-power diode lasers at 975 nm and high-concentration double-cladding Er-doped ZBLAN fibers, several 10-W-level fiber lasers near 3 μm have been achieved recently by using heavily Er^{3+}-doped

ZBLAN fibers and the maximum output power has reached 30 W [57,69-72]. Besides the well known transition $^4I_{11/2} \rightarrow {}^4I_{13/2}$ for emission around 3 μm, the transition $^4F_{9/2} \rightarrow {}^4I_{9/2}$ in Er^{3+} ions can also provide mid-IR laser emission around 3.5 μm. However, it usually requires low operation temperature or has very limited output power [73,74]. Until very recently, an Er^{3+}-doped ZBLAN fiber laser at 3.5 μm using dual-wavelength pumping with a highest output power of 260 mW at room temperature was demonstrated [75].

The partial energy level diagram of Ho^{3+} ions are plotted in Fig. 1.3 (d). Compared with Er^{3+}-doped ZBLAN fiber lasers, Ho^{3+}-doped ZBLAN fiber lasers have a relatively longer emission wavelength which is usually around 2.9 μm for the transition $^5I_6 \rightarrow {}^5I_7$ and closer to the water absorption peak. The lifetime of the $^5I_7$ level (12 ms) is longer than the lifetime of the $^5I_6$ level (3.5 ms) and hence the 2.9 μm transition can be self-terminating. The first CW operation of Ho^{3+}-doped ZBLAN fiber laser near 3 μm was demonstrated by L. Wetenkamp with an output power only less than 13 mW when pumped at 640 nm [76]. High power cascade lasing at 2.9 μm and 2.1 μm has been employed to extend the output power and to remove bottlenecking at the $^5I_7$ level [77]. Maximum total output power of 3 W with a slope efficiency of 65% was obtained in a Ho^{3+}-doped ZBLAN fiber pumped by a Raman fiber laser at 1150nm [78]. In order to improve the efficiency of the 3 μm emission and eliminate the 2 μm lasing, Ho^{3+}-doped fibers were codoped with Pr^{3+} ions since strong energy transfer process from the energy level $^5I_7$ of Ho^{3+} to the energy level $^3F_2$ of Pr^{3+} will rapidly depopulate the lower laser level $^5I_7$ [54,79]. So far, the highest output power of 2.5 W with a slope efficiency of 32% was achieved in a Ho^{3+}/Pr^{3+} codoped ZBLAN fiber pumped by a Yb^{3+}-doped silica fiber laser at 1100nm [54]. However, unlike Er^{3+}-doped ZBLAN fibers, due to the lack of

convenient high-power pump sources, 10-watt-level Ho^{3+}-doped ZBLAN fiber laser at 2.9 μm has not been developed until now. Ho^{3+}-doped ZBLAN fiber lasers with emissions beyond 3 μm in the atmospheric transparency window are also of much interest. A 3.22 μm holmium (Ho^{3+}) doped ZBLAN fiber laser was reported with a few milliwatts output at room temperature [80]. Under cryogenic cooling, a Ho^{3+}-doped ZBLAN fiber laser operating at 3.95 μm with a few milliwatts was achieved [81].

The partial energy-level diagram of Dy^{3+} ions is plotted in Figure 1.3 (g). Infrared Laser emission at 2.9 μm can be obtained from the transition $^6H_{13/2} \rightarrow {}^6H_{15/2}$. Unlike the quasi-four-level transitions in Er^{3+}- and Ho^{3+}-doped ZBLAN fiber lasers, this transition is quasi-three-level in Dy^{3+}-doped ZBLAN fiber lasers. The first CW Dy^{3+}-dope ZBLAN fiber laser was demonstrated in 2003 [55]. Maximum output power of 0.275 W was generated at a slope efficiency of 4.5% when the ZBLAN fiber laser was pumped with a diode-cladding-pumped Yb^{3+}-doped silica fiber laser at about 1100 nm. Later, the slope efficiency was increased to 20% when the ZBLAN fiber laser was pumped by a 1.3 μm Nd:YAG laser because of the increased Stokes efficiency and the reduced ESA of pump photons [56]. However, the output power was 0.18 W limited by the available pump power. With the recent development of high efficiency, high power pump sources, watt-level Dy^{3+}-doped ZBLAN fiber laser are achievable in the near future.

Tellurite and chalcogenide fibers are not excellent candidates for high power RE-doped lasers, however, they are often used in the nonlinear wavelength conversions such as supercontinuum generations and Raman fiber lasers due to their high nonlinearities. For example, the supercontinuum generation with longest wavelength up to ~ 5 μm in tellurite PCFs when pumped by 1550 nm, 100 fs pulses of energy E=1.9 nJ, was reported

by P. Domachuk et al in 2008 [82]. Several cascaded Raman lasers based on chalcogenide glass fiber have been demonstrated and longest laser emission wavelength of 3.77 μm was generated at room temperature [83].

1.2.2 Pulsed lasers

Constrained by the fragility and the susceptibility to opto-mechanic effects of ZBLAN glass, the output power of CW ZBLAN fiber lasers cannot be scaled up dramatically like kW-level silica fiber lasers by launching more pump power into the gain fiber. Although coherent beam combining techniques can be used for the further power scaling of mid-IR fiber lasers, the unavailability of corresponding fiber devices at mid-IR range obstacles their implement in the near future. Besides, in some particular applications such as medical surgeries, high peak power is required but high average power is not preferred. Pulsed mid-IR fiber laser is an alternative approach to achieve high peak power. Pulsed lasers with peak powers some orders of magnitude higher than in the CW regime are highly demanded for in some particular applications such as materials processing, micromachining, laser ablation, range finding, spectroscopy, nonlinear optics, etc. Laser pulses are generally produced by the processes of Q-switching which offers microsecond or nanosecond pulses, or mode-locking which offers picosecond or femtosecond pulses.

Q-switching is a widely used laser technique in which the Q-factor of the laser cavity is modulated actively by a modulator or passively by a saturable absorber. The most common type is the actively Q-switched solid-state bulk laser. The laser resonator

contains an active modulator, which in most cases is an acousto-optic modulator (AOM). Sometimes an electro-optic modulator (EOM) may also be used as an active modulator. Compared to bulky and complicate active Q-switching approaches, passive Q-switching has advantages of simplicity and compactness and no need of additional electric equipment. A saturable absorber is usually used instead of an active modulator in a passively Q-switched laser. Common saturable absorbers for Q-switched lasers are semiconductor saturable absorber mirrors (SESAMs), carbon nanotubes (CNTs), quantum dots, saturable absorber crystals, etc.

Compared to Q-switched lasers, mode-locked lasers offer much higher peak powers and much shorter pulse durations. Mode-locking is a technique in optics by which a laser can produce laser pulses of extremely short duration, on the order of picoseconds or femtoseconds. The basis of the technique is to induce a fixed-phase relationship between the longitudinal modes in the resonant cavity. Interference between these modes causes the laser light to be produced as a train of pulses. Depending on the properties of the laser these pulses may be of extremely brief duration, as short as a few femtoseconds. Similar to Q-switched lasers, mode-locked laser can also be achieved either by an active modulator or a passive saturable absorber. Likewise, active mode-locking can be achieved by an AOM, EOM, or similar device like a semiconductor electroabsorption modulator. Compared with active mode-locking, passive mode-locking can generate much shorter pulses since a saturable absorber can modulate the resonator losses much faster than an active modulator. Besides conventional saturable absorber like SESAMs and quantum dots, passive mode-locking can also be achieved by artificial saturable absorbers based on nonlinear optical effects, including Kerr lens mode locking [84],

nonlinear polarization evolution [85], additive-pulse mode locking [86], etc. However, for passive mode-locking based on nonlinear optical effects, the resonator adjustment is usually very critical and the long-term reliability is usually very poor.

1.2.3 Saturable absorbers for mid-IR pulsed fiber lasers

Since actively modulated pulse lasers tend to be bulky, complicate, and usually require additional electric equipments, passive modulation becomes a more appealing approach to get pulsed lasers. Passively Q-switching or mode-locking is often accomplished by using a saturable absorber. The most commonly used saturable absorber in the mid-IR region is the semiconductor saturable absorber mirrors (SESAMs) [87-89]. Though SESAMs are currently the most prevalent saturable absorbers and have shown their capability for mode-locking mid-IR fiber lasers in the 3 μm region, they usually have a narrow operating wavelength range and require complex fabrication and packaging. Another kind of saturable absorber in the mid-IR region is the transitional metal doped crystals such as Fe^{2+}:ZnSe and Fe^{2+}:ZnS crystals. These saturable absorber crystals possess the advantages of large absorption cross-section, small saturation energy (low saturable loss) and excellent opto-mechanical properties (damage threshold ~2 J/cm^2). However, these crystals have long relaxation time and may not be suitable for passive mode-locking. In recent years, single-wall carbon nanotubes (SWCNTs) with broadband absorption have also emerged as promising saturable absorbers. However, they suffer from substantial non-saturable losses and tend to cluster in the manufacturing process, and they can only work up to 2 μm with current technology.

Graphene, a two-dimensional lattice of carbon atoms in a honeycomb structure, was found to possess extraordinary nonlinearities and ultrafast recovery times of photo-excited electrons in the picosecond and femtosecond timescales [90,91]. Moreover, Graphene is a zero-bandgap material and its absorption is only determined by optical conductivity constant and independent of optical frequency. It has already been verified that graphene has an ultrabroad absorption range from visible to THz waveband [92]. Thus graphene is a promising ultra-broadband saturable absorber. Q-switched and mode-locked operation of Yb^{3+}-, Er^{3+}-, and Tm^{3+}-doped silica fiber lasers based on graphene have been successfully demonstrated in the 1, 1.5 and 2 μm wavelength regions, respectively [93-97]. Therefore, it is of high interest for us to investigate the applicability of graphene as a saturable absorber to generate mid-IR pulses in the 3 μm region. Moreover, nanometer-sized graphene flakes can be deposited on fiber end facet or made to side-polished/tapered fibers to make fiber-based saturable absorbers, which can be used to make compact and reliable Q-switched and mode-locked all-fiber lasers.

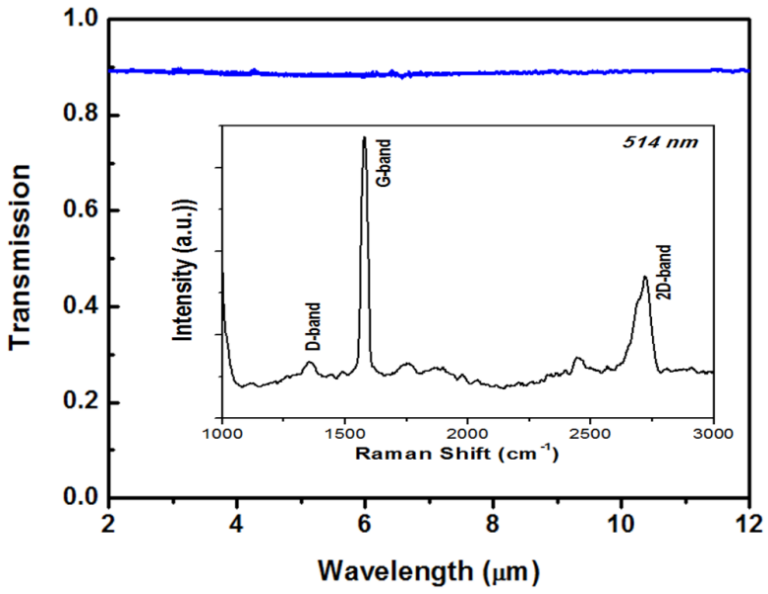

Fig. 1.6 The transmission of 5-layer graphene thin film deposited on silicon substrate. Inset: Raman spectrum of the 5-layer graphene.

In the experiment for graphene Q-swithced Er^{3+}-doped ZBLAN fiber laser, graphene was first obtained by liquid exfoliation of graphite (Bay Carbon) in 1-methyl-2-pyrrolidinone (NMP). In a typical process, 0.1 mg/mL solution was sonicated for 24 hours and allowed to settle overnight. The top 75% of the supernatant was then removed and centrifuged at 1500 rpm for 40 min. This yielded few-layer graphene flakes. The solution containing the graphene flakes were found to be stable for months and were used for the preparation of the saturable absorber. The wavelength-independent absorption of graphene in the infrared range was confirmed by measuring the transmission of few layers of graphene, which was drop cast on silicon substrate. Fig. 1.6 shows the flat infrared transmission of graphene from 2 μm to 12 μm. The absorption coefficient is almost wavelength independent, so it is expected that graphene can be used as a saturable absorber for passively Q-switching in a very wide IR wavelength range. The Raman spectroscopy of the sample with few layers of graphene was measured using a Renishaw Raman system with a pump laser at 514 nm and is shown in the inset. The Raman spectrum is consistent with previous reports [98,99].

In the experiment for graphene mode-locked Er^{3+}-doped ZBLAN fiber laser, I used a thermal chemical vapor deposition (CVD) method [100] to fabricate the graphene thin films, because with this method it is easier to achieve the desired thickness of graphene thin films than with the optically driven deposition method [101]. In addition, the CVD method can make large-area uniform graphene thin films that can be diced into smaller

pieces and used for a variety of laser development and optical characterization efforts. The multilayer graphene thin films were grown on copper foil (100 mm thick, 99.9% purity) by use of the CVD system (base pressure ~5Pa) at a growth temperature of ~1050 ℃ in a mixture of 300 sccm argon gas, 20 sccm hydrogen and 0.8 sccm methane for ~ 8 minutes. A standard PMMA assisted transfer process was used to deposit the graphene thin films onto gold mirrors [102]. We first used $FeCl_3$ to etch away the copper substrate and then rinsed the graphene (with PMMA) multiple times in de-ionized (DI) water to completely get rid of the residual copper etchant. 2 ml of 2% HCl solution in 15 ml of DI water was used to wash away residual iron particles. The graphene sample was then picked up by the gold mirror from DI water. Acetone was used to remove the PMMA to result in a graphene coated gold mirror. The Raman spectrum of the multilayer graphene was measured using a Horiba Jobin Yvon Raman system with a pump laser at 514 nm and is shown in the inset of Fig. 1.7, from which the saturable absorber is estimated to be about 4-6 layers thick. The linear and nonlinear absorption characteristics of the graphene saturable absorber sample were measured by using a mode-locked Er^{3+}-doped ZBLAN fiber laser we just developed. The power-dependent transmittance of the graphene sample is shown in Fig. 1.7. The linear absorption of the multilayer graphene sample was measured to be about 12% and its modulation depth and saturation power intensity were estimated to be ~ 10% and 2 MW/cm^2, respectively.

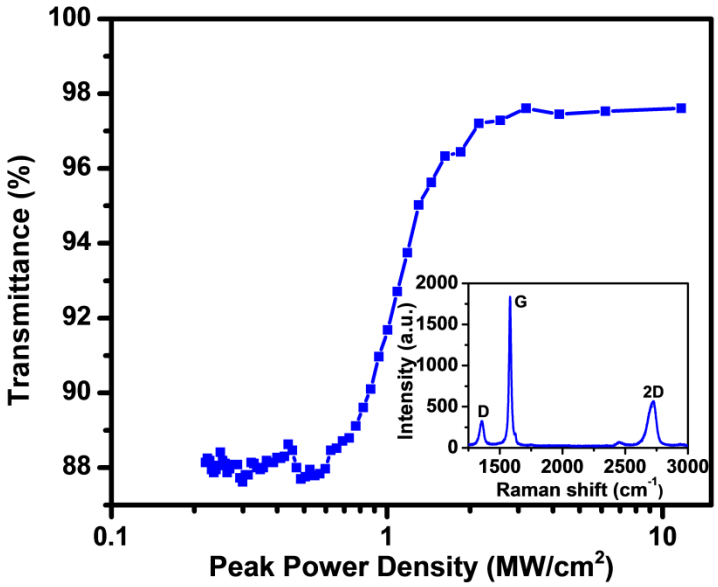

Fig. 1.7 Power-dependent transmittance of the graphene saturable absorber sample. Inset shows the Raman spectrum of the graphene sample used in the mode-locked laser experiment.

1.3 Outline of the dissertation

In this dissertation, I first give a brief introduction of the RE-doped fiber lasers, then the generation and development of mid-IR lasers are briefly discussed, and finally their important applications are presented in chapter 1.

In chapter 2, I report a Singly Ho^{3+}-doped ZBLAN fiber lasers at 3 μm passively Q-switched by Fe^{2+}:ZnSe crystal and graphene saturable absorbers respectively. 800 ns pulses at 2.93 μm with energy of 460 nJ and repetition rate of 105 KHz were obtained when a Fe^{2+}:ZnSe crystal was inserted into a free space collimating and focusing setup. A more compact and reliable Q-switched fiber laser was achieved when a graphene deposited fiber mirror was butt-coupled to the angle-cleaved end of the gain fiber. 1.2 μs

pulses with energy of 1 μJ and repetition rate of 100 KHz were achieved. More than 100 mW average output power was obtained at the maximum available pump power.

In chapter 3, an Er^{3+}-doped ZBLAN fiber amplifier for Q-switched pulses at 2.79 μm is reported. Over 24 μJ of pulse energy at an average output power of 1.0 W was achieved at a maximum available pump power of 9.4 W. The efficiency of this pulsed laser fiber amplifier is about 10%. Our simulation predicts that over 300 μJ pulses can be achieved with this fiber amplifier when a 120 W pump is used.

In chapter 4, an mid-infrared erbium (Er^{3+}) doped ZrF_4–BaF_2–LaF_3–AlF_3–NaF (ZBLAN) fiber laser mode-locked by multilayer graphene saturable absorber was demonstrated. Mode-locked pulses at 2.8 μm with an average output power of 18 mW at a repetition rate of 25.4 MHz, corresponding to a pulse energy of 0.7 nJ, were obtained. The pulse width was measured to be ~ 42 ps by a home-made autocorrelator.

In chapter 5, I report my simulations for the development of 10-watt-level 3-5 μm Raman lasers using tellurite fibers as the nonlinear gain medium and pumped by readily available continuous-wave (cw) and Q-switched erbium-doped fluoride fiber lasers at 2.8 μm. The results show that a watt-level or even ten-watt-level laser source in the 3-5 μm atmospheric transparency window can be achieved by utilizing the 1^{st}- and 2^{nd}-order Raman scattering in the tellurite fiber. A conversion efficiency of 33.8% and 14.1% were obtained for 1^{st}-order and 2^{nd}-order Raman laser respectively with a CW pumping scheme. When a Q-switched pump is used, over 70% conversion efficiency can be obtained with the 1^{st}-order Raman laser and 35% for the 2^{nd}-order Raman laser.

In chapter 6, a brief summary of the dissertation and the prospect are given.

CHAPTER 2

Fe^{2+}:ZnSe and Graphene Q-switched Singly Ho^{3+}-doped ZBLAN Fiber Lasers at 3 μm

2.1 Introduction

Q-switched fiber lasers at 3 μm have already been demonstrated with various active and passive modulation techniques. The first actively Q-switched mid-IR fiber laser near 3 μm was demonstrated in 1994 [58]. An acousto-optic modulator (AOM) and a rotating mirror were used as switching elements in an Er-doped ZBLAN fiber laser. Pulse duration of 100 ns and peak power exceeding 2W were achieved. Tokita, et al. recently reported a 12 W Er^{3+}-doped ZBLAN fiber laser Q-switched by a germanium AOM. Pulses at 2.8 μm with pulse energy of 100 μJ and peak power up to 0.9 kW were obtained [57]. Using a TeO_2 AOM, Hu, et al demonstrated a Q-switched Ho^{3+}/Pr^{3+}-codoped ZBLAN fiber laser at 2.9 μm with a pulse width of 78 ns and tunable repetition rate from 40 to 300 kHz [61]. However, an AOM Q-switched 3 μm laser needs electric equipment for active modulation and careful alignment as well. The gain-switching technique has recently been used in Er^{3+}- and Ho^{3+}-doped ZBLAN fiber lasers to obtain 3 μm pulses [103,104]. However, gain-switching usually requires high energy pump pulses. Passive Q-switching based on saturable absorbers which exhibit reduced absorption at high optical intensity is a preferred technique to achieve high intensity laser pulses because it doesn't require additional electric equipment and high pulse energy pumps and has the advantages of simplicity and compactness as well. The first passively Q-switched Er^{3+}-

doped ZBLAN fiber laser was demonstrated by using InAs epilayers as the saturable absorber [59]. 1.2 μs pulses with energy of 1.25 μJ and peak power of 1.04 W at repetition rate of 1.1 KHz were achieved. However, the damage threshold of InAs epilayers is low and it limits their application in high power mid-IR laser. Most recently an Er^{3+}-doped ZBLAN fiber laser passively Q-switched by a Fe^{2+}:ZnSe crystal was reported [60]. 370 ns pulses at 2.78 μm with pulse energy of 2.0 μJ and peak power of 5.34 W were achieved at a repetition rate of 161 kHz. Since the water absorption peak is at 3 μm and pulsed lasers closer to 3 μm are more efficient for laser surgery and some other particular applications, Ho^{3+}-doped ZBLAN fiber laser, which has an operation wavelength longer than Er^{3+}-doped ZBLAN fiber laser [61-63], is attracting more interest. An actively Q-switched Ho^{3+}/Pr^{3+}-doped ZBLAN fiber laser at 2.87 μm producing 78 ns pulses with a peak power of 77 W at repetition rate up to 300 KHz was reported very recently [61]. In this chapter I report the investigations on singly Ho^{3+}-doped ZBLAN fiber laser passively Q-switched by Fe^{2+}:ZnSe crystal and graphene respectively. Because free-running singly Ho^{3+}-doped ZBLAN fiber lasers generally operate at a longer wavelength than Ho^{3+}/Pr^{3+}-codoped ZBLAN fiber lasers, Q-switched pulses at 2.93 μm were obtained using both saturable absorbers.

2.2 Singly Ho^{3+}-doped ZBLAN fiber laser at 3 μm

Because of low maximum phonon energy of ZBLAN glass, Ho^{3+}-doped ZBLAN can generate laser at 3 μm through radiative transition from energy level $^5I_6$ to level $^5I_7$ as shown in Fig. 2.1. In the low concentration singly Ho^{3+}-doped ZBLAN, the lifetime of the upper laser level $^5I_6$ (3.5 ms) is usually longer than that of the lower laser level $^5I_7$ (12

ms). The 3 μm laser emission is generally self-terminated due to population accumulation in the $^5I_7$ state. The population accumulation in the $^5I_7$ state can be solved by codoping with Pr^{3+} ions and through the energy transfer process between Ho^{3+} and Pr^{3+} ions [52]. The population accumulation in the $^5I_7$ state can also be eliminated through excited state absorption processes in high concentration Ho^{3+}-doped ZBLAN [105]. In a free-running configuration, the operation wavelength of singly Ho^{3+}-doped ZBLAN laser is usually longer than the Ho^{3+}/Pr^{3+} codoped ZBLAN laser due to the relatively large quantity of population staying in the $^5I_7$ state. Therefore, singly Ho^{3+}-doped ZBLAN fiber was used in our experiment to achieve a passively Q-switched fiber laser at a wavelength closer to 3 μm.

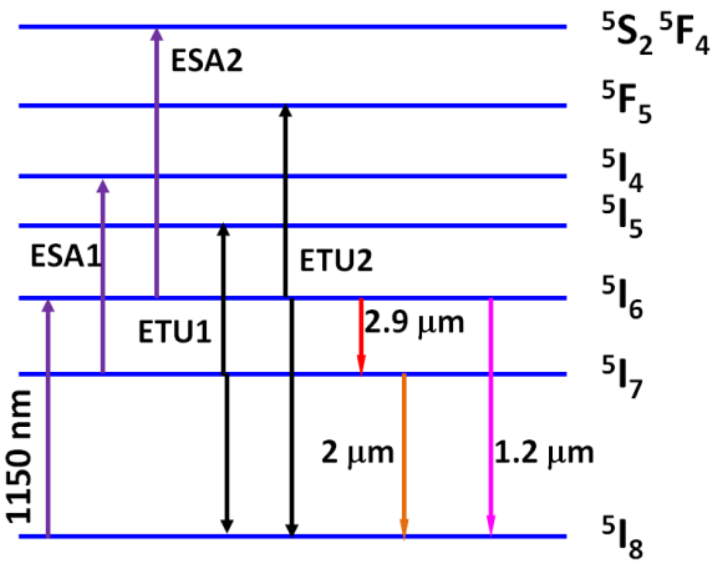

Fig. 2.1 Energy-level diagram of Ho^{3+}-doped ZBLAN and transitions related to the laser emission at 2.9 μm. ESA1 and ESA2 represent exited state absorptions and ETU1 and ETU2 represent energy transfer upconversions.

The absorption spectrum of Ho^{3+}-doped ZBLAN glass was measured and is shown in Fig. 2.2 (a). Besides these strong absorptions in the visible, Ho^{3+}-doped ZBLAN has absorption in the 1.1 μm - 1.2 μm range with a peak at 1150 nm, where semiconductor lasers and Raman fiber lasers pumped by Yb^{3+}-doped silica fiber lasers are readily available. The fluorescence of Ho^{3+}-doped ZBLAN glass was measured and is shown in Fig. 2.2(b). The strong emission at 1.2 μm corresponds to the transition $^5I_6 \rightarrow {}^5I_8$. Although the branch ratio of the transition $^5I_6 \rightarrow {}^5I_8$ to the transition $^5I_6 \rightarrow {}^5I_7$ is about 9:1, the 2.9 μm laser can be easily obtained in a high concentration Ho^{3+}-doped ZBLAN fiber because the 1.2 μm quasi-three-level laser is overwhelmed by the 2.9 μm quasi-four-level laser, in which population inversion can be obtained with a small excitation population [106]. Inset of Fig. 2.2(b) shows the fluorescence of Ho^{3+}-doped ZBLAN in the 3 μm region. The transition $^5I_6 \rightarrow {}^5I_7$ peaks at 2.85 μm and extends up to 3 μm, making Ho^{3+} a favorite active element for 3 μm laser systems. Actively Q-switched singly Ho^{3+}-doped and Ho^{3+}/Pr^{3+} codoped ZBLAN fiber lasers were reported recently [61,62]. However, an acousto-optic modulator (AOM) was used in both demonstrations. That makes the laser expensive and complicated. In this chapter, I report the demonstration of the passively Q-switched singly Ho^{3+}-doped ZBLAN fiber laser operating at 2.93 μm, in which Fe^{2+}:ZnSe crystal and graphene deposited fiber mirror were used as the saturable absorber respectively.

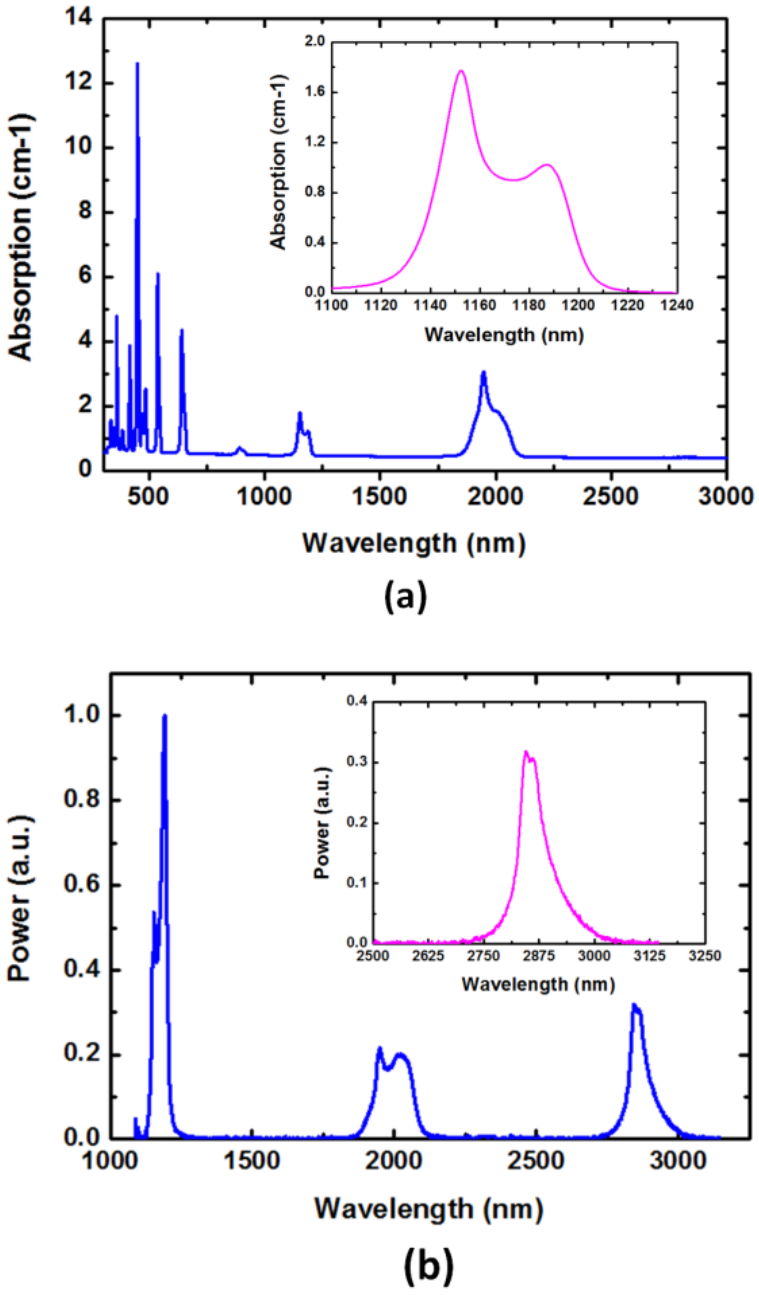

Fig. 2.2 (a) The absorption and (b) fluorescence of 3 mol% Ho^{3+}-doped ZBLAN. Inset of (a) shows the absorption of Ho^{3+}-doped ZBLAN in the 1.1-1.24 μm range; inset of (b) shows the fluorescence of Ho^{3+}-doped ZBLAN in the 3 μm region.

2.3 Fe^{2+}:ZnSe Q-switched Ho^{3+}-doped ZBLAN fiber laser

Fe^{2+}:ZnSe has been used for high power mid-IR laser pulse generation because of its large absorption cross-section and small saturation energy with the excellent opto-mechanical feature (damage threshold ~2 J/cm^2) [60,107]. The Fe^{2+}-doped ZnSe crystal (IPG Photonics) used in our experiment was fabricated by post-growth thermal diffusion of iron in polycrystalline ZnSe. The thickness of the Fe^{2+}: ZnSe crystal was 2 mm. The absorption of the Fe^{2+}:ZnSe crystal in the 2-8 μm range was measured with an FT-IR spectrometer (Spectrum One, Perkin Elmer) and is shown in Fig. 2.3. Clearly, the Fe^{2+}:ZnSe has absorption between 2.5-4.5 μm with a peak around 3 μm. Therefore, Fe^{2+}:ZnSe crystal is an excellent saturable absorber for mid-IR lasers at 3 μm. Because of the high damage threshold, Fe^{2+}:ZnSe crystal has been used in a passively Q-switched mid-IR Er:YAG laser to produce 6-mJ, 50-ns giant pulses at 2.936 μm [107]. Most recently, a Fe^{2+}:ZnSe passively Q-swithced Er^{3+}-doped ZBLAN fiber laser with more than 300 mW average output power only limited by the available pump power was demonstrated [60]. Here, I report the performance of a singly Ho^{3+}-doped ZBLAN fiber laser Q-switched by the Fe^{2+}:ZnSe crystal. Sub-microsecond pulses at 2.93 μm were obtained.

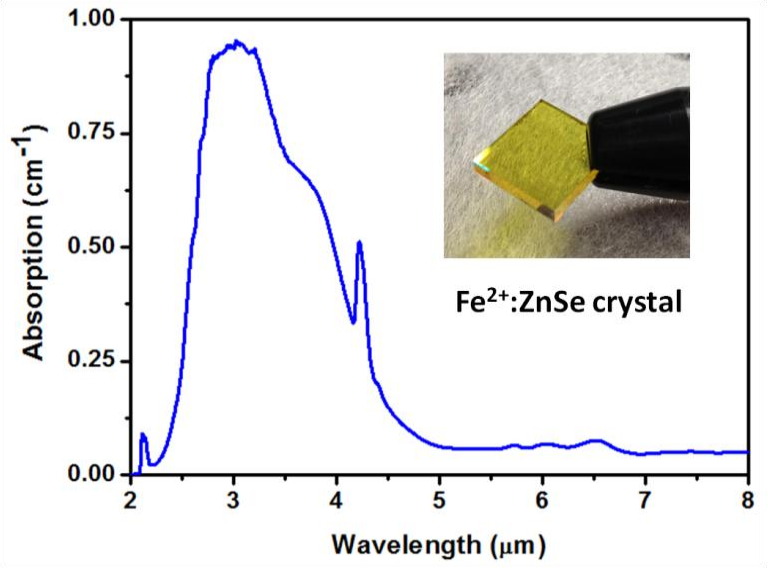

Fig. 2.3 Absorption of the Fe^{2+}:ZnSe crystal used in our experiment. Inset shows the Fe^{2+}-doped ZnSe crystal.

The schematic of the experiment setup is shown in Fig. 2.4. A 1150 nm Raman fiber laser pumped by a 1100 nm Yb^{3+}-doped silica fiber laser was used as the pump. Two sapphire lenses with focal length of 25.4 mm were used to collimate and focus the pump light to the flat cleaved end of the singly Ho^{3+}-doped ZBLAN fiber. A dichroic mirror with a transmission of 89% at 1150 nm and a reflectivity of > 99% at 2.9 μm was placed between the two lenses to couple the laser beam out. The Ho^{3+}-doped ZBLAN fiber has a length of about 2.5 m, a core dopant concentration of 20000 ppm, core NA of 0.16 and core diameter of 10 μm. The flat cleaved end of the Ho^{3+}-doped ZBLAN fiber works as the output coupler of the laser cavity to provide 4% feedback by Fresnel reflection. The other end of the Ho^{3+}-doped ZBLAN fiber was angle cleaved to eliminate the Fresnel reflection. The laser beam coming from the angle cleaved end was collimated and focused onto the Fe^{2+}:ZnSe saturable absorber by two CaF_2 lenses. The transmitted light was then collimated by another CaF_2 lens and reflected by a highly reflective mirror. A

Ge filter was used to block the pump and background noises below ~ 2 μm. An InSb detector with rise time of 7 ns was used to measure the time domain performance of the Q-switched fiber laser. The pulse trains were recorded by an oscilloscope with a bandwidth of 100 MHz (Tektronix TDS 1012). The average power was measured by a thermal power meter (Thorlabs, S310C).

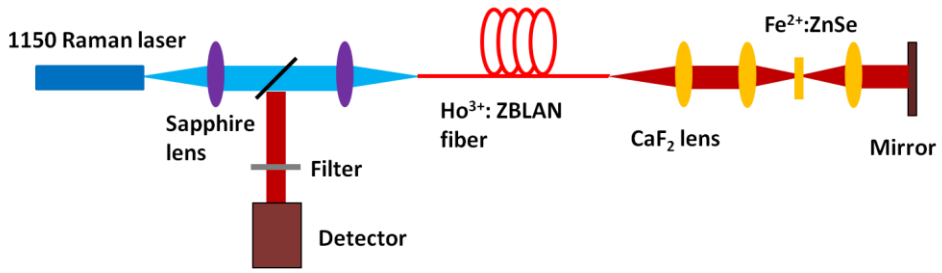

Fig. 2.4 Schematic of experiment setup for Fe^{2+}:ZnSe Q-switched Ho^{3+}-doped ZBLAN fiber laser.

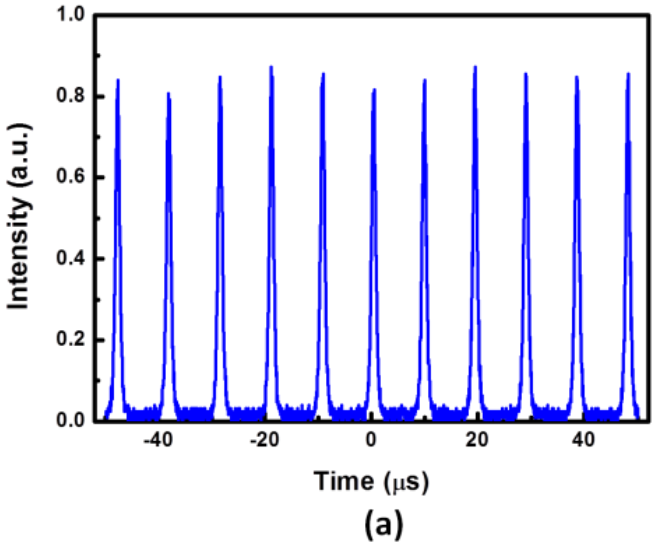

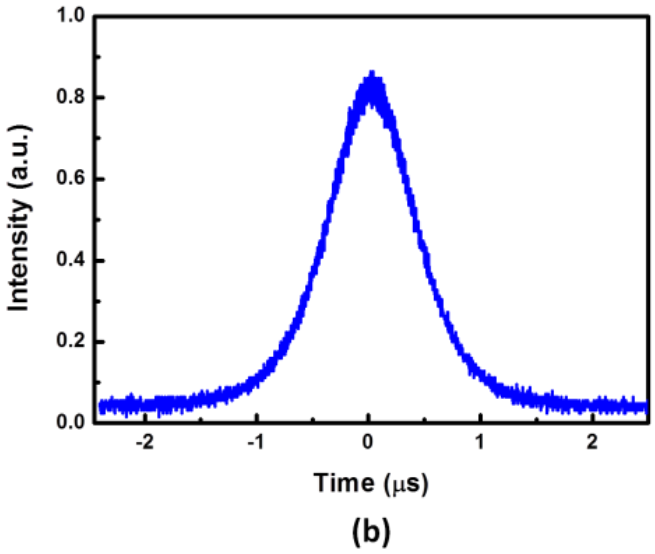

Fig. 2.5 (a) Pulse train and (b) pulse envelop of Fe^{2+}:ZnSe Q-switched Ho^{3+}-doped ZBLAN fiber laser at launched pump power of 1.8 W.

The threshold of this laser was about 0.6 W. But the pulsed operation was not stable. Stable Q-switched pulses were obtained when the launched pump power was 1 W. Fig. 2.5(a) shows a typical pulse train under the launched pump power of 1.8 W. The pulse envelop of the Q-switched pulses at the same launched pump power is shown in Fig. 2.5(b). Pulses with duration of 910 ns were obtained. The measured average output power, repetition rate, pulse duration and calculated pulse energy as a function of the launched pump power are shown in Fig. 2.6. The measured repetition rate increases and the pulse width decreases as the launched pump power increases. The repetition rate increases from 88 KHz to 105 KHz and the pulse duration decreases from 1.15 μs to 0.82 μs in the stable Q-switched regime. When the laser was pumped with the maximum available launched pump power of ~ 2.2 W, the average output power was 47.2 mW and the pulse energy was 450 nJ, corresponding to a peak power of 0.55 W. The slope

efficiency of this laser is 2.5%, which is lower than 12.3% of the tunable Q-switched Ho^{3+}-doped ZBLAN fiber laser [63] due to the large loss of the cavity caused by the Fresnel reflection of the un-anti-reflection coated optics (two sapphire lenses, three CaF_2 lenses, and the Fe^{2+}:ZnSe crystal) and the un-optimized free space optics. Much higher efficiency can be obtained if optics components are optimized for a maximum coupling and anti-reflection coated. The spectrum of the Q-switched Ho^{3+}-doped ZBLAN fiber laser was measured with a monochromator (SPEX 270). As shown in Fig. 2.7, the center wavelength is about 2935 nm, which is a typical wavelength of high concentration Ho^{3+}-doped ZBLAN fiber lasers. Clearly, the wavelength of this passively Q-switched single Ho^{3+}-doped ZBLAN fiber laser is longer than that of the Ho^{3+}/Pr^{3+}-codoped fiber laser.

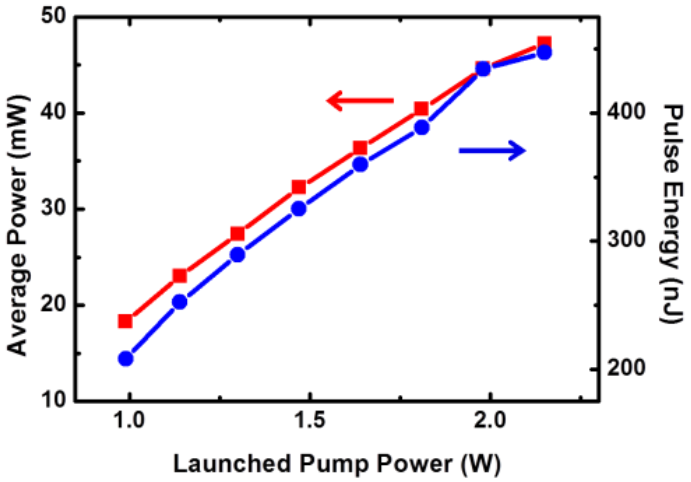

(a)

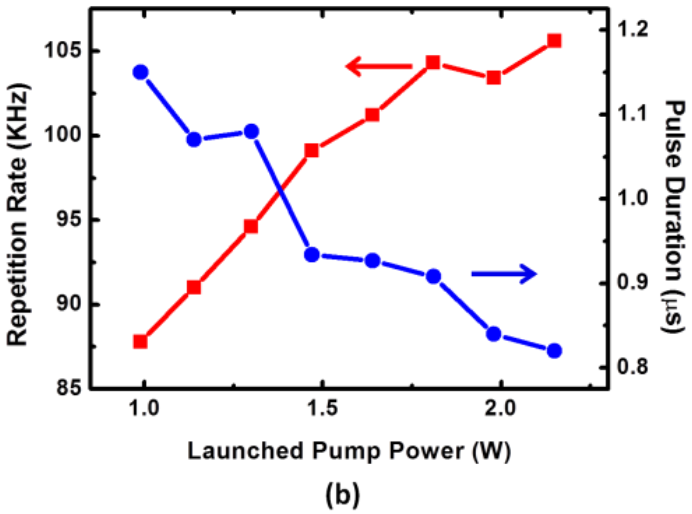

Fig. 2.6 (a) The average output power (red squares) and the pulse energy (blue dots), (b) the repetition rate (red squares) and the pulse duration (blue dots) of the Fe^{2+}:ZnSe Q-switched singly Ho^{3+}-doped ZBLAN fiber laser as a function of the launched pump power.

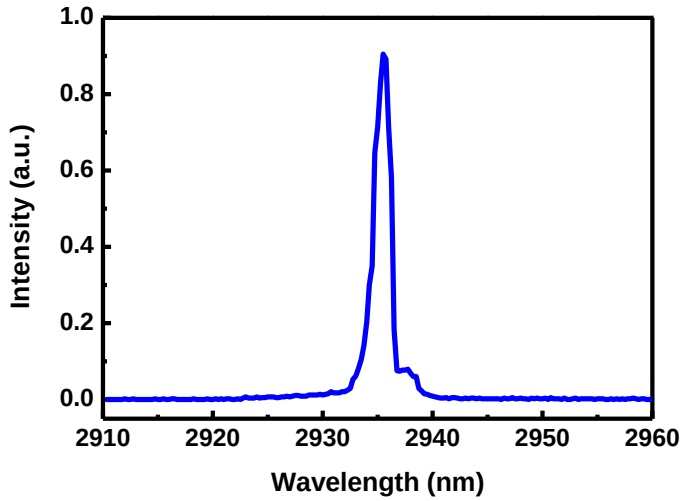

Fig. 2.7 Spectrum of the passively Q-switched singly Ho^{3+}-doped ZBLAN fiber laser at a launched pump power of 1 W.

2.4 Graphene Q-switched singly Ho^{3+}-doped ZBLAN fiber laser

To make a fiber-based saturable absorber for the Ho^{3+}-doped ZBLAN fiber laser, fiber mirror was first fabricated by ion-beam deposition of dichroic thin film (highly reflective @ 2.9 μm and highly transparent @ 1150 nm) onto the end facet of a striped and cleaved optical fiber (Thorlabs AFS105/125). Then the graphene deposited fiber mirror was prepared by the method of optically driven deposition [108]. A 975 nm laser diode was spliced to one end of the fiber mirror (the end without coating) and the other coated end was immersed in the graphene solution. After turning on the 975 nm laser diode for 25 minutes at 30 mW, graphene was deposited on the fiber end facet by optical and thermal gradient forces. The microscopic photographs of the fiber mirror before and after graphene deposition are shown in Fig. 2.8 (a) and (b), respectively. Obviously, a neat graphene thin film was deposited onto the fiber mirror. It is very surprised to us that the graphene thin film is very smooth and homogenous over the entire fiber end facet but not only over the core area. This may manifest that thermal gradient force contributes more significantly to the thin film deposition than optical gradient force. The dichroic thin film may also facilitate the homogeneous deposition. Further investigation on the mechanics of the thin film deposition and how to control the thin film thickness is currently under way. The absorption loss of deposited graphene thin film was measured to be ~33% (-1.74 dB). Considering that the absorption loss of each graphene layer is 2.3% (-0.10 dB) [109], we estimated that about 17 layers of graphene were deposited on the fiber mirror.

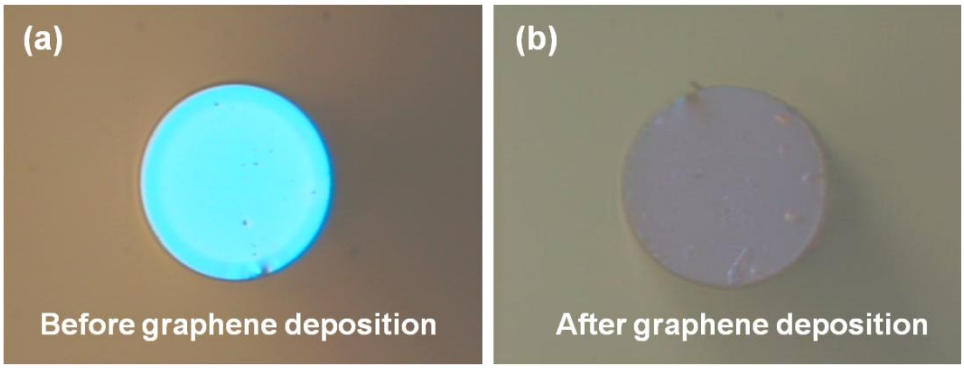

Fig. 2.8 The fiber mirror end before (a) and after (b) graphene was deposited.

The experiment setup of graphene Q-switched Ho^{3+}-doped ZBLAN fiber laser is schematically shown in Fig. 2.9. It is very similar to that of the Fe^{2+}:ZnSe Q-switched Ho^{3+}-doped ZBLAN fiber laser except that a graphene deposited fiber mirror was used to butt-couple to the back end of the Ho^{3+}-doped ZBLAN fiber. The fiber mirror itself is highly reflective at ~ 3 μm and highly transparent at the pump wavelength. The graphene deposited on the fiber mirror acts as a saturable absorber.

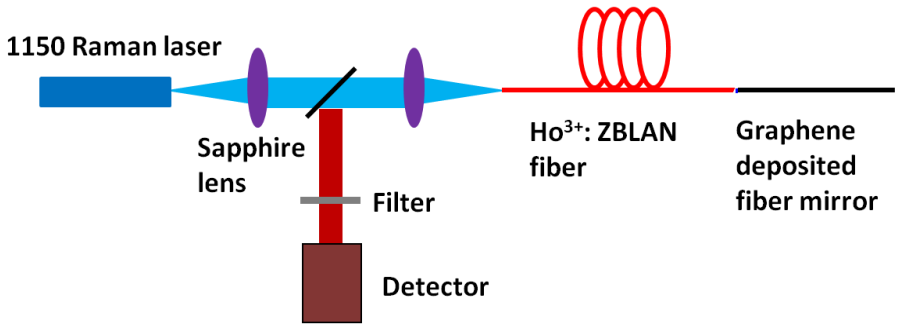

Fig. 2.9 Schematic of experiment setup for graphene Q-switched Ho^{3+}-doped ZBLAN fiber laser.

The threshold of this laser is about 0.4 W which is lower than Fe^{2+}:ZnSe Q-switched laser due to the significantly reduced cavity loss. The stable Q-switched pulses start at 0.6 W and maintain until the launched pump power reaches about 1.5 W. The Q-switched operation was not stable any more when the pump power was further increased. This is probably caused by the thermal effects of the graphene thin film. A typical Q-switched pulse train is shown in Fig. 2.10. As observed in a general Q-switched fiber laser, the repetition rate increases while the pulse width decreases with the increased pump power. The repetition rate increases from 64 KHz to 92 KHz and the pulse duration decreases from 1.40 μs to 1.18 μs in the stable Q-switched regime. The measured average output power, repetition rate, pulse duration and calculated pulse energy as a function of the launched pump power are shown in Fig. 2.11. When the laser was pumped at the pump power of 1.5 W, the average output power was measured to be 102 mW and the pulse duration was 1.18 μs. The pulse energy and the peak power were calculated to be 1.1 μJ and 0.95 W, respectively. The slope efficiency of this fiber laser is 8.9%, which is much higher than that of the Fe^{2+}:ZnSe Q-switched Ho^{3+}-doped ZBLAN fiber laser due to the reduced cavity loss. The efficiency is relatively lower than 12.3% of the tunable Q-switched Ho^{3+}-doped ZBLAN fiber laser [63]. However, by optimizing fiber length and dopant concentration of Ho^{3+}-doped ZBLAN fiber, higher efficiency is expected. The spectrum of this laser was similar to that of the Fe^{2+}:ZnSe Q-switched fiber laser. The peak wavelength, however, was found a little longer than that of the Fe^{2+}:ZnSe Q-switched fiber laser at the same pump power.

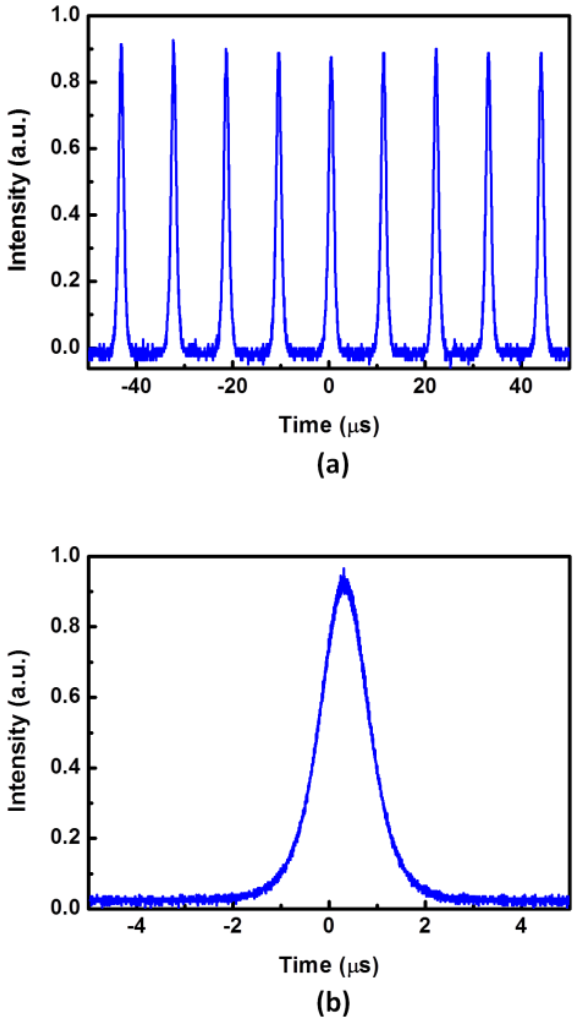

Fig. 2.10 (a) Pulse train and (b) pulse envelop of graphene Q-switched Ho^{3+}-doped ZBLAN fiber laser.

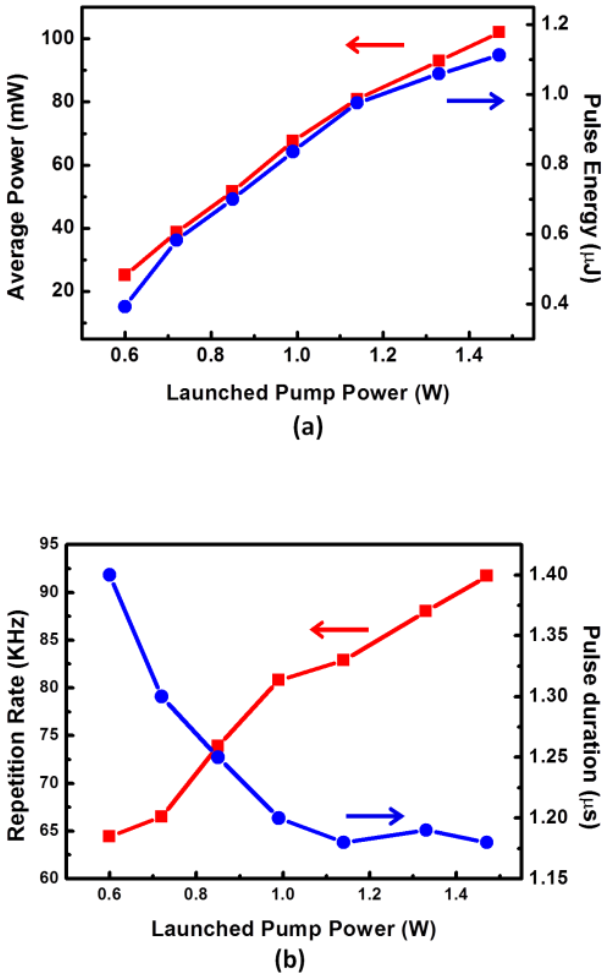

Fig. 2.11 (a) The average output power (red squares) and the pulse energy (blue dots), (b) the repetition rate (red squares) and the pulse duration (blue dots) of graphene Q-switched singly Ho^{3+}-doped ZBLAN fiber laser as a function of the launched pump power.

2.5 Discussions

Q-switched singly Ho^{3+}-doped ZBLAN fiber laser has been obtained by using Fe^{2+}:ZnSe crystal and graphene saturable absorbers, respectively. My experiments demonstrate that both Fe^{2+}:ZnSe crystal and graphene are promising saturable absorbers for mid-IR fiber

lasers at 3 μm. Because Fe^{2+}:ZnSe crystal is a bulk device, a collimating and focusing setup has to be employed and consequently the laser cavity becomes complicated and needs careful alignment. However, Fe^{2+}:ZnSe crystal can be used to generate very high energy mid-IR pulses because of its large damage threshold. Since several 10-watt-level Er^{3+}-doped ZBLAN fiber lasers and watt-level Ho^{3+}-doped ZBLAN fiber lasers have been demonstrated, watt-level or 10-watt-level Q-switched mid-IR fiber lasers can be realized by using Fe^{2+}:ZnSe crystal as the saturable absorber. Graphene is generally in form of nano-sized flake that can be deposited on optical fiber mirror or deformed optical fiber [110] and a fiber optic saturable absorber can be fabricated. Thus compact, rugged, and reliable pulsed mid-IR fiber lasers can be developed with graphene deposited fiber devices.

In the experiments, the Fe^{2+}:ZnSe Q-switched Ho^{3+}-doped ZBLAN fiber laser has lower efficiency than graphene Q-switched Ho^{3+}-doped ZBLAN fiber laser. This is caused by high cavity loss of the Fe^{2+}:ZnSe Q-switched laser due to the Fresnel reflection of uncoated lenses and the crystal and the aberration of un-optimized free space collimating and focusing setup. The performance of the Fe^{2+}:ZnSe Q-switched fiber laser can be improved significantly by using aspherical lenses and anti-reflection coated lenses and the Fe^{2+}:ZnSe crystal. On the other hand, the flat cleaved end of the Ho^{3+}-doped ZBLAN fiber acting as the output coupler has a reflectivity of only 4%, significant improvement in efficiency is expected if a dichroic mirror that has a proper reflectivity at laser wavelength and high transmission at pump wavelength is used as the output coupler. Because Fe^{2+}:ZnSe crystal has high damage threshold and 30 mJ pulses at 2.94 μm has been obtained in a Q-switched Er:YAG laser using Fe^{2+}:ZnSe saturable absorber [111],

Q-switched Ho^{3+}-doped ZBLAN fiber laser with 10-W-level average power is possible due to the advantages of fiber lasers such as outstanding heat-dissipating capability and high efficiency. Because the pulse energy increases and the pulse width decreases with the increased pump power, much higher energy and shorter pulses are expected in Fe^{2+}:ZnSe Q-switched Ho^{3+}-doped or other rare-earth doped ZBLAN fiber lasers.

Since no free space optics was used in the laser cavity, graphene Q-switched Ho^{3+}-doped ZBLAN fiber laser has a higher efficiency and a better stability than the Fe^{2+}:ZnSe Q-switched laser. Although this laser was found to be stable only at a range of pump powers, graphene Q-switched fiber laser can be used as a compact and stable pulsed seed laser for power amplification laser system. Most importantly, since graphene based mode-locked Yb^{3+}-, Er^{3+}-, and Tm^{3+}-doped fiber lasers have been demonstrated at ~ 1 μm, 1.5 μm, and 2 μm, respectively [93,95,97], it is expected graphene mode-locked fiber lasers at 3 μm can be achieved by using a few-layer graphene deposited fiber mirror and optimizing the fiber length and the output coupler.

2.6 Conclusion

In conclusion, I have demonstrated passively Q-switched singly Ho^{3+}-doped ZBLAN fiber laser using Fe^{2+}-doped ZnSe crystal and graphene deposited fiber mirror as the saturable absorber, respectively. For Fe^{2+}:ZnSe crystal Q-switched laser, 460 nJ pulses with repetition of 104 kHz were obtained at the maximum available launched pump power of 2.2 W. Since the damage threshold of Fe^{2+}:ZnSe is as large as 2 J/cm^2, much higher energy pulses 3 μm can be achieved by optimizing the laser cavity and using more

powerful pumps. For graphene Q-switched laser, stable pulses were obtained only at a launched pump power range of 0.6-1.5 W and noticeable time jitter was observed as the pump power was increased to the maximum available pump power of 2.2 W. Nevertheless, 1.1 μJ pulses with repetition rate of 92 kHz, corresponding to an average output power of 102 mW were obtained. Since graphene has been used to mode lock rare-earth doped silica fiber lasers in the near IR, it is expected that mode-locked RE-doped ZBLAN fiber laser at 3 μm can be developed in the near future by using optimizing the graphene deposited fiber mirror and the fiber laser cavity.

CHAPTER 3

Experimental and Numerical Investigations on Q-switched Laser Seeded Fiber MOPA at 2.8 μm

3.1 Introduction

In recent years, graphene, which exhibits saturable absorption over an ultrabroad spectral region has been widely used to develop a variety of compact and reliable Q-switched and mode-locked all-fiber lasers at various wavelengths. Most recently, using a graphene coated fiber mirror as the saturable absorber, Q-switched μJ-level pulses at 3μm in an Er^{3+}-doped and a Ho^{3+}-doped ZBLAN fiber laser were obtained respectively [112,113]. Compared to Fe:ZnSe Q-switched fiber lasers [112], fiber-optic graphene Q-switched fiber lasers have higher efficiency, better stability, and much simpler configuration. However, graphene Q-switched fiber lasers were found to be stable only over a specific range of pump powers. Stable pulses with much higher energy can be achieved with optical fiber amplifiers. In this chapter I report our investigations on an Er^{3+}-doped ZBLAN fiber amplifier for Q-switched pulses at 2.79 μm. Over 24 μJ pulses with an average output power of 1 W were achieved with currently available pump power. Because this single-mode fiber laser has an excellent beam quality ($M^2 = 1$), the laser beam can be focused into a small spot with radiant exposure at a level of 10 J/cm^2, which is high enough for general laser surgeries. Much higher energies are required for other applications such as remote sensing and nonlinear wavelength convertor. Simulation predicts that over 300 μJ of pulse energy can be achieved by using more powerful pumps and effective heat management.

3.2 Experimental setup and results for Q-switched laser seeded fiber amplifier

The schematic of the experiment setup for the pulsed Er^{3+}-doped ZBLAN fiber laser amplifier is shown in Fig. 3.1. A graphene Q-switched Er^{3+}-doped ZBLAN fiber laser at 2.79 μm [113] was used as the signal source. A sapphire lens (focal length 25.4 mm) was used to couple the signal into the core of the amplifier fiber. The amplifier fiber was a 4-m Er^{3+}-doped ZBLAN fiber with a core dopant concentration of 8 mol.%, core NA of 0.1 and core diameter of 15 μm. The inner circular cladding of the fiber had a diameter of 125 μm and an NA of 0.4. The cladding pump absorption was measured to be 6.5 dB/m at 975 nm. Both ends of the Er^{3+}-doped ZBLAN fiber were angle cleaved to prevent parasitic lasing. The amplifier fiber was backward pumped by a fiber-coupled laser diode at 975 nm. The pump laser was collimated and focused into the inner cladding of the Er^{3+}-doped ZBLAN fiber by two sapphire lenses (focal length 25.4 mm). A dichroic mirror which has a high transmission at 975 nm (T = 91%) and a high reflectivity at 2.79 μm (R = 98%) was place at 45° angle of incidence between two sapphire lenses to deliver the amplified signal out. The output power of the fiber amplifier was measured by a thermal detector (Thorlabs, S310C). An InSb detector (Kolmar KISDP-1-J1/DC) with rise time of 7 ns was used to measure the time domain performance of the seed and the amplified pulses. The pulse trains were recorded by an oscilloscope with a bandwidth of 100 MHz (Tektronix TDS 1012). The spectra of the signal before and after the fiber amplifier were measured with a monochromator (SPEX 270).

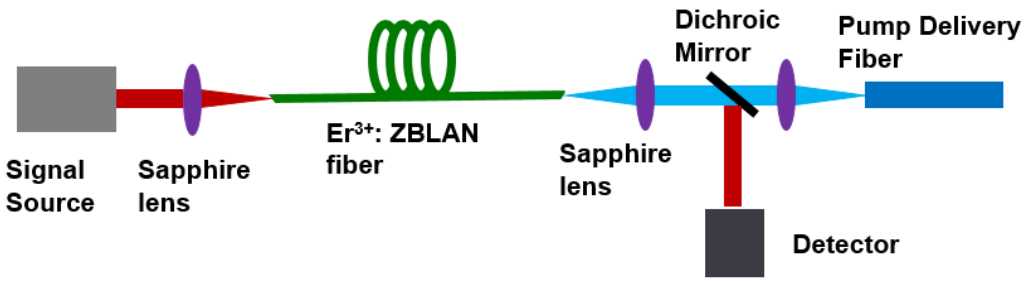

Fig. 3.1 Schematic of the experiment setup of an Er^{3+}-doped ZBLAN fiber amplifier for a pulsed laser at 2.79μm.

In the experiment, the output power of the fiber amplifier for launched signal powers of 1 mW, 5 mW, 10 mW and 20 mW were measured at different pump powers. The different signal powers were obtained by attenuating the output power of the signal source which operated at stable Q-switching with fixed repetition rate of 41.2 KHz and pulse width of 2.1 μs. The maximum available launched pump power is about 9.4 W. The pulse energy and output power as a function of the launched pump power for different signal powers are shown in Fig. 3.2. The efficiency of this fiber amplifier increases with the increased signal power. An efficiency of 10.6% was obtained with the input signal power of 20 mW, which corresponds to an input pulse energy of 0.49 μJ. Further increase of the input signal power didn't result in significant increase of the efficiency. Gain saturation was not observed in our experiment and an average output power of 1.0 W was achieved at the maximum available pump power. The pulse energy of the amplified pulses is estimated to be about 24 μJ. The spectra of the seed laser and the amplified laser were measured and normalized as shown in Fig. 3.3. There is only a slight difference between the seed signal and the amplified signal, which may due to some minor hysteresis in the monochromator. Fig. 3.4 shows the pulse shapes of the seed

laser and the amplified laser at pump power of 2.3 W, 4.7 W, 7.1 W, and 9.4 W respectively. Clearly, the front portion of the pulse is amplified more than the rear portion. However, noticeable distortion of the pulse shape was not measured in our experiment. The inset shows the pulse train of the amplified laser, which is identical to the seed laser. For the four pump powers, the average output powers are 180 mW, 500 mW, 760 mW, and 1.0 W, corresponding to pulse energies of 4.4 μJ, 12.1 μJ, 18.4 μJ, and 24.3 μJ, respectively. Since an Er^{3+}-doped ZBLAN fiber laser has been demonstrated with > 24 W output at a pump power of > 160 W [70], it is very possible to scale up the pulse energy by an order of magnitude by using more powerful pumps and employing active cooling techniques.

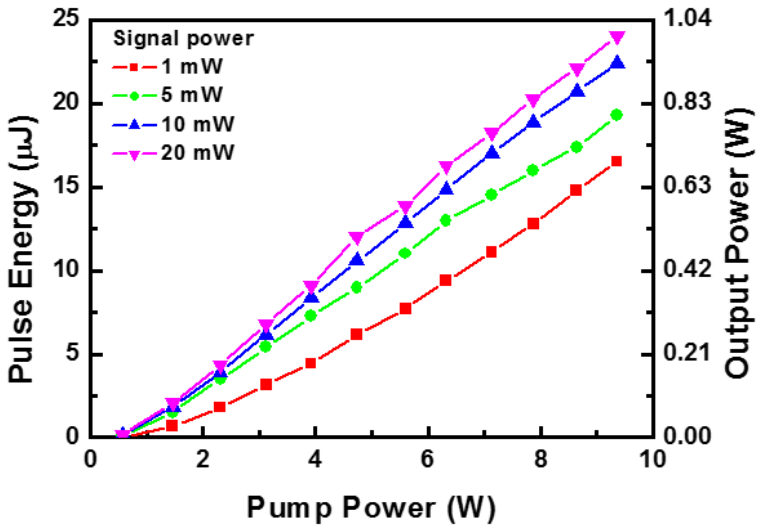

Fig. 3.2 Pulse energy and output power of the Er^{3+}-doped ZBLAN fiber amplifier as a function of the launched pump power for different signal powers (Squares: 1 mw, dots: 5 mW, upward triangles 10 mW, downward triangles 20 mW).

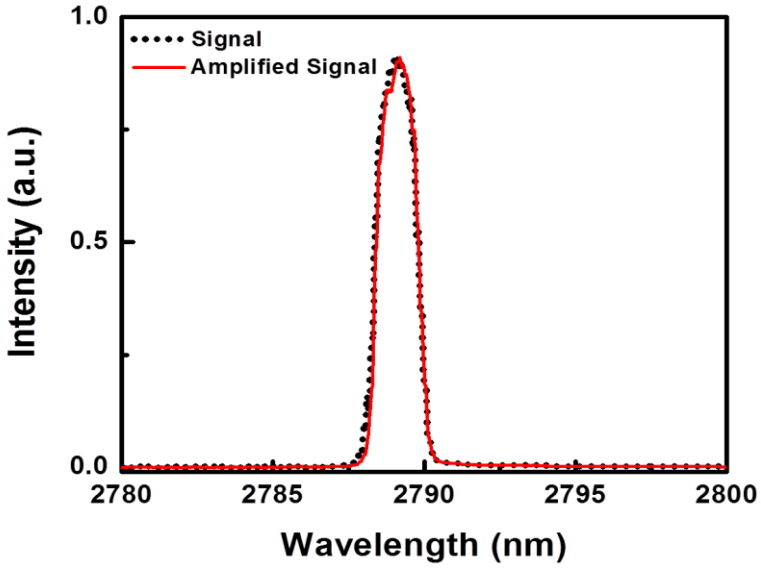

Fig. 3.3 The normalized spectra of the input laser (black dotted curve) and the amplified laser (red solid curve) at a pump power of 9.4 W.

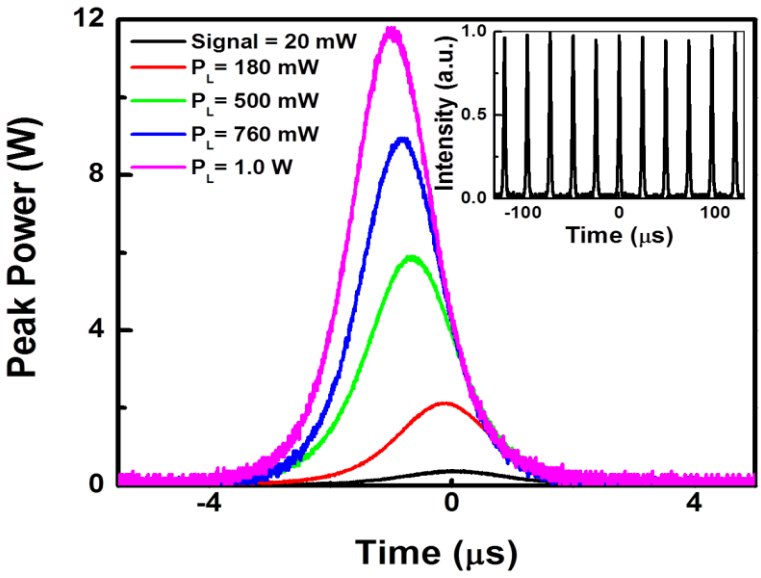

Fig. 3.4 The pulse shapes of the seed pulse and the amplified pulses at different pump powers at a repetition rate of 41.2 KHz. Inset shows the pulse train of the amplified laser at a pump power of 9.4 W.

3.3 Numerical simulation model and results

In order to evaluate the performance of this fiber amplifier and predict its further power scaling, we have conducted a series of simulations based on the laser mechanism shown in Fig. 3.5. The ground state absorption (GSA) at 975 nm corresponds to a transition from the lowest level $^4I_{15/2}$ to the upper level $^4I_{11/2}$. The laser emission at 2.8 μm corresponds to the transition from the upper laser level $^4I_{11/2}$ to the lower laser level $^4I_{13/2}$. Although the lower level $^4I_{13/2}$ has a longer natural lifetime (τ_2 = 9.0 ms) than the upper level $^4I_{11/2}$ (τ_1 = 6.9 ms), population inversion can be established in heavily Er^{3+}-doped ZBLAN by the energy transfer upconversion (ETU) process from the lower laser level ($^4I_{13/2}$, $^4I_{13/2}$) → ($^4I_{15/2}$, $^4F_{7/2}$), which is faster than that from the upper laser level ($^4I_{11/2}$, $^4I_{11/2}$) → ($^4I_{15/2}$, $^4F_{7/2}$) [52,114,115]. Moreover, in the ETU1 process, one pump photon is turned into two laser photons and thus the efficiency of a heavily Er^{3+}-doped ZBLAN fiber laser is improved [69].

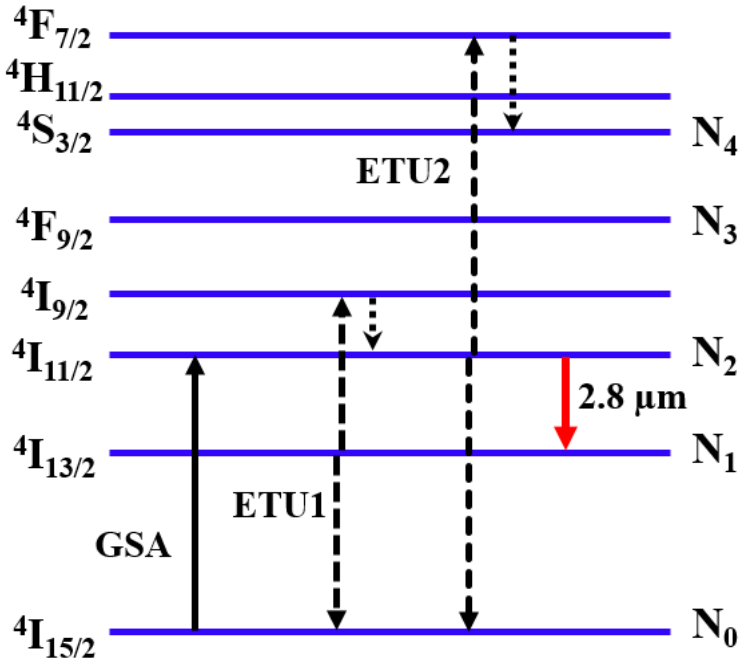

Fig. 3.5 Partial energy-level diagram of Er^{3+}-doped ZBLAN and transitions related to the laser emission at 2.8 μm. GSA represents ground state absorption and ETU represents energy transfer upconversion.

The Er^{3+}-doped ZBLAN fiber amplifier for the Q-switched laser was simulated by solving the dynamic rate equations and calculating the pulse amplification in both temporal and spatial domain using the Runge-Kutta method. The rate equations are

$$\frac{\partial N_4}{\partial t} = k_{2240} N_2^2 - N_4 / \tau_4 \tag{3.1}$$

$$\frac{\partial N_3}{\partial t} = p_{43} N_4 / \tau_4 - N_3 / \tau_3 \tag{3.2}$$

$$\frac{\partial N_2}{\partial t} = R_{02} N_2 - W_{21} N_2 + W_{12} N_1 + k_{1120} N_1^2 - 2k_{2240} N_2^2 - N_2 / \tau_2 + p_{42} N_4 / \tau_4 + p_{32} N_3 / \tau_3 \tag{3.3}$$

$$\frac{\partial N_1}{\partial t} = W_{21}N_2 - W_{12}N_1 - 2k_{1120}N_1^2 + p_{21}N_2/\tau_2 - N_1/\tau_1 + p_{31}N_3/_3 + p_{41}N_4/\tau_4 \quad (3.4)$$

$$\frac{\partial N_0}{\partial t} = -R_{02}N_2 + k_{1120}N_1^2 + k_{2240}N_2^2 + p_{40}N_4/\tau_4 + p_{30}N_3/\tau_3 + p_{20}N_2/\tau_2 + N_1/\tau_1 \quad (3.5)$$

$$N_{Er} = N_4 + N_3 + N_2 + N_1 + N_0 \quad (3.6)$$

where N_4, N_3, N_2, N_1, N_0 are the populations in $^4F_{7/2}/^4S_{3/2}$, $^4F_{9/2}$, $^4I_{9/2}/^4I_{11/2}$, $^4I_{13/2}$, $^4I_{15/2}$ levels respectively and N_{Er} is the concentration of Er^{3+} ions. k_{2240} is the ETU rate of the transition ($^4I_{11/2}$, $^4I_{11/2}$) → ($^4I_{15/2}$, $^4F_{7/2}$) and k_{1120} is the ETU rate of the transition ($^4I_{13/2}$, $^4I_{13/2}$) → ($^4I_{15/2}$, $^4I_{9/2}$). τ_4, τ_3, τ_2, τ_1 are the fluorescence lifetimes of the 4 levels respectively and p_{ij} represents the branching ratio of the decay from level i to lower level j. The values of lifetime τ_i, and branching ratio p_{ij} can be found in Ref. [115] and the ETU rate k_{ijk} can be found in Ref. [116,117]. $R_{02} = \sigma_{a,\lambda_p}P_p/(h\nu_p A_{eff})$ is the absorption rate of the pump laser. $W_{21} = \sigma_{e,\lambda_s}P_s/(h\nu_s A_{eff})$ is the emission rate of the laser from $^4I_{11/2}$ level to $^4I_{13/2}$ level and $W_{12} = \sigma_{a,\lambda_s}P_s/(h\nu_s A_{eff})$is the absorption rate of the signal from $^4I_{13/2}$ level to $^4I_{11/2}$ level. In the above equations, h is the Plank constant, σ_{a,λ_p} is the absorption cross section at the pump wavelength, σ_{e,λ_s} and σ_{a,λ_s} are the emission and absorption cross sections at the signal wavelength, respectively. P_p and P_s are the pump power and laser power respectively, ν_p and ν_s are the frequencies of the pump and the laser respectively, and A_{eff} is the effective mode area. The governing equation for P_p (t) and P_s (t) can be expressed as

$$\left(\frac{\partial}{\partial z}+\frac{1}{V_p}\frac{\partial}{\partial t}\right)P_p(t,z)=-F_p(\sigma_{a,\lambda_p}N_0(t,z)+\alpha_p)P_p(t,z) \quad (3.7)$$

$$\left(\frac{\partial}{\partial z}+\frac{1}{V_s}\frac{\partial}{\partial t}\right)P_s(t,z)=F_s(\sigma_{e,\lambda_s}N_2(t,z)-\sigma_{a,\lambda_s}N_1(t,z)-\alpha_s)P_s(t,z) \quad (3.8)$$

where V_p and V_s are the group velocity of the pump and the signal, α_p and α_s are the loss of the pump and signal and F_p and F_s are the spatial overlaps of the pump and signal modes with the fiber core, respectively.

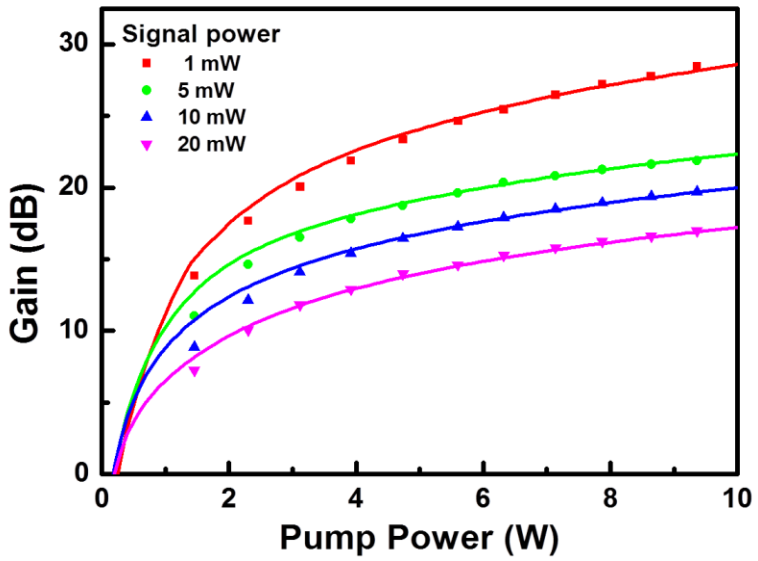

Fig. 3.6 Measured and calculated net gain of the Er^{3+}-doped ZBLAN fiber amplifier as a function of the pump power for different signal powers. The dots represent the experiment results and the curves represent the simulation results.

In order to validate the modeling of the Er^{3+}-doped ZBLAN fiber amplifier for Q-switched pulses, the gain as a function of the pump power for different signal powers was calculated and compared with the experimental data as shown in Fig. 3.6. The simulation

results agree well with the experimental data. The gain as a function of the signal power for different pump powers was calculated and is shown in Fig. 3.7. Both experimental data and simulation results show that the gain increases with the pump power but decreases with the signal power. Since no saturation was observed in our experiment, it is possible to achieve much higher pulse energy by launching more pump power into the gain fiber. Fig. 3.8 shows the calculated pulse energy and output power of the 15-μm-core Er^{3+}-doped ZBLAN fiber amplifier as a function of the pump power for different signal powers. The slope efficiency of the fiber amplifier increases with the increased signal power. But the increase is not significant when the signal power is larger than 20 mW. When the pump power is 120 W and the seed signal power is 20 mW, a pulse energy of over 300 μJ can be obtained. The inset shows the pulse shape of the amplified pulses at pump powers of 20 W and 120 W and that of the input seed pulse. The saturation energy of the 15-μm-core fiber is 60 μJ. Therefore, due to the gain saturation, the pulse shape is distorted at high pump power. Since over 20 W continuous-wave laser and over 10 W actively Q-switched laser have been demonstrated with heavily Er^{3+}-doped ZBLAN fibers [57,70-72], 3 μm pulses with energy of 300 μJ can be achieved by currently available ZBLAN fiber laser technology.

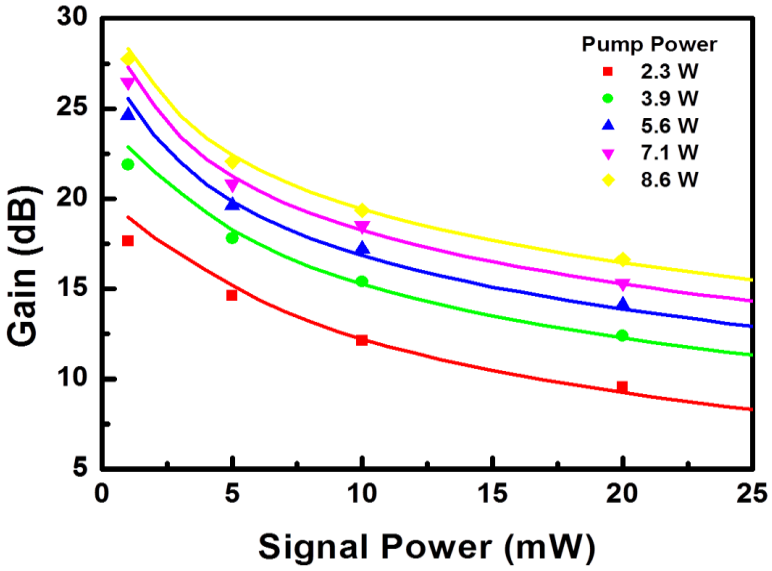

Fig. 3.7 Measured and calculated net gain of the Er^{3+}-doped ZBLAN fiber laser amplifier as a function of the signal power for different pump powers. The dots represent the experiment results and the curves represent the simulation results.

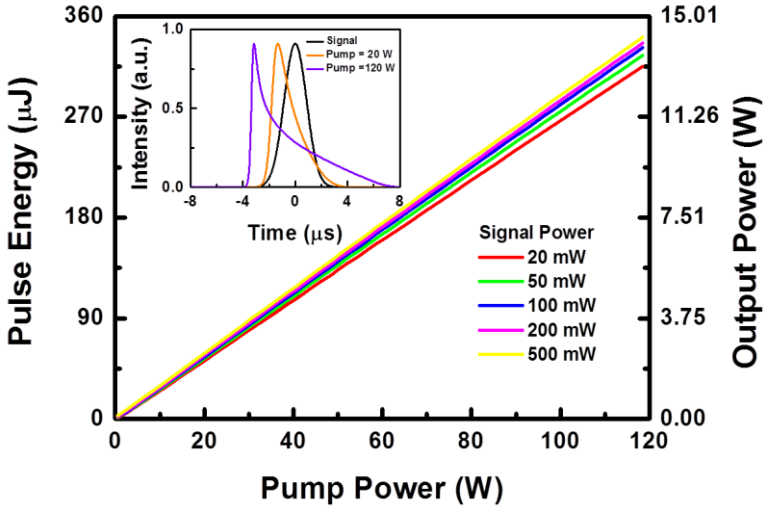

Fig. 3.8 Calculated average output power of the 15-μm-core Er^{3+}-doped ZBLAN fiber amplifier as a function of the pump power for different signal powers. Inset shows the 20 mW seed pulse shape (black) and the amplified pulse shape at a pump power of 20 W (orange) and 120 W (violet).

3.4 Conclusion

In conclusion, an Er^{3+}-doped ZBLAN fiber amplifier for pulsed lasers at 2.8 μm was investigated experimentally and numerically. Amplified pulses with energy over 24 μJ and an average output power of 1 W were achieved. More powerful pulses are expected when higher pump power is used and active cooling is employed. The simulations predict that the pulse energy can be scaled up to over 300 μJ at an average power of 10-W when a pump power of 120 W is launched in the Er^{3+}-doped ZBLAN fiber amplifier. Further scaling of the pulse energy can be accomplished by using a large-core active fiber and reducing the repetition rate of the pulses as well. Multi-mJ mid-IR pulses at 2.8 μm will be achievable by employing current ZBLAN fiber laser technology and active cooling techniques.

CHAPTER 4

Graphene Mode-locked Fiber Laser at 2.8 μm

4.1 Introduction

Mode-locked operation of an Er^{3+}-doped ZBLAN fiber laser in the 3 μm wavelength region was first demonstrated by Frerichs and Unrau using the flying mirror technique and an InAs saturable absorber [59]. However, the mode-locked operation was Q-switched and non-continuous. A continuous-wave mode-locked Er^{3+}-ZBLAN fiber laser was recently demonstrated by C. Wei et al using a Fe^{2+}:ZnSe saturable absorber [118]. Stable and continuous mode-locked pulses at 2.78 μm with a pulse duration of 19 ps and an average power of 51 mW were obtained [118]. Meanwhile, J. Li et al reported a partially mode-locked Ho^{3+}-Po^{3+}-codoped ZBLAN fiber laser at 2.87 μm by using a GaAs-based semiconductor saturable absorber mirror (SESAM) [89]. Most recently, they demonstrated a mode-locked Ho^{3+}-Po^{3+}-codoped ZBLAN fiber laser with improved stability by employing a ring cavity fiber laser configuration with a transmissive semiconductor saturable absorber [119]. A SESAM-mode-locked Er^{3+}-doped ZBLAN fiber laser at 2.8 μm was also recently demonstrated by A. Haboucha et al [88]. Though SESAMs are currently the most prevalent saturable absorbers and have shown their capability for mode-locking mid-IR fiber lasers in the 3 μm region, they usually have a narrow operating wavelength range and require complex fabrication and packaging. In recent years, graphene-based devices have emerged as innovative and remarkable saturable absorbers for mode-locking lasers because of their ultra-broad absorption band, low saturation intensity, and ultrafast recovery time [90, 120]. A graphene mode-locked

laser was first demonstrated in 2009 in the 1.5 μm wavelength region due to the readily available fiber components in this telecommunication window [91,121]. The ultra-broad operating wavelength range of graphene-based saturable absorbers has been validated by their use in mode-locked solid-state lasers and fiber lasers in the 1 μm, 2 μm and even 2.5 μm wavelength region [97,122,123]. Most recently a Q-switched Er^{3+}-doped ZBLAN fiber laser at 2.8 μm and Ho^{3+}-doped ZBLAN fiber laser at 2.93 μm using graphene deposited fiber mirrors as the saturable absorbers were demonstrated [101,124]. These developments suggested the pursuit of mode-locked fiber lasers in the 3 μm region by using a graphene device with proper absorption and modulation depth as the mode locker. In this chapter I report the mode-locked operation of an Er^{3+}-doped ZBLAN fiber laser at 2.78 μm induced by a multiple layer graphene coated gold mirror as the saturable absorber.

4.2 Experiment setup for the graphene mode-locked fiber laser

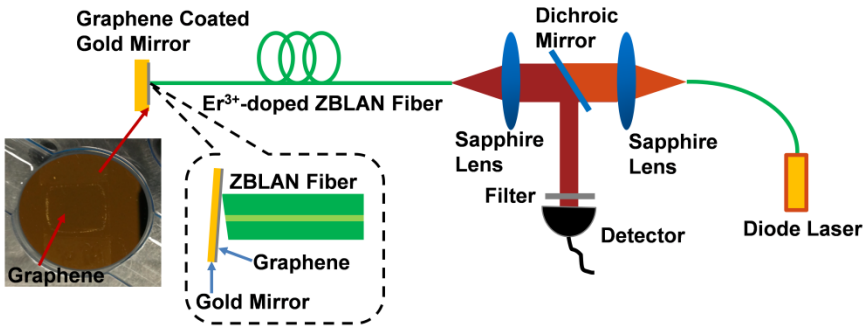

Fig. 4.1 Schematic of the experimental setup of a multi-layer graphene mode-locked Er^{3+}-doped ZBLAN fiber laser at 2.78 μm

The schematic of the experimental setup is shown in Fig. 4.1. A fiber-coupled diode laser at 975 nm was used as the pump source. Two identical plano-convex

sapphire lenses (focal length 25.4 mm) were used to collimate and focus the pump laser to the inner cladding of the 4-m Er^{3+}-doped double-clad ZBLAN fiber (FiberLabs Inc.). The Er^{3+}-doped ZBLAN fiber has a core with dopant concentration of 8 mol.%, NA of 0.1 and diameter of 15 μm, an inner cladding with a diameter of 125 μm, and NA of 0.4. The front end of the Er^{3+}-doped ZBLAN fiber was flat cleaved to work as the output coupler of the laser cavity and provide ~ 4% feedback, while the rear end is angle cleaved (~8^o) to eliminate the influence of Fresnel reflection. A multilayer graphene coated gold mirror was placed close to the angle-cleaved Er^{3+}-doped ZBLAN fiber end as shown in the inset of Fig. 4.1 and used to serve as the saturable absorber and cavity mirror. It is noted that the graphene coated gold mirror was adjusted at an angle (~ 4^o) to the vertical direction and thus the laser beam can be coupled back into the gain fiber core with a very low loss (< 0.1 dB) because the air gap between the gold mirror and the fiber core (~ 15 μm) is much smaller than the Rayleigh range (~ 144 μm). Between the two collimating and focusing sapphire lenses a dichroic mirror with high transmissivity at 975 nm (T = 91%) and high reflectivity at 2.78 μm (R = 98%) was placed at a 45^o angle of incidence to outcouple the signal laser. A long-pass filter was used to block the light below 1.7 μm. An InSb detector with a rise time of 7 ns was used to measure the time domain performance of the mode-locked laser. The pulse train was recorded by an oscilloscope (Tektronix TDS 1012) and the average output power was measured by a thermal detector (Thorlabs, S310C).

4.3 Experimental results and discussions

The threshold of the Er^{3+}-doped ZBLAN fiber laser was measured to be 350 mW. However, the mode-locked operation was not stable until the pump power was increased to 420 mW. Stable mode-locked operation of the Er^{3+}-doped ZBLAN fiber laser was maintained at a pump power of 420-470 mW. Pulse trains of the graphene mode-locked fiber laser at a pump power of 470 mW over 500 ns and 5 μs durations were recorded with a digital oscilloscope and are shown in Figs. 4.2(a) and 4.2(b), respectively. The variation of the pulse peaks is about 6%, indicating the fairly stable operation of this mode-locked fiber laser, which is degraded mainly by the Fresnel reflection of the uncoated plano-convex sapphire lens and self-pulsing in the highly Er^{3+}-doped ZBLAN fiber [125,126]. The average output power of this mode-locked fiber laser at a pump power of 470 mW was measured to be about 18 mW. The repetition rate is about 25 MHz, which corresponds to a cavity length of 4 meters. As the pump power was further increased, the mode-locked operation of the Er^{3+}-doped ZBLAN fiber laser became very unstable but was maintained even at a pump power of 2 W with more than 100 mW average output power. The mode-locked operation at high pump power may be primarily attributed to self-pulsing in the Er^{3+}-doped ZBLAN fiber, which is usually caused by saturable absorption of the ion clusters in heavily ion doped fibers [125,126]. When the pump power was more than 2 W, the multilayer graphene was usually damaged and the output of the fiber laser decreased.

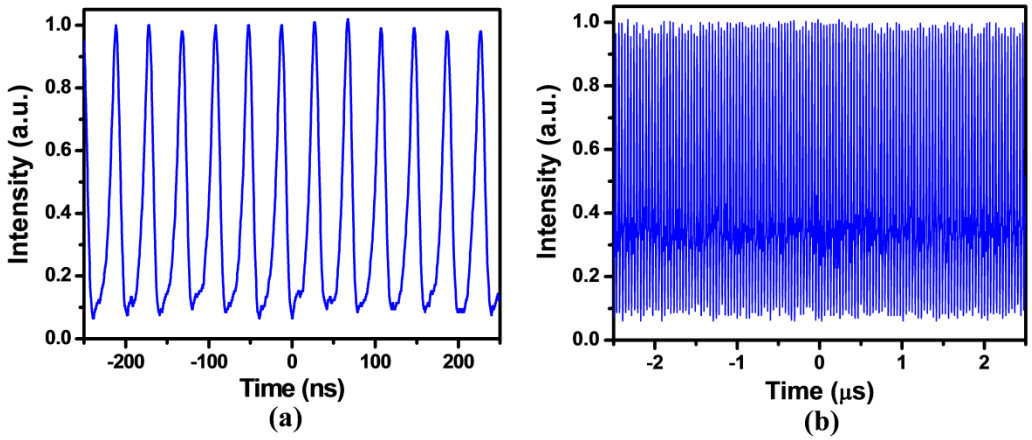

Fig. 4.2 The pulse train of the graphene mode-locked Er^{3+}-doped ZBLAN fiber laser over (a) a 500 ns and (b) a 5 μs duration at a pump power of 470 mW.

The spectrum of the multilayer graphene mode-locked Er^{3+}-doped ZBLAN fiber laser at a pump power of 470 mW was measured with a Yokogawa AQ6375 optical spectrum analyzer at a resolution of 0.05 nm and is shown in Fig. 4.3. The central wavelength is about 2784.5 nm with a full width at half-maximum (FWHM) of 0.21 nm, corresponding to a pulse width of 39 ps for $sech^2$-shaped and transform limited pulses. The radio frequency (RF) spectrum of the multilayer graphene mode-locked Er^{3+}-doped ZBLAN fiber laser at a pump power of 470 mW was measured with a spectrum analyzer (Advantest R3267) and is shown in Fig. 4.4. The signal-to-noise ratio (SNR) of the RF spectrum was measured to be about 43.5 dB at a resolution bandwidth of 1 kHz. The RF spectrum over 0-100 MHz was measured and is shown in the inset of Fig. 4.4.

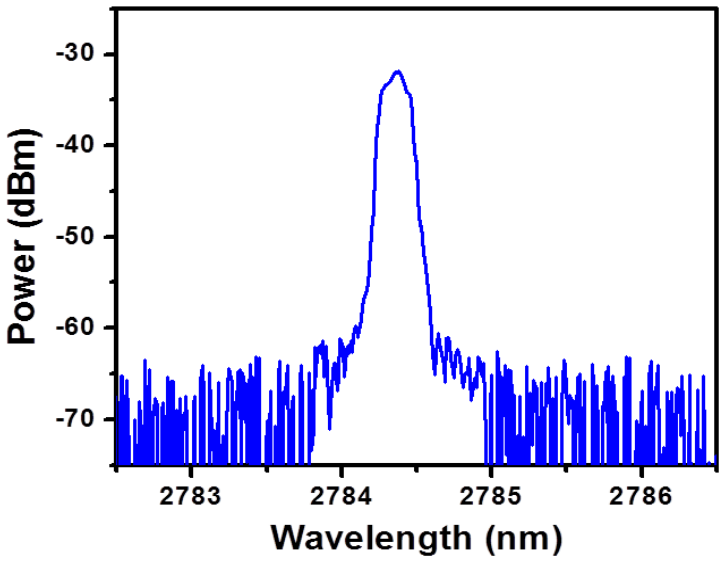

Fig. 4.3 The optical spectrum of the multilayer graphene mode-locked Er^{3+}-doped ZBLAN fiber laser at a pump power of 470 mW.

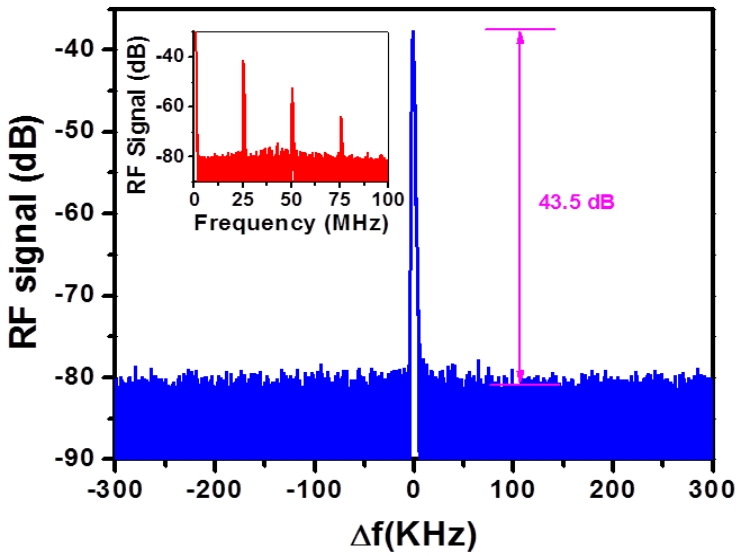

Fig. 4.4 The RF spectrum of the mode-locked pulses centered at 25.4 MHz with a SNR of 43.5 dB. The pump power is 470 mW. (Inset, the RF spectrum over a 100 MHz range).

The pulse duration of the multilayer graphene mode-locked Er^{3+}-doped ZBLAN fiber laser at 2.78 μm was measured with a home-made autocorrelator. The schematic of the autocorrelator is shown in Fig. 4.5(a). A 45:55 pellicle beam splitter is used to split the incident beam into two beams and direct them onto retroflectors 1 and 2, respectively. The two beams reflected from the two retroreflectors meet at the beam splitter and their transmitted and reflected beams are overlapped and combined into an interfered beam. The combined beam was focused by a CaF_2 lens onto an InGaAs detector, which can generate an electrical signal due to the two-photon absorption even though its linear absorption wavelength range is 700-1800 nm. Retroreflector 1 was fixed while Retroreflector 2 was mounted on a motorized translation stage to change the temporal overlap of the pulses reflected from the two retroreflectors. The incident beam was modulated by a chopper and a lock-in amplifier (SR830 DSP) was used to detect the two-photon absorption signal. A long-pass filter was placed in front of the InGaAs detector to eliminate background noise. Since the 18 mW average output power of the mode-locked fiber laser oscillator was too low to be detected with this home-made autocorrelator, we amplified the signal average power to about 300 mW using a 3-m Er^{3+}-doped ZBLAN fiber amplifier [127]. Since the pulse width of this mode-locked laser is estimated to be 39 ps and the peak power is about 17 W, the accumulated nonlinear phase shift (B-integral) of the 3-m Er^{3+}-doped ZBLAN fiber amplifier is less than 0.2 and we can assume that the pulse width changes very little after the amplification. The autocorrelation trace of the amplified pulses was recorded by an oscilloscope that was connected to the lock-in amplifier and is shown in Fig. 4.5(b). Since we used a lock-in amplifier to detect the two-photon absorption signal, the interferometric signal inside the

autocorrelation trace was averaged out. The full width at half maximum (FWHM) of the autocorrelation trace was calculated to be 65 ps by fitting the autocorrelation trace with a $sech^2$ function, yielding an FWHM pulse width of 42 ps. The time-bandwidth product of this mode-locked laser is 0.342. Therefore, the pulses of this multilayer graphene mode-locked Er^{3+}-doped ZBLAN fiber laser are nearly transform-limited.

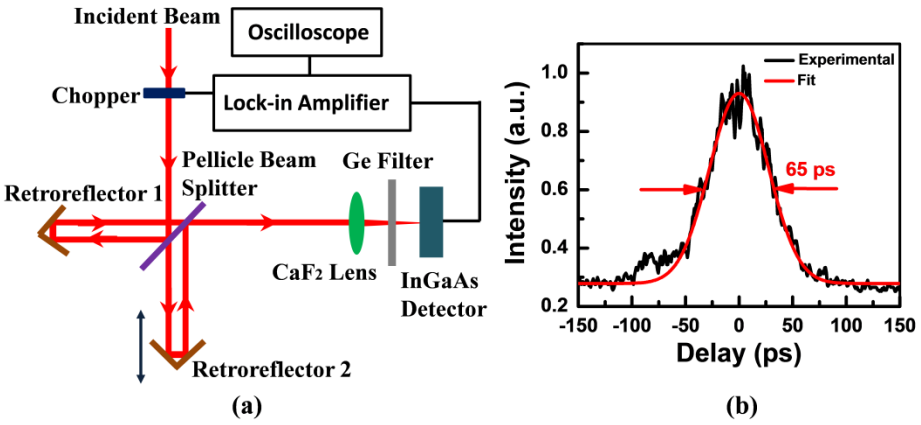

Fig. 4.5 (a) Schematic of the interferometric autocorrelator based on two-photon absorption in an InGaAs detector; (b) the autocorrelation trace recorded by the oscilloscope. The black line represents the experimental results and the red line represents the fitting results.

4.4 Conclusion

In conclusion, mode-locked operation of an Er^{3+}-doped ZBLAN fiber laser induced by multilayer graphene was demonstrated for the first time, to the best of our knowledge. Mode-locked pulses at 2.78 μm with an average output power of 18 mW and a pulse width of 42 ps at a repetition rate of 25.4 MHz were obtained. Our experiment has validated that graphene is a remarkable saturable absorber for mode-locking lasers in the

3 μm region. More stable and much shorter mode-locked pulses at 3 μm can be obtained by employing a ring cavity incorporating a transmissive graphene saturable absorber and carefully managing the dispersion of the ring cavity.

CHAPTER 5

Towards Ten-watt-level 3-5 μm Raman Lasers Using Tellurite Fiber

5.1 Introduction

Mid-IR lasers at 3-5 have attracted great attention because of the atmospheric transparency window [128] and numerous molecular absorption fingerprints [28] at this wavelength range. In the last decade, mid-IR fiber lasers have been extensively studied and much progress has been made with ZBLAN fiber laser technology. Watt-level and even 10-watt-level CW erbium (Er^{3+}), holmium (Ho^{3+}), and dysprosium (Dy^{3+}) ion-doped ZBLAN fiber lasers have been demonstrated around 2.8 μm -3 μm range and pulsed operation of these lasers has also been demonstrated with various active or passive Q-switching and mode-locking techniques recently. However, the emission wavelengths of these fiber lasers are not within the atmospheric transparency window. Some rare-earth (RE) doped ZBLAN fiber lasers in the 3-4 μm range have been demonstrated [75,80, NOTEREF _Ref425842680 \h 81]. However, the emission wavelengths of these RE-doped glass fiber lasers are limited to specific wavelengths by the allowable transitions between energy levels of the RE ions and their power scaling is usually restricted by the significant thermo-optic effects that occur due to the low quantum efficiency. Because non-radiative decay is predominant over direct radiative transitions when the laser wavelength is longer than 4 μm, it is extremely hard to obtain a > 4 μm laser output from a RE-doped ZBLAN fiber laser. Although RE-doped chalcogenide fiber lasers may be able to achieve laser emission beyond 4 μm [11], it is still very difficult to achieve watt-

level output due to the low achievable RE doping level (~ 0.1 mol%) and low damage threshold of chalcogenide. In recent years, fiber lasers based on stimulated Raman scattering have attracted much interest for their capability to generate coherent radiation at any wavelength within the transparency region of the fiber material. Since over 20-watt output at 3 μm has been obtained from RE-doped ZBLAN fiber lasers[70-72], it should be very promising to develop watt-level or even 10-watt-level laser sources at 3-5 μm using Raman laser technology based on mid-IR optical fibers.

Raman fiber lasers using optical fibers as the nonlinear medium can generate laser that cannot be obtained through direct transition between two energy levels of ions. The first Raman fiber laser was demonstrated by K. O. Hill et al. by employing single-mode glass fibers in a Fabry-Perot resonator configuration [129]. Later P. N. Kean et al. reported the first compact and stable all-fiber Raman laser based on fiber Bragg gratings in 1988 [130]. Most recently, V. R. Supradeepa et al. demonstrated a more than 300 W cw Raman fiber laser at 1.5 μm with an optical efficiency of 64% [131]. However, these Raman lasers mainly use silica fibers that are opaque in the mid-IR range. ZBLAN, tellurite, and chalcogenide fibers that are highly transparent in mid-IR range have been used in Raman fiber lasers. V. Fortin et al. demonstrated the first Raman laser based on ZBLAN fiber in 2011 [132] and later a watt-level cw Raman fiber laser operating beyond 2.2 μm was achieved by using a pump source at 1.98 μm [133]. However, ZBLAN glass fiber is not an ideal gain medium for Raman lasers due to its inherent low nonlinearity, fragility and hydroscopicity. Chalcogenide fiber having very large nonlinearity [134] and high transparency in the entire mid-IR wavelength range is a good alternative for Raman fiber lasers in the mid-IR region. M. Bernier et al. demonstrated the first Raman fiber

laser above 3 μm using a single-mode As_2S_3 chalcogenide glass fiber and a pulsed pump source at 3.005 μm [64]. Most recently, they developed a cascaded Raman chalcogenide glass fiber laser at 3.77 μm by using two pairs of FBGs directly inscribed in the chalcogenide fiber. A laser output peak power in excess of 100 mW is obtained with a conversion efficiency of about 8.3% with respect to the launched pump power [83]. Some simulation work on chalcogenide fiber Raman lasers has also been done by P. A. Thielen et al. and a 8 W mid-IR fiber Raman laser operating at 6.46 μm pumped by a 10 W 5.59 μm carbon monoxide laser was theoretically proposed [135]. However, chalcogenide fibers have very low damage threshold, which limits their output power and pulsed pumping schemes are often used to reduce thermal effects. Moreover, chalcogenide fibers have relatively narrow Raman gain bandwidth (~50 cm^{-1}) and small Raman shifts (~350 cm^{-1}) [136]. The operating wavelength of a chalcogenide fiber laser based on 2nd-order Raman scattering is still below 4 μm [**Error! Bookmark not defined.**]. In order to achieve a laser output at 5 μm, at least 4th order Raman scattering has to be employed. In this case, the construction of the Raman fiber laser will be complex and the efficiency will become very low. Compared to chalcogenide fibers, tellurite fibers have the advantages of better thermal stability [10], stronger corrosion resistance, broader Raman gain bandwidth (~300 cm^{-1}) and larger Raman shift (~750 cm^{-1}) [137]. By taking advantage of this broad gain bandwidth and large Raman shift, A. Mori et al. demonstrated a tellurite fiber Raman amplifier near 1.5 μm with a gain bandwidth of 160 nm [138] and G. Qin et al. reported a widely tunable (1495–1600 nm) ring-cavity tellurite fiber Raman laser with more than 100 nm tunable range [17]. However, all these demonstrations have been at near-infrared wavelengths, where silica

fiber lasers are predominant. We have previously developed a 10-watt cw laser and several pulsed lasers around 3 μm. Therefore, it is promising to develop high power fiber laser sources operating within the 3-5 μm atmospheric transparency window by using our fiber lasers as pump sources for tellurite Raman fiber lasers. In order to obtain insight into tellurite fiber Raman lasers pumped at 3 μm and provide valuable guidance for future 3-5 um Raman fiber laser development, it is essential to investigate the performance of the Raman fiber lasers with different designs. In this chapter, I present the numerical simulation studies on 1^{st}- and 2^{nd}-order Raman lasers based on tellurite fibers. The calculations show that watt-level or even 10-watt-level Raman fiber lasers can be achieved by pumping sub-meter tellurite fibers with 20 W Er^{3+}-doped ZBLAN fiber lasers at 2.8 μm.

5.2 Theoretical model for Raman tellurite fiber lasers

Tellurite glass, which has the lowest phonon energy among oxide glasses, has been extensively used in nonlinear photonics devices in the mid-IR due to its good optical transparency in the wavelength range of 0.5-5 μm and high nonlinear refractive index of 5.9×10^{-19} m^2/W [139]. Compared to other mid-IR transmitting glasses such as ZBLAN and chalcogenide glasses, tellurite glass not only exhibits better physical and chemical performance, but also has better Raman scattering properties including broad Raman gain bandwidth and large Raman shift [10]. All these advantages make tellurite glass fibers uniquely suitable for high power mid-IR Raman fiber lasers. Generally, the optical properties of a tellurite fiber depend on the glass compositions [137]. In the simulation, the Raman gain coefficient of TeO_2-Bi_2O_3-ZnO-Na_2O (TBZN) tellurite fiber that can be

fabricated in our lab is used. The Raman gain coefficient as a function of Raman shift is shown in Fig. 5.1 [137]. Due to the large Raman shift and high Raman gain of tellurite fibers, a Raman fiber laser operating in the 3-5 μm atmospheric transparency window can be achieved by using the 1st- and 2nd-order Raman scattering with a pump wavelength of 2.8 μm. The propagation loss of a tellurite fiber is shown in the inset of Fig. 5.1. The low propagation loss (< 0.5 dB/m) at 1-4.5 μm indicates that the tellurite fiber is a suitable platform for a mid-IR Raman laser. Although the propagation loss significantly increases as the wavelength approaches 5 μm due to the increased probability of multi-phonon decay, my calculations, as shown below, confirm that a 3-5 μm Raman laser can be achieved by using sub-meter length tellurite fibers.

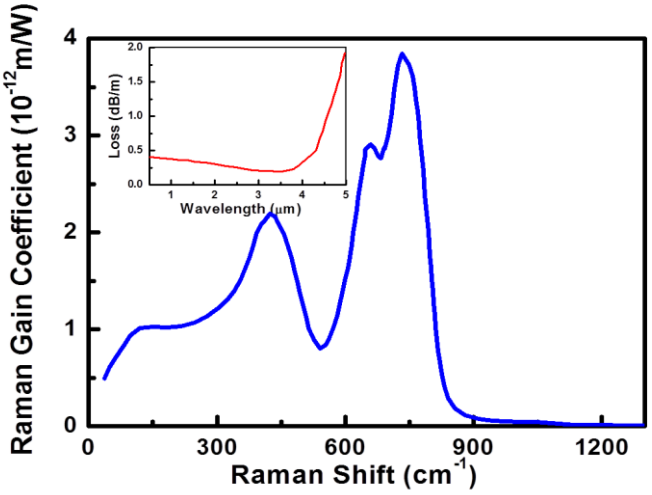

Fig. 5.1 Raman gain coefficient of a TBZN tellurite fiber as a function of the Raman shift. Inset shows the propagation loss of the tellurite fiber at 0.5-5 μm wavelength range.

The schematics of Raman fiber lasers based on the 1st- and 2nd-order Raman scattering are shown in Figs. 5.2(a) and 2(b), respectively. In all cases, a high reflectance (HR) fiber Bragg grating (FBG) works as the cavity mirror, while a

partially reflective (PR) FBG acts as the output coupler. In order to increase the efficiency of the Raman fiber laser, an HR FBG at the pump wavelength is employed to reflect the residual pump back into the gain fiber. In the 2nd-order Raman fiber laser, a pair of HR FBGs is utilized to convert the pump light to 1st-order Raman light most efficiently.

For the slowly varying optical fields of the pump and the 1st-order Raman scattered light, the governing equations for the forward and backward powers can be expressed via the following coupled equations [140,141]:

$$\frac{1}{P_p^f(z,t)}\left[\frac{\partial P_p^f(z,t)}{\partial z}+\frac{1}{v_p}\frac{\partial P_p^f(z,t)}{\partial t}\right]=\frac{1}{-P_p^b(z,t)}\left[\frac{\partial P_p^b(z,t)}{\partial z}+\frac{1}{v_p}\frac{\partial P_p^b(z,t)}{\partial t}\right] \tag{5.1}$$
$$=-\alpha_p-\frac{\omega_p}{\omega_1}\gamma_1\left[P_1^f(z,t)+P_1^b(z,t)\right],$$

$$\frac{1}{P_1^f(z,t)}\left[\frac{\partial P_1^f(z,t)}{\partial z}+\frac{1}{v_1}\frac{\partial P_1^f(z,t)}{\partial t}\right]=\frac{1}{-P_1^b(z,t)}\left[\frac{\partial P_1^b(z,t)}{\partial z}+\frac{1}{v_1}\frac{\partial P_1^b(z,t)}{\partial t}\right] \tag{5.2}$$
$$=-\alpha_1+\gamma_1\left[P_p^f(z,t)+P_p^b(z,t)\right].$$

For the 2nd-order Raman fiber laser, the time dependent partial differential equation for the pump power is the same as (5.1), while the power of the 1st-order Stokes wave is determined by

$$\frac{1}{P_1^f(z,t)}\left[\frac{\partial P_1^f(z,t)}{\partial z}+\frac{1}{v_1}\frac{\partial P_1^f(z,t)}{\partial t}\right]=\frac{1}{-P_1^b(z,t)}\left[\frac{\partial P_1^b(z,t)}{\partial z}+\frac{1}{v_1}\frac{\partial P_1^b(z,t)}{\partial t}\right]$$
$$=-\alpha_1+\gamma_1\left[P_p^f(z,t)+P_p^b(z,t)\right] \quad (5.3)$$
$$-\frac{\omega_1}{\omega_2}\gamma_2\left[P_2^f(z,t)+P_2^b(z,t)\right],$$

and that of the 2nd-order stokes wave is determined by

$$\frac{1}{P_2^f(z,t)}\left[\frac{\partial P_2^f(z,t)}{\partial z}+\frac{1}{v_2}\frac{\partial P_2^f(z,t)}{\partial t}\right]=\frac{1}{-P_2^b(z,t)}\left[\frac{\partial P_2^b(z,t)}{\partial z}+\frac{1}{v_2}\frac{\partial P_2^b(z,t)}{\partial t}\right] \quad (5.4)$$
$$=-\alpha_2+\gamma_2\left[P_1^f(z,t)+P_1^b(z,t)\right].$$

In the equations 1-4, P_p represents the pump power; P_1, P_2, represent the power of the 1st- and 2nd-order Stokes waves; the superscripts *f*, *b* represent the forward and backward propagation directions, respectively; ω_p, ω_1 and ω_2 are the frequencies of the pump, the 1st- and 2nd-order stokes waves, respectively; γ_1, γ_2 are the Raman gain coefficients of the 1st- and 2nd-order Stokes waves; and v_p, v_1 and v_2 are the group velocities of the pump, the 1st- and 2nd-order Stokes wave, respectively.

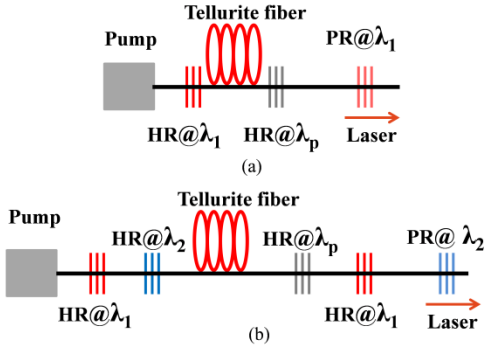

Fig. 5.2 Schematic of the 1st- (upper) and 2nd-order (lower) Raman tellurite fiber laser. HR FBG and PR FBG represent high reflectance fiber Bragg grating and partially reflective fiber Bragg grating, respectively. λ_p, λ_1 and λ_2 represent the wavelengths of the pump, the 1st- and 2nd-order Stokes waves, respectively.

The boundary conditions for the powers of the pump and the Stokes at the input and output ends of the Raman fiber laser are given by

$$P_p^f(0) = P_{in}, \quad P_p^b(L) = R_p P_p^f(L), \tag{5.5}$$

$$P_k^f(0) = R_k^b P_k^b(0), \quad P_k^b(L) = R_k^f P_k^f(L), \quad (k = 1,2). \tag{5.6}$$

Where R_p is the reflectance of the HR FBG for the pump, R_k^f and R_k^b represent the reflectances of the HR and PR FBGs at λ_k respectively. P_{in} is the launched pump power and L is the length of the tellurite Raman fiber. The output power of the Raman fiber laser can be obtained by

$$P_{out} = (1 - R_n^f) P_n^f(L), \quad (n = 1,2). \tag{5.7}$$

The simulations of the Raman fiber lasers are accomplished by using the Runge-Kutta method to numerically solve the coupled equations.

5.3 Results and discussion

5.3.1 Continuous-wave Raman fiber lasers

Both cw and Q-switched RE-doped ZBLAN fiber lasers at 3 μm can be used to pump a Raman tellurite fiber laser in the 3-5 μm wavelength range. In this subsection, the simulation results of cw Raman fiber lasers pumped at the typical wavelength of a free-running cw and a Q-switched Er^{3+}-doped ZBLAN fiber laser are presented. Tellurite fiber with a core diameter of 8 μm and a numerical aperture (NA) of 0.15 is used as the

Raman gain fiber. All the HR FBGs are assumed to have a reflectance of 99.5% at the desired wavelengths.

5.3.1.1 First-order Raman fiber lasers

1^{st}-order Raman fiber lasers pumped by a 20 W cw Er^{3+}-doped ZBLAN fiber laser at 2.8 μm were investigated first. Since the Raman gain peak of tellurite glass is at a frequency shift of 740 cm^{-1} as shown in Fig. 5.1, the output power of the 1^{st}-order Raman laser operating at 3.53 μm was calculated as a function of the fiber length and the reflectance of the output FBG coupler and is presented by a contour plot shown in Fig. 5.3. It is found that a maximum output power of 6.75 W can be obtained at 3.53 μm, when the Raman fiber length is 1 m and the output FBG coupler has a reflectance of 90%. The most attractive feature of a Raman fiber laser is that it can operate at any wavelength within the Raman gain band. Therefore, it is essential to investigate the operating wavelength range of the Raman fiber laser. When the Raman fiber length and the reflectance of the output FBG coupler are fixed at 1 m and 90%, respectively, the output power of the Raman fiber laser as a function of operating wavelength was calculated and is shown in Fig. 5.4. The maximum output power of 7.42 W can be obtained at 3.16 μm, which is larger than that of 3.53 μm at the Raman gain peak due to the larger quantum efficiency. Because the Raman gain coefficient around 3.3 μm is less than 1×10^{-12}m/W, the 20 W pump power is still below the laser threshold and lasing cannot be established at 3.26 μm – 3.36 μm when the fiber length is 1 m and the output coupler reflectance is 90%. The laser threshold of the Raman fiber laser at 3.3 μm can be reduced by increasing the reflectance of the output coupler and the fiber length as will be demonstrated below.

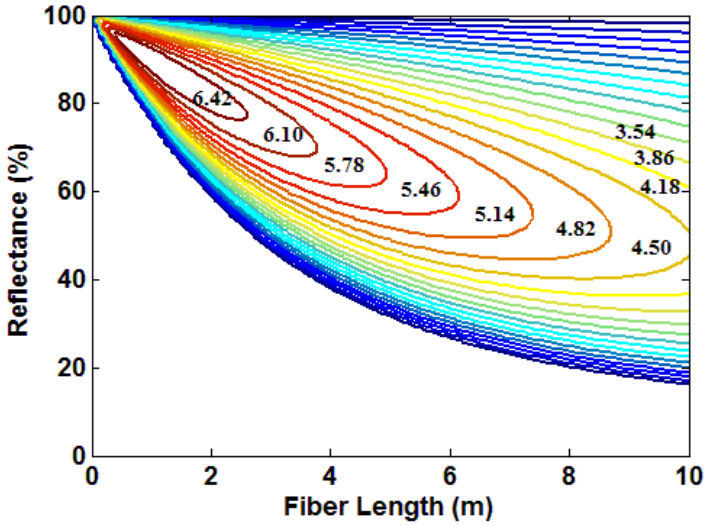

Fig. 5.3 Output power of a 3.53 μm 1st-order Raman fiber laser as a function of the Raman fiber length and the reflectance of the output FBG coupler at a pump power of 20 W. The numbers besides the contour curves are the output powers.

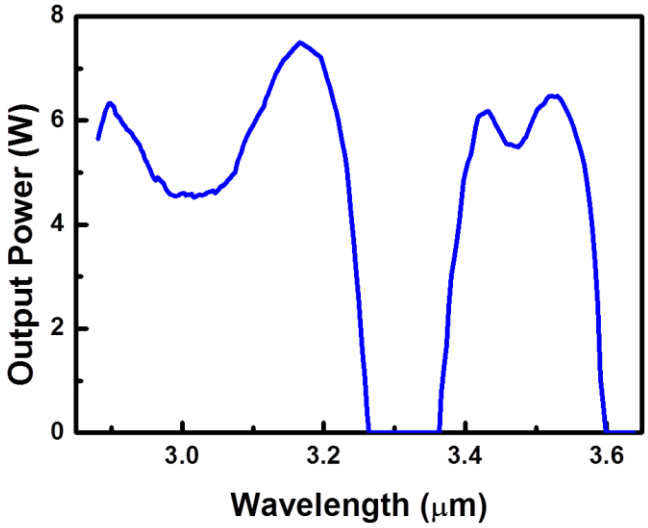

Fig. 5.4 Output power of the 1st-order Raman fiber laser as a function of wavelength at a pump power of 20 W when the Raman gain fiber length and the reflectance of the output FBG coupler are fixed at 1 m and 90%, respectively.

In order to achieve clear insight into the dependence of the output power of the 3.53 μm 1st-order Raman fiber laser on the length of the Raman gain fiber and the reflectance of the output FBG coupler, the output power as a function of the length of the Raman fiber for different reflectance of the output FBG coupler and as a function of the reflectance of the output FBG coupler for different lengths of the Raman fiber were calculated and are shown in Figs. 5.5(a) and 5(b), respectively. As seen in Fig. 5.5(a), the Raman fiber laser starts to lase with a shorter fiber length as the reflectance of the output FBG coupler becomes higher. Fig. 5.5(a) also indicates that the optimum fiber length giving the maximum output reduces with the increased reflectance of the output FBG coupler and the dependence of the output power on the Raman gain fiber length becomes critical as the reflectance of the output FBG coupler becomes large. Fig. 5.5(b) shows the optimum reflectance of the output FBG coupler increases with reduced Raman fiber length and the dependence of the output power on the reflectance of the output FBG coupler becomes critical as the Raman fiber becomes short. Both figures provide sufficient information and guidance for the design and development of the 1st-order Raman fiber laser.

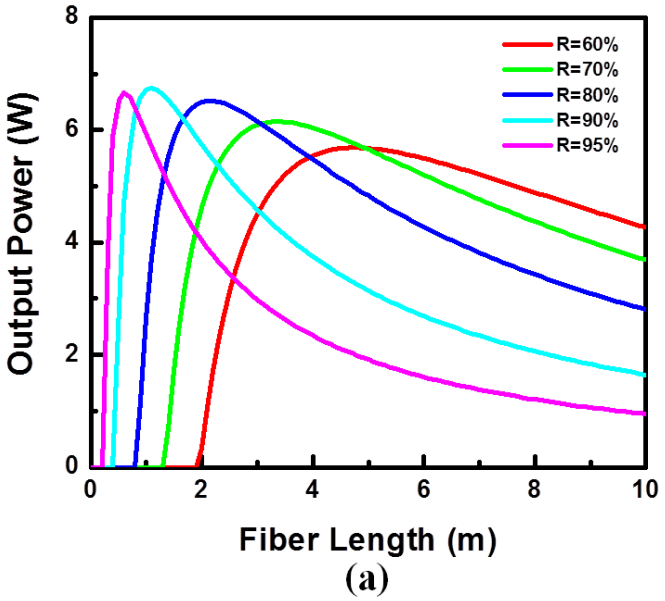

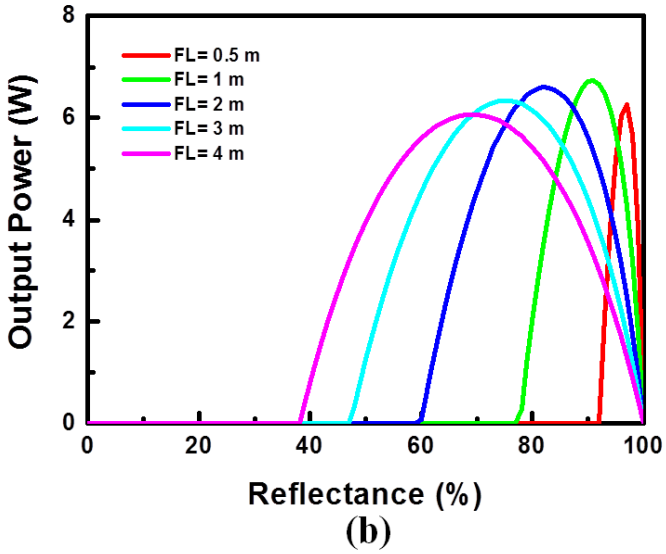

Fig. 5.5 Output power of the 3.53 μm 1st-order Raman fiber laser (a) as a function of the fiber length for different reflectance of the output FBG coupler and (b) as a function of the reflectance of the output FBG coupler for different fiber lengths when the pump power is 20 W.

The output power as a function of the pump power for different fiber lengths when the reflectance of the output FBG coupler is 90% and for different reflectances of the output FBG coupler when the Raman gain fiber length is 1m is shown in Figs. 5.6(a) and 6(b), respectively. Clearly, the pump threshold power of the 3.53 μm 1st-order Raman fiber laser increases with increased Raman fiber length, while it reduces with increased reflectance of the output FBG coupler. Its slope efficiency reduces with increased Raman fiber length, while it increases with increased reflectance of the output FBG coupler. Therefore, there is a tradeoff between high slope efficiency and low pump threshold. Elaborate design of the Raman fiber laser is necessary to achieve the required specifications.

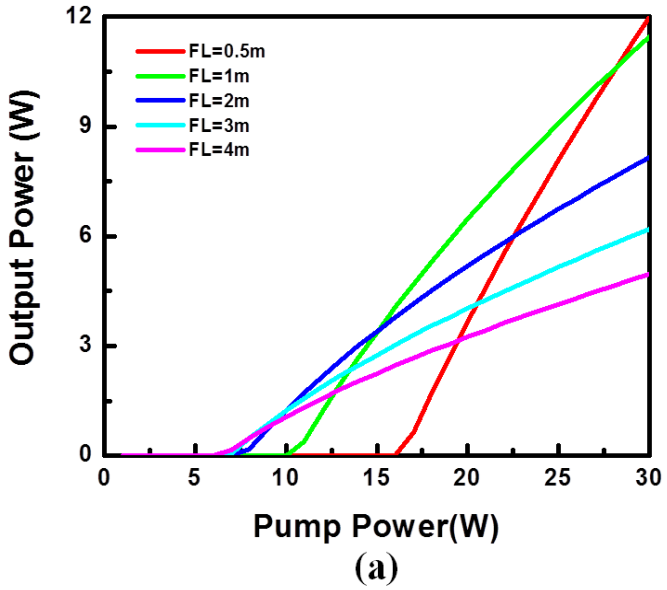

(a)

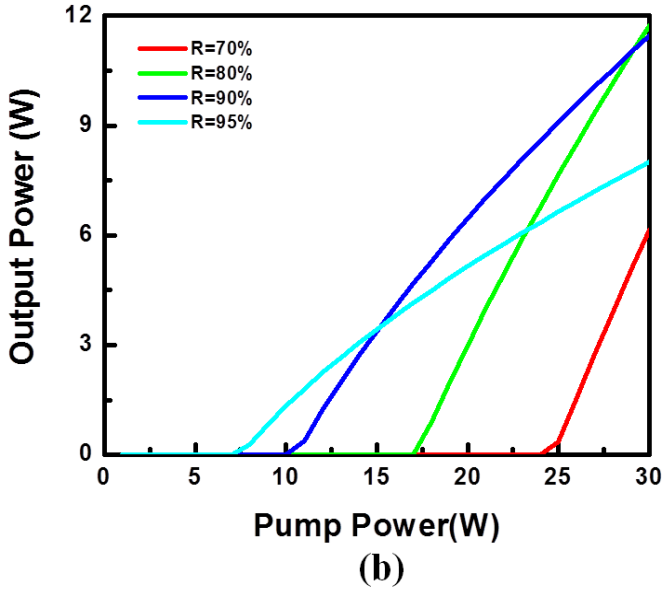

Fig. 5.6 Output power of the 3.53 μm Raman fiber laser as a function of the pump power (a) for different fiber lengths when the reflectance of the output FBG coupler is 90% and (b) for different reflectances of the output FBG coupler when the Raman gain fiber length is 1 m.

The Raman gain coefficient of tellurite glass has a minimum (0.8×10^{-12} m/W) at a Raman shift of 542 cm^{-1}, corresponding to a Raman laser wavelength of 3.3 μm for a pump wavelength of 2.8 μm. As shown in Fig. 5.4, the 3.3 μm 1st-order Raman fiber laser with a fiber length of 1 m and the output FBG coupler of 90% cannot lase even at a power of 20 W. Therefore, it is critical to study the performance of the 3.3 μm 1st-order Raman fiber laser and optimize the Raman laser to achieve the maximum output power at 3.3 μm. The output power of the 1st-order Raman fiber laser at 3.3 μm as a function of the fiber length and the reflection of the output FBG coupler is presented in a contour plot shown in Fig. 5.7. A maximum output power of 0.78 W can be obtained when the Raman

fiber length is 1.25 m and the reflectance of the output FBG coupler is 98%. However, the maximum conversion efficiency of the 3.3 μm Raman fiber laser is only about 3.9% due to the small Raman gain coefficient. When the Raman fiber length and the reflection of the output FBG coupler are fixed at 1.25 m and 98%, respectively, the output power of the Raman fiber laser as a function of the wavelength is calculated and is shown in Fig. 5.8. In this case, a Raman fiber laser operating in a wavelength range from 2.9 μm to 3.62 μm can be obtained. The output power at 3.3 μm is a minimum due to a minimum Raman gain coefficient at a Raman shift of 542 cm^{-1}. Nevertheless, the efficiency of a Raman fiber laser at 3.3 μm can be significantly increased by changing the pump wavelength. As shown in Fig. 5.8(b), the output power at 3.3 μm will be 6.3 W and the efficiency will be as high as 31.5% when the pump wavelength is 2.9 μm.

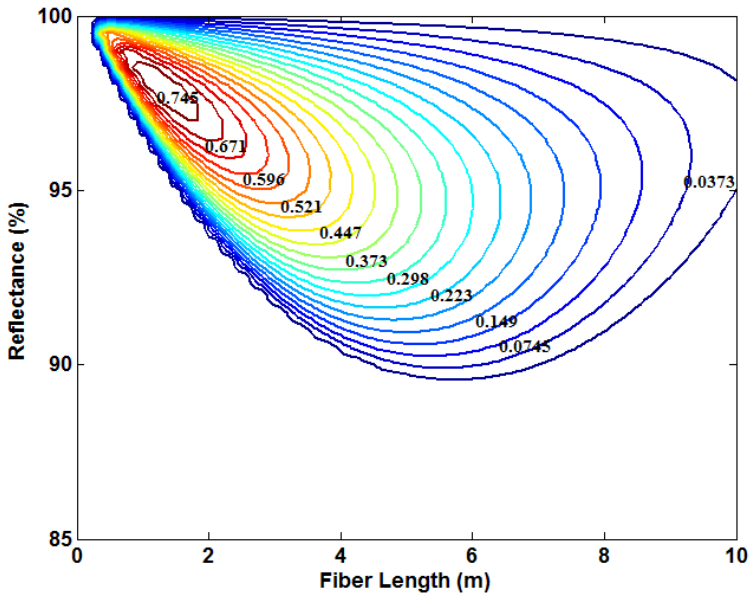

Fig. 5.7 Output power of a 3.3 μm 1st-order Raman fiber laser as a function of the Raman fiber length and the reflectance of the output FBG coupler at a pump power of 20 W. The values beside the contour curves are the output powers.

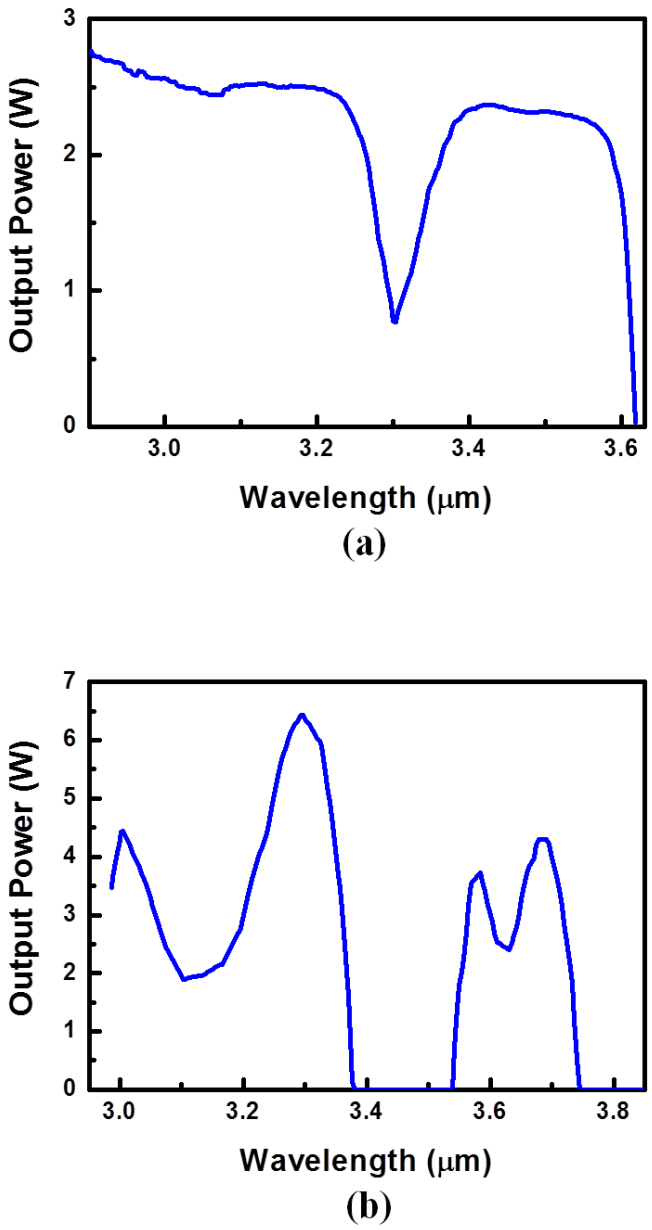

Fig. 5.8 Output power of the 1st-order Raman fiber laser as a function of wavelength at a pump power of 20 W. (a) The Raman gain fiber length and the reflectance of the output FBG coupler are fixed at 1.25 m and 98%, respectively and the pump laser is at 2.8 μm; (b) the Raman gain fiber length and the reflection of the output FBG coupler are fixed at 1 m and 90%, respectively and the pump laser is at 2.9 μm.

5.3.1.2 Second-order Raman fiber lasers

Because the wavelength of a 1st-order Raman fiber laser pumped at 2.8 μm cannot exceed 3.62 μm, a Raman fiber laser operating a wavelength beyond 3.62 μm can be achieved by either increasing the pump wavelength or by using 2nd-order Raman scattering. Because the emission wavelength of a high efficiency RE-doped ZBLAN fiber laser is usually limited to be below 3.1 μm [50], using 2nd-order Raman scattering is the most effective approach to extend the operating wavelength of a Raman laser. The configuration of a 2nd-order Raman fiber laser is depicted in Fig. 5.2. A pair of HR FBGs at a wavelength within the Raman shift relative to the pump wavelength is used to form a high Q-value fiber cavity for the 1st-order Raman Stokes, which is converted to the 2nd-order Raman Stokes by the nested cavity consisting of the HR and PR FBGs as well as the tellurite fiber. In this subsection, the simulation results for the 2nd-order Raman fiber laser are presented.

First, a 2nd-order Raman fiber laser in which both the 1st- and 2nd-order Raman shifts are at the Raman gain peak (740 cm^{-1}) is investigated. The operating wavelength of this Raman fiber pumped at 2.8 μm is 4.77 μm. Referring to the configuration illustrated in Fig. 5.2(b), two highly reflective FBGs at 3.53 μm and the tellurite fiber form the 1st-order Raman fiber laser cavity. A highly reflective FBG and a partially reflective FBG at 4.77 μm nested with the 1st-order Raman fiber laser form a cascaded Raman fiber laser, i.e., the pump power is transferred to the 1st-order Raman laser at 3.53 μm first, and then transferred to the 2nd-order Raman laser at 4.77 μm. The output power of the 2nd-order Raman fiber laser as a function of the fiber length and the reflectance of the output FBG

coupler at a pump power of 20 W are presented by a contour plot shown in Fig. 5.9. A maximum output power of 2.82 W can be obtained when the Raman fiber length is 0.34 m and the reflectance of the output FBG coupler is 40.5%. When the Raman fiber length and the reflectance of the output FBG coupler are fixed at 0.34 m and 40.5%, respectively, the output power of a Raman fiber laser operating from 3.7 μm to 5 μm was calculated and is shown in Fig. 5.10. Due to the small Raman gains close to the pump wavelength and at a Raman shift of 542 cm^{-1}, a 2nd-order Raman laser cannot be established in the two wavelength ranges 4.25 - 4.5 μm and 3.6 - 4.05 μm when the pump power is 20 W. This problem can be solved by properly selecting the Raman shifts of the 1st and 2nd order Raman scattering.

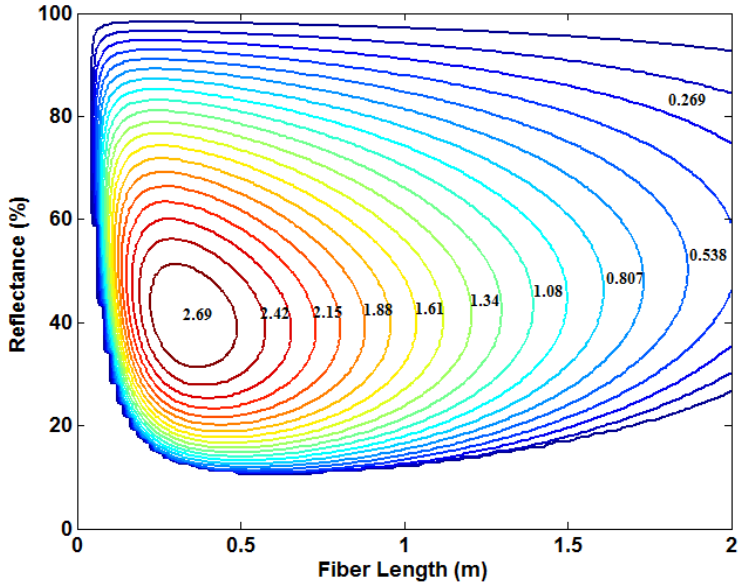

Fig. 5.9 Output power of a 4.77 μm 2nd-order Raman fiber laser as a function of the Raman fiber length and the reflectance of the output FBG coupler when the pump power is 20 W and the 1st-order Stokes oscillates at 3.53 μm. The values beside the contour curves are the output powers.

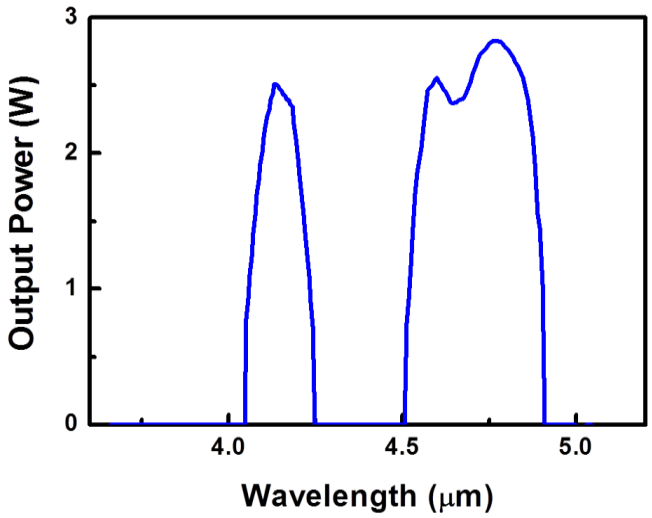

Fig. 5.10 Output power of the 2nd-order Raman fiber laser as a function of wavelength at a pump power of 20 W when the Raman gain fiber length and the reflectance of the output FBG coupler are fixed at 0.34 m and 40.5%, respectively, and the 1st-order Stokes oscillates at 3.53 μm.

For instance, a Raman fiber laser can operate at 4.36 μm when the 1st-order Raman shift is at 740 cm^{-1} and the 2nd-order Raman shift is at 542 cm^{-1}, i.e., the maximum reflectance wavelength of the HR FBGs for the 1st-order Raman laser is at 3.53 μm and that of the 2nd-order Raman laser is at 4.36 μm. It was found that a maximum output power of 1.51 W at a pump power of 20 W can be obtained when the Raman fiber length is 0.19 m and the reflectance of the output FBG coupler is 88%. Under the same conditions, the output power of the Raman fiber laser as a function of the wavelength was calculated and is shown in Fig. 5.11(a). Clearly, the Raman fiber laser can operate at any wavelength between 3.6 μm and 5.0 μm. The efficiency of the Raman fiber laser based on this configuration, however, is much lower than that shown in Fig. 5.10. Nevertheless, the simulation results summarized in Fig. 5.11(b) confirm that a Raman

tellurite fiber laser pumped at 2.8 μm can operate at any wavelength within the 3-5 μm atmospheric transparency window by elaborately designing the Raman laser cavity.

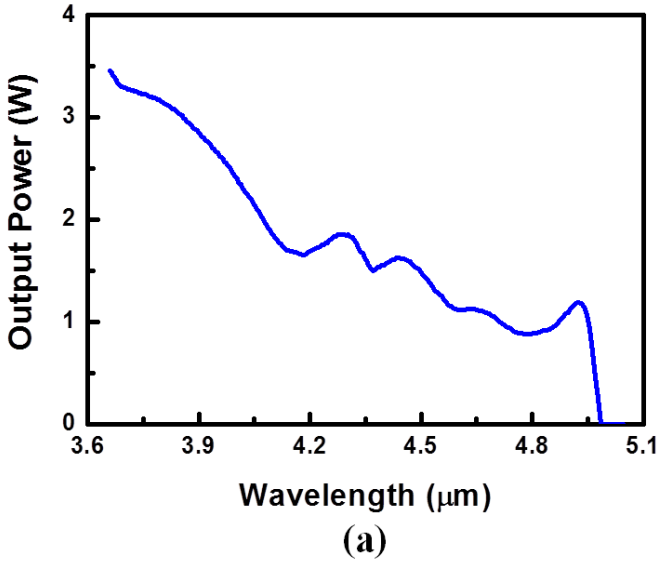

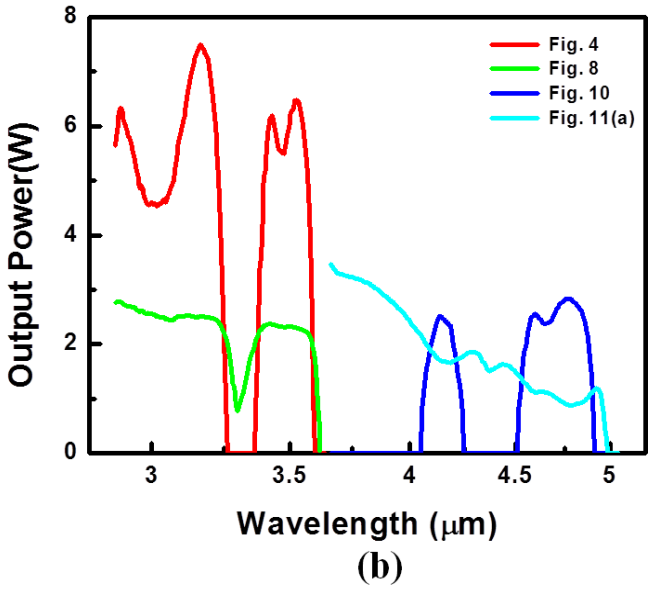

Fig. 5.11 (a) Output power of the 2nd-order Raman fiber laser as a function of wavelength at a pump power of 20 W when the Raman gain fiber length and the reflectance of the output FBG coupler are fixed at 0.19 m and 88%, respectively, and the 1st-order Stokes oscillates at 3.53 μm. (b) Summary of the calculation results plotted in Fig. 5.4, Fig. 5.8,

Fig. 5.10 and Fig. 5.11(a) shows the feasibility of obtaining a fiber laser at any wavelength between 3-5 μm by utilizing 1st-order and 2nd-order Raman scattering in tellurite fiber.

5.3.2 Q-switched laser pumped Raman tellurite fiber lasers

Q-switched lasers usually have higher peak power than cw lasers and thus enable high-efficiency low threshold Raman lasers. Q-switched fiber lasers at 3 μm have been extensively studied [58,60,112,113]. We have successfully demonstrated Q-switched Er^{3+}-doped and Ho^{3+}-doped ZBLAN fiber lasers using Fe^{2+}:ZnSe and graphene saturable absorbers [60,112,113]. Q-switched pulses with pulse energies of 1.67 μJ and peak powers of 0.58 W have been obtained [113]. Using an Er^{3+}-doped ZBLAN fiber amplifier, we have increased the pulse energy to 24 μJ with a peak power of 11.4 W. It is quite feasible to obtain a pulse energy of 300 μJ with a peak power of 143 W by using more powerful pump sources [127]. Therefore, Q-switched fiber lasers at 3 μm are very promising pump sources for high-efficiency tellurite fiber Raman lasers. In this subsection, tellurite fiber Raman lasers pumped by 2 μs Q-switched fiber lasers at a repetition rate of 40 kHz are investigated.

For comparison, a 1st-order Raman laser operating at the Raman gain peak with a Raman shift of 740 cm^{-1}, corresponding to a Raman laser wavelength of 3.53 μm when pumped at 2.8 μm, is investigated first. When the average power of the Q-switched laser source is 20 W, the output power of the 3.53 μm Raman fiber laser as a function of the fiber length and the reflectance of the output FBG coupler is presented as a contour plot shown in Fig. 5.12(a). A maximum output power of 13.6 W can be obtained when the

fiber length is 0.5 m and the reflectance of the PR FBG coupler is 48%. Clearly, compared to a cw laser pumping scheme, the conversion efficiency of the Raman laser pumped by a Q-switched laser is increased by a factor of two. When the fiber length is 0.5 m and the reflectance of the output FBG coupler is 48%, the output power of the Q-switched 3.53 μm Raman fiber laser as a function of the average pump power was calculated and is shown by the red curve in Fig. 5.12(b). For comparison, the output power of the cw 3.53 μm Raman fiber laser as a function of the pump power when the fiber length is 1 m and the reflectance of the output FBG coupler is 90% is also plotted as a blue curve in Fig. 5.12(b). Obviously, even though the gain fiber of the Q-switched Raman laser is 0.5 m, which is half of the 1 m gain fiber of the cw Raman laser, the threshold of the Q-switched Raman laser is still lower than that of the cw Raman laser. The conversion efficiency of the Q-switched Raman laser can be as high as 70%, which is significantly larger than that of the cw Raman laser. The pulse shapes of the pump pulse and the output Raman signal pulse are plotted in Fig. 5.13. Because the Raman gain is nonlinearly dependent on the pump power, the Raman signal pulse doesn't have long tails like the pump pulse and its pulse width is also slightly narrower than that of the pump pulse.

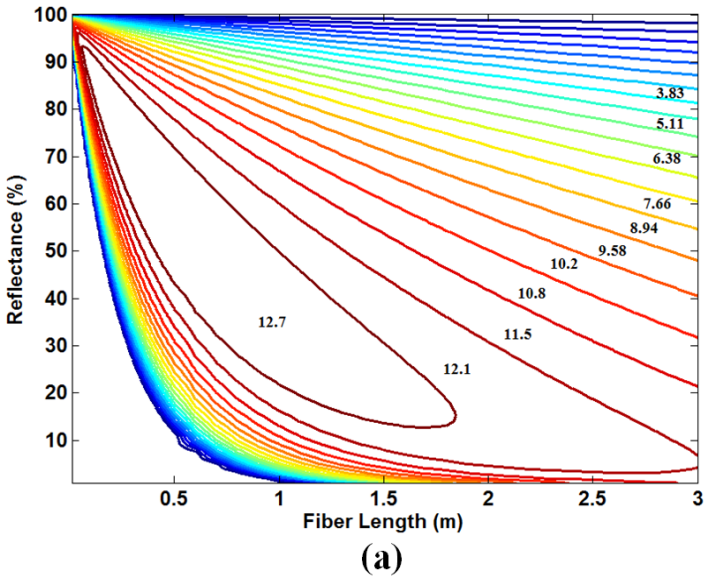

(a)

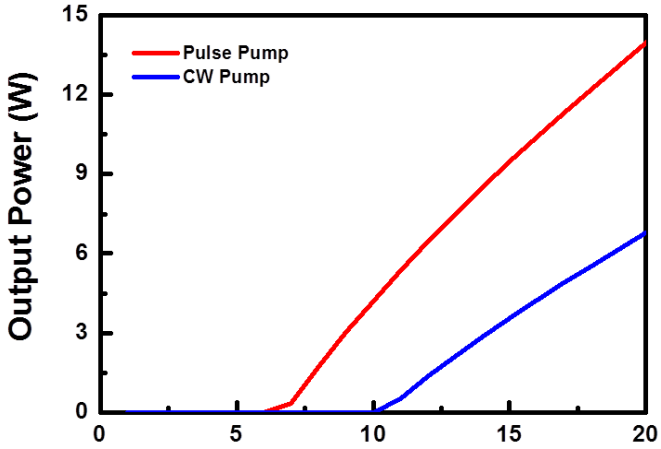

(b)

Fig. 5.12 Output power of Q-switched 1st-order Raman fiber laser at 3.53 μm as a function of the Raman fiber length and the reflectance of the output FBG coupler when the Q-switched 2.8 μm pump laser has an average power of 20 W. (a) The contour plot and (b) the output power of the Q-switched (red) and cw (blue) Raman fiber laser at 3.53 μm as a function of the pump power.

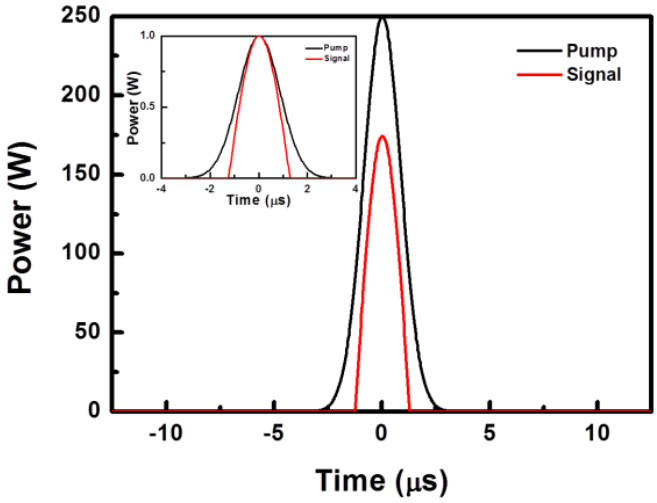

Fig. 5.13 The pulse shapes of the pump pulse and the output Raman signal pulse when the Raman gain fiber length is 0.5 m and the reflectance of the output FBG coupler is 48%. The inset shows the normalized pulse shapes of the pump and the Raman signal (the input pulse is assumed to be Gaussian).

2nd-order Raman fiber lasers pumped by a Q-switched laser at 2.8 μm have also been investigated. The output power of a Q-switched 2nd-order Raman fiber laser operating at 4.77 μm as a function of the fiber length and the reflectance of the output FBG coupler was calculated and a maximum output power of 7.0 W can be obtained when the Raman fiber length is 0.5 m and the reflectance of the output FBG coupler is 40%. The conversion efficiency of the Q-switched 2nd-order Raman laser is 35%, which is nearly 2.5 times of that of the cw laser counterpart. The output power of the Q-switched 2nd-order Raman laser as a function of the pump power is plotted as a red curve in Fig. 5.14. Obviously, the conversion efficiency of the Q-switched laser is significantly larger than that of the cw 2nd-order Raman laser, which is presented as a blue curve in Fig. 5.14. The threshold of the Q-switched 2nd-order Raman laser is only 3 W, which is much smaller

than the 13 W threshold of the cw 2nd-order Raman laser. Therefore, the tellurite fiber Raman laser pumped by a Q-switched Er-doped fiber laser at 2.8 μm will exhibit better performance than when pumped by a cw laser in terms of higher conversion efficiency and much lower pump threshold.

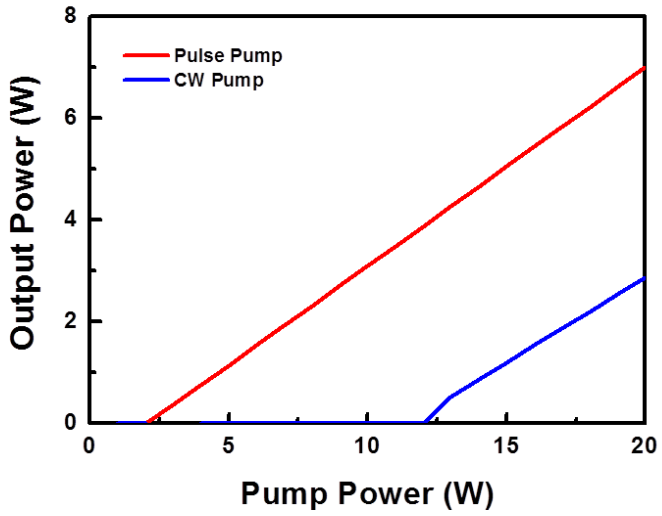

Fig. 5.14 The output power of the Q-switched (red) and cw (blue) 2nd-order Raman fiber laser at 4.77 μm as a function of the pump power.

5.4 Conclusion

In this chapter numerical simulations of tellurite fiber Raman lasers pumped by readily available Er^{3+}-doped ZBLAN fiber lasers have been presented. The simulation results have shown that fiber laser sources operating at any wavelength within the 3-5 μm atmospheric transparency window can be achieved by employing 1st-and 2nd-order Raman scattering of tellurite fibers. Q-switched Raman fiber lasers have much higher conversion efficiency and much lower threshold than corresponding cw Raman fiber

lasers. The calculation results can provide useful guidance for the design and development of high power tellurite fiber Raman lasers at 3-5 μm.

CHAPTER 6

Summary and Prospect

6.1 Summary

In this dissertation, I first report a singly Ho^{3+}-doped ZBLAN fiber lasers at 3 μm passively Q-switched by Fe^{2+}:ZnSe crystal and graphene saturable absorbers respectively. 800 ns pulses at 2.93 μm with energy of 460 nJ and repetition rate of 105 KHz are obtained when a Fe^{2+}:ZnSe crystal was inserted into a free space collimating and focusing setup. A more compact and reliable Q-switched fiber laser is achieved when a graphene deposited fiber mirror is butt-coupled to the angle-cleaved end of the gain fiber. 1.2 μs pulses with energy of 1 μJ at a repetition rate of 100 KHz were achieved. More than 100 mW average output power was obtained at the maximum available pump power.

However, constrained by the inherent property of the saturable absorbers, the output power of the Q-switched laser cannot be scaled up just by launching more pump power into the gain fiber. To obtain stable pulses with much higher power, an Er^{3+}-doped ZBLAN fiber amplifier for Q-switched pulses at 2.79 μm is demonstrated. Over 24 μJ of pulse energy at an average output power of 1.0 W is achieved at a maximum available pump power of 9.4 W. The efficiency of this pulsed laser fiber amplifier is about 10%. The simulation predicts that over 300 μJ pulses can be achieved with this fiber amplifier when a 120 W pump is used with proper cooling techniques.

To achieve higher peak powers and shorter pulse durations, a mid-infrared erbium (Er^{3+}) doped ZBLAN fiber laser mode-locked by multilayer graphene saturable absorber is demonstrated. Mode-locked pulses at 2.8 μm with an average output power of 18 mW at a repetition rate of 25.4 MHz, corresponding to a pulse energy of 0.7 nJ, were obtained. The pulse width was measured to be ~ 42 ps by a home-made autocorrelator.

In the last part, I report the simulations for the development of 10-watt-level 3-5 μm Raman lasers using tellurite fibers as the nonlinear gain medium and pumped by readily available continuous-wave (CW) and Q-switched erbium-doped fluoride fiber lasers at 2.8 μm. My simulation results have shown that fiber laser sources operating at any wavelength within the 3-5 μm atmospheric transparency window can be achieved by employing 1^{st}-and 2^{nd}-order Raman scattering of tellurite fibers. Q-switched Raman fiber lasers have much higher conversion efficiency and much lower threshold than corresponding CW Raman fiber lasers. The calculation results can provide useful guidance for the design and development of high power tellurite fiber Raman lasers at 3-5 μm.

6.2 Prospect

Graphene Q-switched fiber laser with over 24 μJ pulse energy and an average output power of 1 W have been demonstrated by utilizing a fiber amplifier. Since an Er^{3+}-doped ZBLAN fiber laser has been demonstrated with over 24 W output at a pump power of >160 W [70], it is very possible to scale up the pulse energy by an order of magnitude by using more powerful pumps and employing active cooling techniques. At a launched pump power of 120 W, the pulse energy can be scaled up to over 300 μJ at an average

power of 10-W. Further scaling of the pulse energy can be accomplished by using a 2-stage fiber amplifier with large-core active ZBLAN fiber as shown in Fig. 6.1 and reducing the repetition rate of the pulses as well. Multi-mJ mid-IR pulses at 2.8 μm will be achievable by employing current ZBLAN fiber laser technology and active cooling techniques.

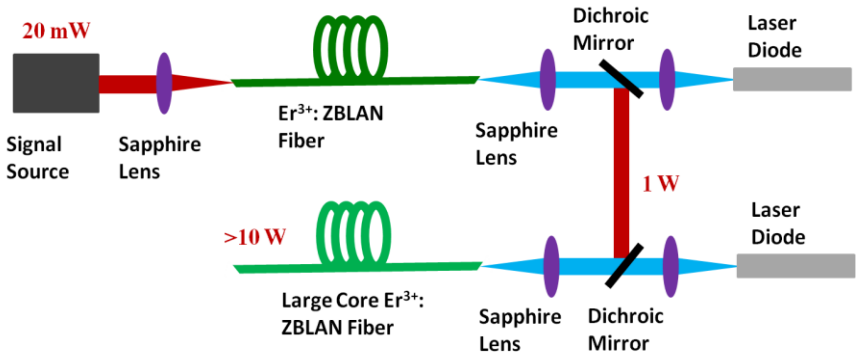

Fig. 6.1 Schematic of the experiment setup of a 2-stage Er^{3+}-doped ZBLAN fiber amplifier for a pulsed laser at 2.8 μm.

The graphene mode-locked Er^{3+}-doped ZBLAN fiber laser genetates only 10-ps-level pulses with a low reflection output coupler provided by the cleaved end of the ZBLAN fiber. The high intracavity loss is not suitable for the generation of high energy, stable ultrashort pulses. We can expect significant improvement in efficiency and stability if a proper FBG or dichroic mirror is used as the output coupler [88]. More stable and much shorter mode-locked pulses at 3 μm can also be obtained by employing a ring cavity incorporating a transmissive graphene saturable absorber [119] to eliminate spatial hole burning and carefully managing the dispersion of the ring cavity. Since sub-ps-level graphene mode-locked laser have been demonstrated at 1.5 μm, 2 μm and 2.5 wavelength regions [102,120,123], sub-ps-level graphene mode-locked Er^{3+}-doped

ZBLAN fiber lasers at 2.8 μm are promising with the improved experiment setup as shown in Fig. 6.2. Mode-locked lasers with watt-level or even 10-watt-level of average power is achievable with chirped pulse amplification scheme.

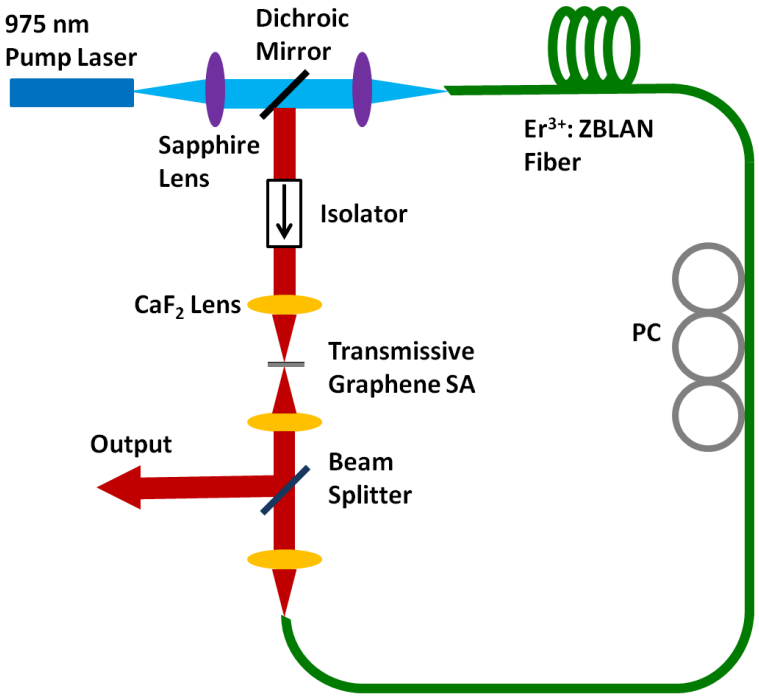

Fig. 6.2 Schematic of the experimental setup of the graphene mode-locked Er^{3+}-doped ZBLAN fiber laser at 2.8 μm using a ring laser cavity.

The numerical simulation on Raman lasers based on mid-infrared tellurite fibers provides useful guidance for the design and development of high power fiber Raman lasers at 3-5 μm atmospheric transparency window. High power Raman tellurite fiber lasers 3-5 μm are expected when we can write high efficiency FBGs on tellurite fiber. Since chalcogenide fibers have low loss in the entire mid-IR wavelength range [15], cascaded Raman lasers based on mid-IR chalcogenide fibers operating in the 3 - 12 μm are possible with high power pump sources and proper FBGs as shown in Fig. 6.3.

Wavelength up to 12.9 μm is achievable with an 8th-order cascaded Raman chalcogenide fiber laser when pumped at 2.8 μm.

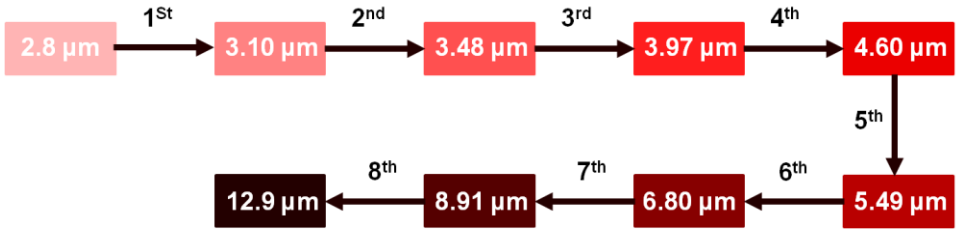

Fig. 6.3 Wavelength evolution of the cascaded Raman chalcogenide fiber lasers in the mid-IR region when pumped 2.8 μm.

REFERENCE

1. T. H. Maiman, “Stimulated optical radiation in ruby”, Nature **187**, 493-494 (1960).
2. E. Snitzer, “Proposed fiber cavities for optical masers”, J. Appl. Phys. **32** (1), 36-39 (1961).
3. W. A. Gambling, “The rise and rise of optical fibers”, IEEE J. Sel. Top. Quantum Electron. **6** (6), 1084-1093 (2000).
4. S. Xu, Z. Yang, W. Zhang, X. Wei, Q. Qian, D. Chen, Q. Zhang, S. Shen, M. Peng, and J. Qiu, “400 mW ultrashort cavity low-noise single-frequency Yb-doped phosphate fiber laser,” Opt. Lett. **36** (18), 3708-3710 (2011).
5. K. Ohsawa, T. Shibata, K. Nakamura, and S. Yoshida, “Fluorozirconate glasses for infrared transmitting optical fibers,” in Proceedings of the 7th European Conference on Optical Communication (ECOC), 1.1-1–1.1-4, Copenhagen, Danmark, September 1981.
6. X. Zhu and N. Peyghambarian, “High-power ZBLAN glass fiber lasers: review and prospect,” Adv. Optoelectron. **2010**, 501956 (2010).
7. D. C. Tran, G. H. Sigel, and B. Bendow, “Heavy metal fluoride glasses and fibers: A review”, J. Lightwave Technol. **2** (5), 566-586 (1984).
8. R. Paschotta, N. Moore, W. A. Clarkson, A. C. Tropper, D. C. Hanna, and G. Maze, “230 mW of blue light from a Tm-doped upconversion fiber laser”, IEEE J. Sel. Top. Quantum Electron. **3** (4), 1100-1102 (1997).
9. M. Liao, X. Yan, G. Qin, C. Chaudhari, T. Suzuki, and Y. Ohishi, “A highly non-linear tellurite microstructure fiber with multi-ring holes for supercontinuum generation,” Opt. Express **17**(18), 15481–15490 (2009)
10. J. S. Wang, E. M. Vogel, and E. Snitzer, “Tellurite glass: new candidate for fiber devices,” Opt. Mater. **3**(3), 187–203 (1994).
11. J. S. Sanghera, L. B. Shaw, and I. D. Aggarwal, “Chalcogenide glass-fiber-based mid-IR sources and applications,” IEEE J. Sel. Top. Quantum Electron. **15**(1), 114-119 (2009).

12. J. Hu, C. R. Menyuk, L. B. Shaw, J. S. Sanghera, and I. D. Aggarwal, "Maximizing the bandwidth of supercontinuum generation in As_2Se_3 chalcogenide fibers," Opt. Express **18**(7), 6722–6739 (2010).

13. D. Dooling et al, "ZBLAN continues to show promise," http://science.nasa.gov/science-news/science-at-nasa/1998/msad05feb98_1/

14. C. Wei, X. Zhu, R. A. Norwood, F. Song, and N. Peyghambarian, "Numerical investigation on high power mid-infrared supercontinuum fiber lasers pumped at 3 μm," Opt. Express **21**(24), 29488-29504 (2013).

15. http://www.coractive.com/

16. T. J. Whitley, C. A. Millar, R. Wyatt, M. C. Brierley, and D. Szebesta, "Upconversion pumped green lasing in erbium doped fluorozirconate fibre", Electron. Lett. **27**(20), 1785-1786 (1991).

17. G. Qin, M. Liao, T. Suzuki, A. Mori, and Y. Ohishi, "Widely tunable ring-cavity tellurite fiber Raman laser," Opt. Lett. **33**(17), 2014-2016 (2008).

18. R. E. Slusher, G. Lenz, J. Hodelin, J. Sanghera, L. B. Shaw, and I. D. Aggarwal, "Large Raman gain and nonlinear phase shifts in high-purity As_2Se_3 chalcogenide fibers," Journal of the Optical Society of America B **21**(6), 1146–1155 (2004)

19. R. Paschotta, "Rare-earth-doped fibers," http://www.rp-hotonics.com/rare_earth_doped_ fibers.html.

20. V. Gapontsev, V. Fomin, A. Ferin and M. Abramov, "Diffraction limited ultra-high power fiber lasers," Paper AWA1 in Proc. Adv. Solid-State Photon. Topical Meeting (OSA, 2010).

21. C. Jauregui, J. Limpert and A. Tünnermann, "High-power fiber lasers," Nature Photon. **7**, 861-867 (2013).

22. T. Eidam, J. Rothhardt, F. Stutzki, F. Jansen, S. Hädrich, H. Carstens, C. Jauregui, J. Limpert, and A. Tünnermann, "Fiber chirped-pulse amplification system emitting 3.8 GW peak power," Opt. Express **19**(1), 255–260 (2011).

23. S. D. Jackson, "Towards high-power mid-infrared emission from a fiber laser," Nature Photon. **6**, 423-431 (2012).

24. F. K. Tittel, D. Richter, and A. Fried, "Mid-Infrared Laser Applications in Spectroscopy," Solid-State Mid-Infrared Laser Sources, Topics Appl. Phys. **89**, 445–516 (2003).

25. M. Skorczakowski, J. Swiderski, W. Pichola, P. Nyga, A. Zajac, M. Maciejewska, L. Galecki, J. Kasprzak, S. Gross, A. Heinrich, and T. Bragagna, "Mid-infrared Q-switched Er:YAG laser for medical applications," Laser Phys. Lett. **7**, 498–504 (2010).

26. B. Jean and T. Bende, "Mid-IR laser applications in medicine," Solid-State Mid-Infrared Laser Sources, **89**, Heidelberg, Germany: Springer, 2003, 511-546.

27. A. Vogel and V. Venugopalan, "Mechanisms of pulsed laser ablation of biological tissues," Chem. Rev. **103** (2), 577-644 (2003).

28. A. Schliesser, N. Picqué and T. W. Hänsch, "Mid-infrared frequency combs," Nature Photon. **6**, 440-449 (2012).

29. P. Werle, F. Slemr, K. Maurer, R. Kormann, R. Mucke, and B. Janker, "Near- and mid-infrared laser-optical sensors for gas analysis," Opt.Laser Eng., **37**, 101–114 (2002).

30. S. Zlatanovic, J. S. Park, S. Moro, J. M. Chavez Boggio, I. B. Divliansky, N. Alic, S. Mookherjea, and S. Radic, "Mid-infrared wavelength conversion in silicon waveguides using ultracompact telecom-band-derived pump source," Nature Photon. **4**, 561-564 (2010).

31. G. Zhu, L. Geng, X. Zhu, L. Li, Q. Chen, R. A. Norwood, T. Manzur, and N. Peyghambarian, "Towards ten-watt-level 3-5 μm Raman lasers using tellurite fiber," Opt. Express **23**(6), 7559-7573 (2015).

32. D. M. Wieliczka, S. Weng, and M. R. Querry, "Wedge shaped cell for highly absorbent liquids: infrared optical constants of water," Appl. Opt. **28**(9), 1714-1719 (1989).

33. J. T. Walsh, Jr., T. J. Flotte, and T. F. Deutsch, "Er:YAG laser ablation of tissue: Effect of pulse duration and tissue type on thermal damage," Lasers Surg. Med. **9**, 314-326, (1989).

34. A. Schliesser, N. Picque, and T. W. Hänsch, "Mid-infrared frequency combs," Nat. Photonics **6**, 440 (2012).

35. J. F. Butler, A. R. Calawa, and R. H. Rediker, "Properties of the PbSe diode laser", IEEE J. Quantum Electron. **1**(1), 4-7 (1965).

36. J. Chen, T. Hosoda, G. Kipshidze, L. Shterengas, G. Belenky, A. Soibel, C. Frez, and S. Forouhar, "Single spatial mode room temperature operated 3.15μm diode lasers", Electron. Lett. **46**(5), 367-368 (2010).

37. A. Bauer, K. Roßner, T. Lehnhardt, M. Kamp, S. Hofling, L. Worschech, and A. Forchel, "Mid-infrared semiconductor heterostructure lasers for gas sensing applications," Semi. Sci. Technol. **26**(1), 014032 (2011).

38. T. Day, M. Pushkarsky, D. Caffey, K. Cecchetti, R. Arp, A. Whitmore, M. Henson, E. B. Takeuchi, "Quantum cascade lasers for defense & security," Proc. SPIE **8898**, 889802 (2013).

39. G. J. Wagner, T. J. Carrig, R. H. Page K. I. Schaffers, J. Ndap, X. Ma, and A. Burger, "Continuous-wave broadly tunable Cr^{2+}:ZnSe laser," Opt. Lett. **24**(1), 19-21(1999).

40. V. V. Fedorov et al, "3.77–5.05-μm tunable solid-state lasers based on Fe^{2+}-doped ZnSe crystals operating at low and room temperatures," IEEE J. Lightwave Technol. **42**(9), 907-917(2006).

41. S. Mirov, V. Fedorov, I. Moskalev, D. Martyshkin, and C. Kim, "Progress in Cr^{2+} and Fe^{2+} doped mid-IR laser materials," Laser & Photon. Rev. **4** (1), 21-41 (2010).

42. E. Lippert, H. Fonnum, G. Arisholm, and K. Stenersen , “A 22-watt mid-infrared optical parametric oscillator with V-shaped 3-mirror ring resonator,” Opt. Express **18**(25), 26475-26483 (2010).

43. F. Rotermund, V. Petrov, and F. Noack, “Difference-frequency generation of intense femtosecond pulses in the mid-IR (4-12 μm) using $HgGa_2S_4$ and $AgGaS_2$,” Opt. Commun. **185**(1-3), 177-183 (2000).

44. K. C. Burr, C. L. Tang, M. A. Arbore, and M. M. Fejer, “Broadly tunable mid-infrared femtosecond optical parametric oscillator using all-solid-state-pumped periodically poled lithium niobate,” Opt. Lett. **22**(19), 1458–1460 (1997).

45. C. Erny, K. Moutzouris, J. Biegert, D. Kühlke, F. Adler, A. Leitenstorfer, and U. Keller, “Mid-infrared difference-frequency generation of ultrashort pulses tunable between 3.2 and 4.8 μm from a compact fiber source,” Opt. Lett. **32**(9), 1138-1140 (2007).

46. A. V. V. Nampoothiri, A. Ratanavis, N. Campbell, and W. Rudolph, “Molecular C_2H_2 and HCN lasers pumped by an optical parametric oscillator in the 1.5-um band,” Opt. Express **18**, 1946-1951(2010).

47. C. K. N. Patel, “Continuous-wave laser action on vibrational-rotational transitions of CO_2,” Phys. Rev. **136** (5A), A1187–A1193 (1964).

48. A. M. Jones, A. V. V. Nampoothiri, A. Ratanavis, T. Fiedler, N. V. Wheeler, F. Couny, R. Kadel, F. Benabid, B. R. Washburn, K. L. Corwin, and W. Rudolph, “Mid-infrared gas filled photonic crystal fiber laser based on population inversion,” Opt. Express **19**(3), 2309–2316 (2011).

49. A. V. V. Nampoothiri, A. M. Jones, A. Ratanavis, R. Kadel, N. V. Wheeler, F. Couny, F. Benabid, B. R. Washburn, K. L. Corwin, and W. Rudolph, “Mid-IR laser emission from a C_2H_2 gas filled hollow core photonic crystal fiber,” Proc. SPIE **7580**, 758001 (2010).

50. M. C. Brierley and P. W. France, “Continuous wave lasing at 2.7 μm in an erbium-doped fluorozirconate fiber,” Electron. Lett. **24**(15), 935–937 (1988).

51. X. Zhu and N. Peyghambarian, “High-power ZBLAN glass fiber lasers: review and prospect,” Adv. Optoelectron. **2010**, 501956 (2010).

52. X. Zhu and R. Jain, “Compact 2 W wavelength-tunable Er:ZBLAN mid-infrared fiber laser,” Opt. Lett. **32**(16), 2381–2383 (2007).

53. X. Zhu and R. Jain, “Watt-Level 100-nm tunable 3-μm fiber laser,” IEEE Photon. Technol. Lett. **20**(2), 156-158 (2008).

54. S. D. Jackson, “Single-transverse-mode 2.5-W holmium-doped fluoride fiber laser operating at 2.86 μm,” Opt. Lett. **29**(4), 334-336 (2004).

55. S. D. Jackson, “Continuous wave 2.9 μm dysprosium-doped fluoride fiber laser,” Appl. Phys. Lett. **83**(7), 1316 -1318 (2003).

56. Y. H. Tsang, A. E. El-Taher, T. A. King, and S. D. Jackson, “Efficient 2.96 μm dysprosium-doped fluoride fiber laser pumped with a Nd:YAG laser operating at 1.3 μm,” Opt. Express **14**, 678-685 (2006).

57. S. Tokita, M. Murakami, S. Shimizu, M. Hashida, and S. Sakabe, “12 W Q-switched Er:ZBLAN fiber laser at 2.8 μm,” Opt. Lett. **36**, 2812–2814 (2011).

58. C. Frerichs and T. Tauermann, “Q-switched operation of laser diode pumped erbium-doped fluorozirconate fibre laser operating at 2.7 μm,” Electron. Lett. **30**(9), 706–707 (1994).

59. C. Frerichs and U. B. Unrau, “Passive Q-switching and mode-locking of erbium-doped fluoride fiber lasers at 2.7 μm,” Opt. Fiber Technol. **2**, 358–366 (1996).

60. C. Wei, X. Zhu, R. A. Norwood, and N. Peyghambarian, “Passively Q-Switched 2.8-μm Nanosecond Fiber Laser, ” IEEE Photon. Technol. Lett. **24**, 1741-1744 (2012).

61. T. Hu, D. D. Hudson, and S. D. Jackson, “Actively Q-switched 2.9 μm Ho^{3+} Pr^{3+}-doped fluoride fiber laser,” Opt. Lett. **37**, 2145 (2012).

62. J. Li, T. Hu, and S. D. Jackson, "Dual wavelength Q-switched cascade laser," Opt. Lett. **37**, 228 (2012).

63. J. Li, Y. Yang, D. D. Hudson, Y. Liu, and S. D. Jackson, "A tunable Q-switched Ho^{3+}-doped fluoride fiber laser," Laser Phys. Lett. **10**, 045107 (2013).

64. M. Bernier, V. Fortin, N. Caron, M. El-Amraoui, Y. Messaddeq, and R. Vallée, "Mid-infrared chalcogenide glass Raman fiber laser," Opt. Lett. **38**(2), 127–129 (2013).

65. R. S. Quimby, W. J. Miniscalco, and B. Thompson, "Excited state absorption at 980 nm in erbium doped glass," in Fiber Laser Sources and Amplifiers III, Proc. SPIE **1581**, 72–79 (1991).

66. S. Bedo, M. Pollnau, W. Luthy, and H. P. Weber, "Saturation of the 2.71 μm laser output in erbium doped ZBLAN fibers," Opt. Commun. **116**, 81-86 (1995).

67. M. Pollnau, Ch. Ghisler, W. Luthy, and H. P. Weber, "Cross-sections of excitedstate absorption at 800 nm in erbium-doped ZBLAN fiber," Appl. Phys. B **67**, 23-28 (1998).

68. M. Pollnau, Ch. Ghisler, W. Luthy, H. P. Weber, J. Schneider, and U. B. Unrau, "Three-transition cascade erbium laser at 1.7, 2.7, and 1.6 μm," Opt. Lett. **22**(9), 612–614 (1997).

69. X. Zhu and R. Jain, "10-W-level diode-pumped compact 2.78 μm ZBLAN fiber laser," Opt. Lett. **32**, 26–28 (2007).

70. S. Tokita, M. Murakami, S. Shimizu, M. Hashida, and S. Sakabe, "Liquid-cooled 24 W mid-infrared Er:ZBLAN fiber laser," Opt. Lett. **34**, 3062–3064 (2009).

71. D. Faucher, M. Bernier, G. Androz, N. Caron, and R. Vallée, "20 W passively cooled single-mode all-fiber laser at 2.8 μm," Opt. Lett. **36**, 1104-1106 (2011).

72. Fortin, M. Bernier, S. T. Bah, and R. Vallée, "30 W fluoride glass all-fiber laser at 2.94 μm," Opt. Lett. **40**(12), 2882-2885 (2015).

73. H. Tobben, "CW lasing at 3.45 μm in erbium-doped fluorozirconate fibres," Frequenz 45(9-10), 250-252 (1991).

74. H. Tobben, "Room temperature CW fibre laser at 3.5 μm in Er^{3+}-doped ZBLAN glass," Electron. Lett. **28**(14), 1361-1362 (1992).

75. O. Henderson-Sapir, J. Munch, and D. J. Ottaway, "Mid-infrared fiber lasers at and beyond 3.5 μm using dual-wavelength pumping," Opt. Lett. **39**(3), 493-496 (2014).

76. L. Wetenkamp, "Efficient CW operation of a 2.9 μm Ho^{3+}-doped fluorozirconate fiber laser pumped at 640 nm," Electron. Lett. **26**(13), 883-884 (1990).

77. T. Sumiyoshi and H. Sekita, "Dual-wavelength continuous-wave cascade oscillation at 3 and 2 μm with a holmium-doped fluoride-glass fiber laser," Opt. Lett. **23**(23), 1837-1839 (1998).

78. T. Sumiyoshi, H. Sekita, T. Arai, S. Sato, M. Ishihara, and M. Kikuchi, "High-power continuous-wave 3- and 2-μm cascade Ho^{3+}:ZBLAN fiber laser and its medical applications," IEEE J. Sel. Top. Quantum Electron. **5**(4), pp. 936–943 (1999).

79. S. D. Jackson, "Singly Ho^{3+}-doped fluoride fiber laser operating at 2.92 μm," Electron. Lett.**40**(22), 1400-1401 (2004).

80. C. Carbonnier, H. Tobben, and U. B. Unrau, "Room temperature CW fiber laser at 3.22 μm," Electron. Lett. **34**(9), 893-894 (1998).

81. J. Schneider, C. Carbonnier, and U. B. Unrau, "Characterization of a Ho^{3+}-doped fluoride fiber laser with a 3.9-μm emission wavelength," Appl. Opt. **36**(33), 8595-8600 (1997).

82. P. Domachuk, N. A.Wolchover, M. Cronin-Golomb, A. Wang, A. K. George, C.M.B.Cordeiro, J.C. Knight, F. G. Omenetto, "Over 4000 nm bandwidth of mid-IR supercontinuum generation in sub-centimeter segments of highly nonlinear tellurite PCFs," Opt. Express **16**(10), 7161-7168 (2008).

83. M. Bernier, V. Fortin, M. El-Amraoui, Y. Messaddeq, and R. Vallée, "3.77 μm fiber laser based on cascaded Raman gain in a chalcogenide glass fiber," Opt. Lett. **39**(7), 2052-2055 (2014).

84. T. Brabec, Ch. Spielmann, P. F. Curley, and F Krausz, “Kerr lens mode locking”, Opt. Lett. **17**(18), 1292-1294 (1992).

85. M. E. Fermann, M. J. Andrejco, Y. Silberberg, and M. L. Stock, “Passive mode locking by using nonlinear polarization evolution in a polarization-maintaining erbium-doped fiber”, Opt. Lett. **18**(11), 894-896 (1993).

86. J. Mark, L. Y. Liu, K. L. Hall, H. A. Haus, and E. P. Ippen, “Femtosecond pulse generation in a laser with a nonlinear external resonator”, Opt. Lett. **14**(1), 48-50 (1989).

87. U. Keller, K. J. Weingarten, F. X. Kartner, D. Kopf, B. Braun, I. D. Jung, R. Fluck, C. Honninger, N. Matuschek, and J. A. d. Au, “Semiconductor saturable absorber mirrors (SESAMs) for femtosecond to nanosecond pulse generation in solid-state lasers”, IEEE J. Sel. Top. Quantum Electron. **2**(3), 435-453 (1996).

88. A. Haboucha, V. Fortin, M. Bernier, J. Genest, Y. Messaddeq, and R. Vallée, “Fiber Bragg grating stabilization of a passively mode-locked 2.8 μm Er^{3+}: fluoride glass fiber laser,” Opt. Lett. **39**(11), 3294-3297 (2014).

89. J. Li, D. D. Hudson,Y. Liu, and S. D. Jackson, “Efficient 2.87 μm fiber laser passively switched using a semiconductor saturable absorber mirror,” Opt. Lett. **37**(18), 3747-3749 (2012).

90. A. K. Geim and K. S. Novoselov, “The rise of graphene,” Nature Mater. **6**, 183-191 (2007).

91. Q. L. Bao, H. Zhang, Y. Wang, Z. Ni, Y. Yan, Z. X. Shen, K. P. Loh, and D. Y. Tang, “Atomic layer graphene as saturable absorber for ultrafast pulsed laser,” Adv. Funct. Mater. **19**, 3077 (2009).

92. J. M. Dawlaty, S. Shivaraman, J. Strait, P. George, M. Chandrashekhar, F. Rana, M. G. Spencer, D. Veksler, and Y. Chen, “Measurement of the optical absorption spectra of epitaxial graphene from terahertz to visible,” Appl. Phys. Lett. **93**, 131905 (2008).

93. J. Liu, S. Wu, Q. Yang, and P. Wang, "Mode-locked and Q-switched Yb-doped Fiber Lasers with Graphene Saturable Absorber," Proc. SPIE **8192**, 819244 (2011).

94. D. Popa, Z. Sun, T. Hasan, F. Torrisi, F. Wang, and A. C. Ferrari, "Graphene Q-switched, tunable fiber laser," Appl. Phys. Lett. **98**, 073106 (2011).

95. G. Sobon, J. Sotor, I. Pasternak, K. Grodecki, P. Paletko, W. Strupinski, Z. Jankiewicz, and K. M. Abramski, "Er-Doped Fiber Laser Mode-Locked by CVD-Graphene Saturable Absorber," J. Lightwave Technol. **30**, 2770-2775 (2012).

96. M. Jiang, H. Ma, Z. Ren, X. Chen, J. Long, M. Qi, D. Shen, Y. Wang and J. Bai, "A graphene Q-switched nanosecond Tm-doped fiber laser at 2 μm," Laser Phys. Lett. **10**, 055103 (2013).

97. M. Zhang, E. J. R. Kelleher, F. Torrisi, Z. Sun, T. Hasan, D. Popa, F. Wang, A. C. Ferrari, S. V. Popov, and J. R. Taylor, "Tm-doped fiber laser mode-locked by graphene-polymer composite," Opt. Express **20**, 25077-25084 (2012).

98. A. C. Eerrari, J. C. Meyer, V. Scardaci, C. Casiraghi, M. Lazzeri, F. Mauri, S. Piscanec, D. Jiang, K. S. Novoselov, S. Roth, and A. K. Geim, "Raman spectrum of graphene and graphene layers," Phys. Rev. Lett. **97**, 187401 (2006).

99. Y. Hernandez, V. Nicolosi, M. Lotya, F. M. Blighe, Z. Sun, S. De, I. T. McGovern, B. Holland, M. Byrne, Y. K. Gun'Ko, J. J. Boland, P. Niraj, G. Duesberg, S. Krishanamurthy, B. Goodhue, J. Hutchison, V. Scardaci, A. C. Ferrari, and J. N. Coleman, "High-yield production of graphene by liquid-phase exfoliation of graphite," Nature Nanotech. **3**, 563-568 (2008).

100. X. Li, W. Cai, J. An, S. Kim, J. Nah, D. Yang, R. Piner, A. Velamakanni, I. Jung, E. Tutuc, S. K. Banerjee, L. Colombo, and R. S. Ruoff, "Large-area synthesis of high-quality and uniform graphene films on copper foils," Science **324**(5932), 1312-1314 (2009).

101. C. Wei, X. Zhu, F. Wang, Y. Xu, K. Balakrishnan, F. Song, R. A. Norwood, and N. Peyghambarian, "Graphene Q-switched 2.78 μm Er^{3+}-doped fluoride fiber laser," Opt. Lett. **38**(17), 3233-3236 (2013).

102. A. A. Lagatsky, Z. Sun, T. S. Kulmala, R. S. Sundaram, S. Milana, F. Torrisi, O. L. Antipov, Y. Lee, J. H. Ahn, C. T. A. Brown, W. Sibbet, and A. C. Ferrari, "2 μm solid-state laser mode-locked by single-layer graphene," Appl. Phys. Lett. **102**, 013113 (2013).

103. J. T. Hu, and S. D. Jackson, "Q-switched induced gain switching of a two-transition cascade laser," Opt. Express **20**(12), 13123-13128 (2012).

104. M. Gorjan, R. Petkovsek, M. Marincek, and M. Copic, "High-power pulsed diode-pumped Er:ZBLAN fiber laser," Opt. Lett. **36**(10), 1923-1925 (2011).

105. A. F. Librantz, S. D. Jackson, L. Gomes, S. J. Ribeiro, and Y. Messaddeq, "Pump excited state absorption in holmium-doped fluoride glass, " J. Appl. Phys. **103**, 023105 (2008).

106. X. Zhu, J. Zong, R. A. Norwood, A. Chavez-Pirson, and N. Pegyhambarian, "Homulium-doped ZBLAN fiber lasers at 1.2 μm," Proc. SPIE **8237**, 823727 (2012).

107. A. A. Voronov, V. I. Kozlovskii, Y. V. Korostelin, A. I. Landman, Y. P. Podmar'kov, V. G. Polushkin, M. P. Frolov, "Passive Fe^{2+}:ZnSe single-crystal Q switch for 3-μm lasers," Quantum Electron. **36**, 1–2 (2006).

108. J. W. Nicholson, R. S. Windeler, and D. J. DiGiovanni, "Optically driven deposition of single-walled carbon-nanotube saturable absorbers on optical fiber end-faces," Opt. Express **15**, 9176 (2007).

109. R. R. Nair, P. Blake, A. N. Grigorenko, K. S. Novoselov, T. J. Booth, T. Stauber, N. M. R. Peres, and A. K. Geim, "Fine structure constant defines visual transparency of graphene," Science **320**, 1308 (2008).

110. S. Yamashita, "A tutorial on nonlinear photonic application of carbon nanotube and graphene," J. Lightwave Technol. **30**, 427-447 (2012).

111. V. A. Akimov, M. P. Frolov, Y. V. Korostelin, V. I. Kozlovsky, A. I. Landman, Y. P. Podmar'kov, V. G. Polushkin, and A. A. Voronov, "2.94 μm Er:YAG q-switched laser with FE^{2+}:ZnSe passive shutter, " Proc. SPIE **6610**, 661008 (2007).

112. G. Zhu, X. Zhu, K. Balakrishnan, R. A. Norwood and N. Peyghambarian, "Fe^{2+}:ZnSe and graphene Q-switched singly Ho^{3+}-doped ZBLAN fiber lasers at 3 μm," Opt. Mater. Express **3**(9), 1365–1377 (2013).

113. C. Wei, X. Zhu, F. Wang, Y. Xu, K. Balakrishnan, F. Song, R. A. Norwood, and N. Peyghambarian, "Graphene Q-switched 2.78 μm Er^{3+}-doped fluoride fiber laser," Opt. Lett. **38**(17), 3233-3236 (2013).

114. S. D. Jackson, T. A. King, and M. Pollnau, "Modelling of high-power diode-pumped erbium 3 μm fibre lasers," J. Modern Opt. **47**(11), 1987–1994 (2000).

115. M. Pollnau and S. D. Jackson, "Energy recycling versus lifetime quenching in erbium-doped 3-μm fiber lasers," IEEE J. Quantum Electron. **38**(2), 162-169 (2002).

116. M. Gorjan M. Marincek, and M. Copic, "Role of interionic processes in the efficiency and operation of erbium-doped fluoride fiber lasers," IEEE J. Quantum Electron. **47**(2), 262-273 (2011).

117. J. Li and S. D. Jackson, "Numerical modeling and optimization of diode pumped heavily-erbium-doped fluoride fiber lasers," IEEE J. Quantum Electron. **48**(4), 454-464 (2012).

118. C. Wei, X. Zhu, R. A. Norwood, and N. Peyghambarian, "Passively continuous-wave mode-locked Er^{3+}-doped ZBLAN fiber laser at 2.8 μm," Opt. Lett. **37**(18), 3849-3851 (2012).

119. T. Hu, D. D. Hudson, and S. D. Jackson, "Stable, self-starting, passively mode-locked fiber ring laser of the 3 μm class," Opt. Lett. **39**(7), 2133-2136 (2014).

120. J. Tarka, G. Sobon, J. Boguslawski, J. Sotor, J. Jagiello, M. Aksienionek, L. Lipinska, M. Zdrojek, J. Judek, and K. M. Abramski, "168 fs pulse generation from graphene-chitosan mode-locked fiber laser," Opt. Express **4**(10), 1981-1986 (2014).

121. T. Hasan, Z. Sun, F. Wang, F. Bonaccorso, P. H. Tan, A. G. Rozhin, and A. C. Ferrari, "Nanotube-polymer composites for ultrafast photonics," Adv. Mater. **21**, 3874-3899 (2009).

122. L. M. Zhao, D. Y. Tang, H. Zhang, X. Wu, Q. Bao, and K. P. Loh, "Dissipative soliton operation of an ytterbium-doped fiber laser mode locked with atomic multilayer graphene," Opt. Lett. **35**(21), 3622-3624 (2010).

123. M. N. Cizmeciyan, J. W. Kim, S. Bae, B. H. Hong, F. Rotermund, and A. Sennaroglu, "Graphene mode-locked femtosecond Cr: ZnSe laser at 2500 nm," Opt. Lett. **38**(3), 341-343 (2013).

124. G. Zhu, X. Zhu, K. Balakrishnan, R. A. Norwood, and N. Peyghambarian, "Fe^{2+}:ZnSe and graphene Q-switched singly Ho^{3+}-doped ZBLAN fiber lasers at 3 μm," Opt. Mater. Express **3**(9), 1365-1377 (2013).

125. F. Sanchez and G. Stephan, "General analysis of instabilities in erbium-doped fiber lasers," Phys. Rev. E **53**(3), 2110-2122 (1996).

126. F. Z. Qamar and T. A. King, "Self pulsations and self Q-switching in Ho^{3+},Pr^{3+}:ZBLAN fiber lasers at 2.87 μm," Appl. Phys. B **81**, 821-826 (2005).

127. G. Zhu, X. Zhu, R. A. Norwood, and N. Peyghambarian, "Experimental and numerical investigations on Q-switched laser seeded fiber MOPA at 2.8 μm," IEEE J. Lightwave Technol. **32**(23), 3951-3955 (2014).

128. J. W. Salisbury and D. M. D'Aria, "Emissivity of terrestrial materials in the 3–5 μm atmospheric window," Remote Sens. Environ. **47**(3), 345-361 (1994).

129. K. O. Hill, B. S. Kawasaki, and D. C. Johnson, "Low-threshold cw Raman laser," Appl. Phys. Lett. **29** (3), 181-183 (1976).

130. P. N. Kean, B. D. Sinclair, K. Smith, W. Sibbett, C. J. Rowe, and D. C. Reid, "Experimental evaluation of a fiber Raman oscillator having fiber grating reflectors," J. Mod. Opt. **35** (3), 397-406 (1988).

131. V. R. Supradeepa and J. W. Nicholson, "Power scaling of high-efficiency 1.5 μm cascaded Raman fiber lasers," Opt. Lett. **38**(14), 2538-2541 (2013).

132. V. Fortin, M. Bernier, J. Carrier, and R. Vallée, "Fluoride glass Raman fiber laser at 2185 nm," Opt. Lett. **36**(21), 4152-4154 (2011).

133. V. Fortin, M. Bernier, D. Faucher, J. Carrier, and R. Vallée, "3.7 W fluoride glass Raman fiber laser operating at 2231 nm," Opt. Express **20**(17), 19412-19419 (2012).

134. J. Hu, C. R. Menyuk, L. B. Shaw, J. S. Sanghera, and I. D. Aggarwal, "Maximizing the bandwidth of supercontinuum generation in As_2Se_3 chalcogenide fibers," Opt. Express **18**(7), 6722–6739 (2010).

135. P. A. Thielen, L. B. Shaw, J. S. Sanghera, and I. D. Aggarwal, "Modeling of a mid-IR chalcogenide fiber Raman laser," Opt. Express **11**(24), 3248-3253 (2003).

136. G. Dong, H. Tao, S. Chu , X. Xiao, S. Wang, X. Zhao, Q. Gong, "Structural dependence of ultrafast third-order optical nonlinearity of Ge–Ga–Ag–S chalcogenide glasses," J. Non-Cryst. Solids **354**(2-9), 440-444 (2008).

137. G. Qin, R. Jose, and Y. Ohishi, "Stimulated Raman scattering in tellurite glasses as a potential system for slow light generation," J. Appl. Phys. **101**, 093109 (2007).

138. A. Mori, H. Masuda, K. Shikano, and M. Shimizu, "Ultra-wide-band tellurite-based fiber Raman amplifier," IEEE J. Lightwave Technol. **21**(5), 1300-1306 (2003).

139. M. Liao, X. Yan, G. Qin, C. Chaudhari, T. Suzuki, and Y. Ohishi, "A highly non-linear tellurite microstructure fiber with multi-ring holes for supercontinuum generation," Opt. Express **17**(18), 15481-15490 (2009).

140. S. D. Jackson and P. H. Muir, "Theory and numerical simulation of nth-order cascaded Raman fiber lasers," J. Opt. Soc. Am. B **18**(9), 1297-1306 (2001).

141. M. Rini, I. Cristiani, and V. Degiorgio, "Numerical modeling and optimization of cascaded CW Raman fiber lasers," IEEE J. Quantum Electron. **36**(10), 1117-1122 (2000).